

V. PEM STACK COMPONENT COST REDUCTION¹

A. High-Performance, Matching PEM Fuel Cell Components and Integrated Pilot Manufacturing Processes

Mark K. Debe and Judith B. Hartmann (primary contact)

3M Company

3M Center, Building 201-1C-30

St. Paul, MN 55144-1000

(651) 736-1772, fax: (651) 575-1187, e-mail: jbhartmann@mmm.com

DOE Program Manager: JoAnn Milliken

(202) 586-2480, fax: (202) 586-9811, e-mail: JoAnn.Milliken@ee.doe.gov

ANL Technical Advisor: James F. Miller

(630) 252-4537, fax: (630) 972-4537, e-mail: millerj@cmt.anl.gov

Contractor: 3M Company, St. Paul, Minnesota

Prime Contract No. DE-FC02-99EE50582, September 1999-December 2001

Subcontractor: Energy Partners, Inc., West Palm Beach, Florida

Objectives

- Develop a set of high-performance, matching polymer electrolyte membrane (PEM) fuel cell components and pilot manufacturing processes to facilitate high-volume, high-yield stack production.
- Demonstrate the matched component performance in a subcontractor's 10-kW fuel cell stack.

OAAT R&D Plan: Task 13; Barriers A and B

Approach

- Phase 1
 - Increase surface area of the 3M-patented, nanostructured, thin-film catalyst support system consistent with high-volume manufacturing process.
 - Develop anode catalyst compositions and structures with higher reformat tolerance and/or a non-precious metal replacement for Ru by using a catalyst deposition process that easily generates new compositions and structures.
 - Investigate catalyst compositions and structures to produce higher-activity cathodes.
 - Develop carbon electrode backing (EB) media, optimized for performance with the catalyst system and flow field.
 - Optimize the fuel cell flow field design for optimized water management and air bleed utilization with the catalyst and EB components.
 - Carry out pilot manufacturing scale-up of the processes for fabrication of catalysts, catalyst-coated membrane assemblies, and electrode-backing media.

¹ The DOE draft technical targets for fuel cell system and fuel cell stack components, sensors, and catalysts can be found in Tables 3, 4a, and 4b, Appendix B. Because the targets in Appendix B were updated after the reports were written, the reports may not reflect the updated targets.

- Phase 2
 - Evaluate matched component system performance in stack tests.
 - Fabricate and deliver a 10-kW stack.

Accomplishments

- Demonstrated a quantitative correlation of fuel cell performance and measured surface area, showing sixfold fundamental enhancement of catalyst utilization of nanostructured thin-film catalysts vs. conventional catalysts. Demonstrated multiple approaches to increase the surface area of the nanostructured catalyst support and demonstrated a method to control the Pt crystallite size independent of the catalyst loading.
- Demonstrated Pt_xM_y binary anode catalysts with performance equivalent to that of PtRu, by using non-precious metals, M, for Ru replacement.
- Demonstrated several Pt_xM_y binary cathode catalyst constructions that outperform the Pt control, by using non-precious metals, M.
- Successfully resolved water management issues with thin-layer catalyst by developing electrode backing (EB) media with matched properties for desired operating conditions. Improved 30 psig current density by 50%. Demonstrated stable 75°C (300 h, 0.6 A/cm²) operation with totally dry air and hydrogen inlet gases. Determined the feasibility for operation at 120°C.
- Developed the matched EB media by using an EB type that is amenable to high-volume manufacturing processes. Scaled up the dispersion preparation process, conducted large-scale pilot plant coating evaluations, and identified a coating method having the potential for meeting volume and quality requirements.
- Developed advanced *in-situ* membrane electrode assembly (MEA) characterization techniques, including a 16-sample cell/16-channel potentiostat system for simultaneous characterization of catalyst surface areas; fast Fourier transform electrochemical impedance spectroscopy on large area MEAs; and techniques to obtain cross-over, H-pump, and anode over-potentials.
- Completed in-depth study of thermal cycling conditioning protocol that increases MEA current density performance by 50–150% over entire voltage range and identified area of fundamental mechanism.
- Made substantial progress on the scale-up and optimization of nanostructured catalyst, PEM, and catalyst-coated membrane (CCM) fabrication processes by using pilot-scale equipment for all processes. Significantly increased the catalyst support system fabrication rates and installed equipment for continuous processing and on-line monitoring. Reduced defects and improved the reproducibility of the PEM fabrication process. Conducted pilot-scale experiments and selected a path for continuous fabrication of CCMs with on-line inspection.

Future Directions

- Continue down-selection of the catalyst and catalyst support components, optimizing their properties and constructions to improve performance of the baseline MEA.
- Continue final down-selection of EB coating materials and coating process to optimize performance with selected flow field and CCM.
- Continue optimization of the fabrication processes for the catalyst, membrane, and catalyst-coated membrane to improve yields, quality, and performance.
- Define the final MEA and flow field parameters for the 10-kW stack build of Phase 2.

Introduction

The membrane electrode assembly (MEA) is the core component set of a PEM fuel cell stack. An MEA consists of five basic components: anode and cathode catalysts, ion exchange polymer membrane,

and anode and cathode gas diffusion layers. The functions of these basic components are intimately related, and the interfaces formed between them are critical for optimum performance. For large-scale volume fabrication at the costs and quality targets

required by transportation applications, very high yields and in-line process control of integrated processes based on cost-effective materials are required. This contract is directed toward demonstrating high-performance, matching PEM fuel cell components manufacturable by integrated pilot processes, utilizing a patented nanostructured thin film catalyst support system. It builds on an initial contract, completed in FY 2000, which demonstrated the feasibility of such an approach.

Approach

Our approach to developing high-performance, matching PEMFC components and integrated pilot manufacturing processes has several facets. These include optimization of the individual components, such as the anode and cathode catalysts and their supports and the electrode-backing and gas-diffusion layers, which are all made by processes consistent with high-volume manufacturing methods. Other facets include understanding and improving the process yields, rates, and quality. During materials or process optimization of a particular component by multiple MEA sample testing, the appropriate performance metric must be used, and the other components must be held as constant as possible. At the next level, these individually optimized components are matched for best overall performance at a particular set of operating conditions. Figure 1 illustrates this concept.

For the anode and cathode catalyst development, the unique nanostructured support and catalyst coating methods offer many combinations of materials and process conditions to generate new

catalyst compositions and structures. The major focus areas are generating higher surface area supports, fabricating and testing new Pt_xM_y binary constructions for anodes and cathodes, and reducing air bleed — all with goals of increasing performance and stability and reducing precious metal loading. Development of carbon EB media has included evaluation of different types of electrode backing materials, coatings, coating configurations, and coating processes. Evaluation involves measurement of a variety of physical properties and of fuel cell performance under a broad range of controlled conditions using nominally identical CCMs. Because this component is the interface between the CCM and flow field, and water management in the catalyst layers is an important function of this component, performance screening in different flow fields is also key to achieving matched components.

The flow field is an integral component of the MEA system. The different operating characteristics of the thin-layer-catalyst approach may benefit from a different flow field design than traditional dispersed catalysts. Our approach involves modeling the gas flow velocity and pressure distributions for various flow field types to obtain more uniform reactant distributions. The gas permeability properties of the various electrode backing and gas diffusion layers are key inputs for this modeling and have to be determined independently. Multiple flow field designs are then tested with the various EB materials to achieve the desired performance.

Scale-up of the processes for producing the catalyst support structures, membranes, CCMs, and EB media is being done in pilot plant facilities. Process optimization and quality improvement studies are being conducted, and improvements to the processes and equipment, including on-line monitoring and inspection methods, are being made as the need is identified through the experiments.

Results

In the past year, significant progress has been made on all the component developments indicated in Figure 1, which will potentially go into improving the baseline MEA. The baseline MEA has effectively the same CCM as when the contract started, no air bleed (AB) optimization, and no final EB materials or flow field optimization.

The performance of the baseline MEA on reformate is compared in Figure 2 to model targets

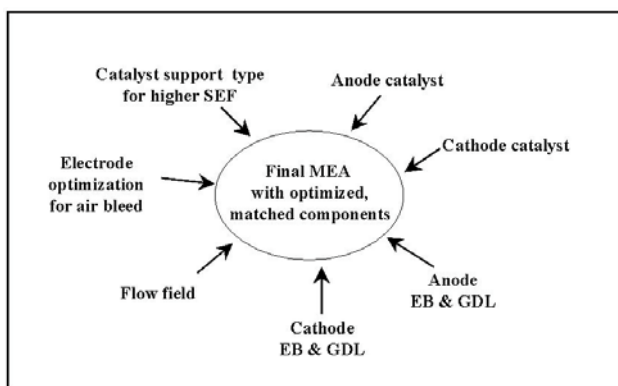


Figure 1. Illustration of how individual components are being optimized and matched to form the final integrated MEA, building on the initial baseline MEA.

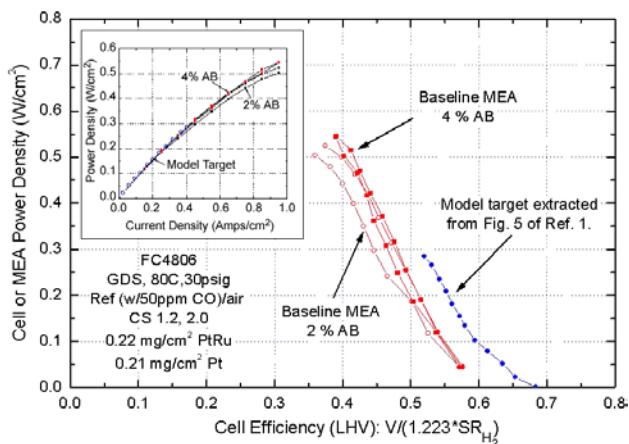


Figure 2. Comparison of performance of our baseline MEA, on reformate containing 50 ppm CO, with target extracted from Figure 5 of Reference 1, a systems model for an 80-kW fuel cell system operating at 80°C, 3 atmospheres, and reformate/air stoichiometries of 1.2 and 2.0.

extracted from an 80-kW automotive fuel cell system model done by Argonne National Laboratory and reported in Reference 1. The baseline MEA does not have optimized anode or cathode catalysts, catalyst supports, electrode backing, air bleed utilization, or flow fields. We have chosen to compare performance on the basis of cell power density versus cell efficiency (lower heating value [LHV] at temperature and pressure, corrected for stoichiometry) because it reflects the important parameters of capital costs versus operating costs and shows the disparity more clearly than does, for example, power density versus current density (see inset in Figure 2). For any given power density, our baseline performance is approximately 5% below this model’s suggested cell performance. The DOE FY2000 target of 0.9 g of Pt/peak kW (stack) is essentially met by the catalyst loadings used in this baseline MEA example.

Work completed to date on optimizing and matching the various components illustrated in Figure 1 has shown the potential for gaining the additional efficiency. Improving the catalyst activities and surface areas are important tasks under investigation. A wide range of binary Pt_xM_y catalysts is being screened to find a cathode catalyst with greater mass activity and/or stability. The continuous process for fabricating the nanostructured catalysts allows a wide range of new constructions to be made and tested. Besides catalyst

composition (M, x, and y), the physical structure and surface finish are controlled. Figure 3 illustrates three-dimensional plots of cathode activity performance metrics versus these composition and structure factors obtained thus far for cobalt and nickel binaries.

Screening for better or less-expensive anode catalysts is also a major task. Finding a replacement for Ru is a primary goal, along with reducing the amount of Pt required for adequate reformate tolerance. To facilitate the rapid screening of many new catalyst constructions having different compositions and structures, anode over-potential (AOP) and AC impedance measurements are made by using advanced techniques developed specifically for these tasks. Figure 4 shows the best example to-date of a new binary anode catalyst containing no Ru and 0.1 mg/cm² of Pt, which has less AOP than the PtRu control. By using AC impedance, Figure 5 compares the charge transfer resistance under

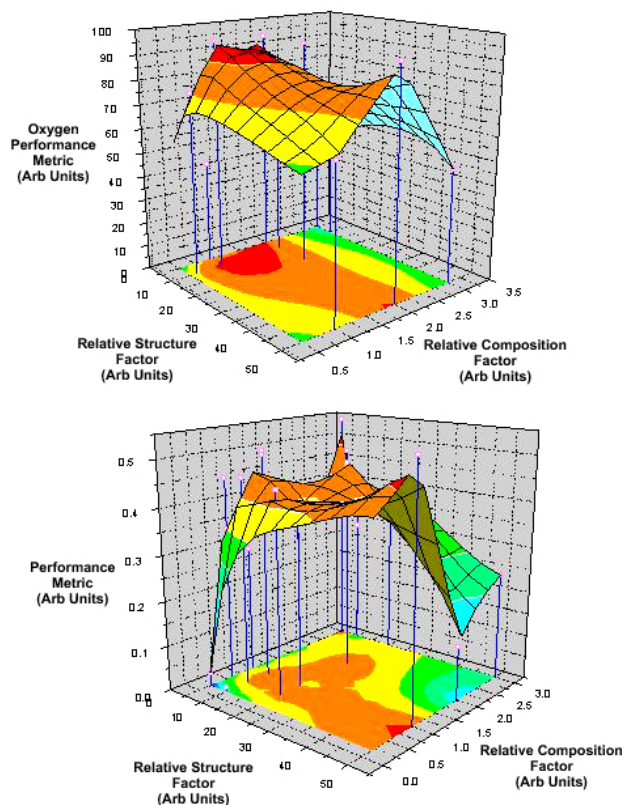


Figure 3. Example data summary plots for Pt_xCo_y (top) and Pt_xNi_y (bottom) cathode binary catalyst screening, showing the relative performance metric plotted as a function of the independently controlled catalyst structure and composition variables.

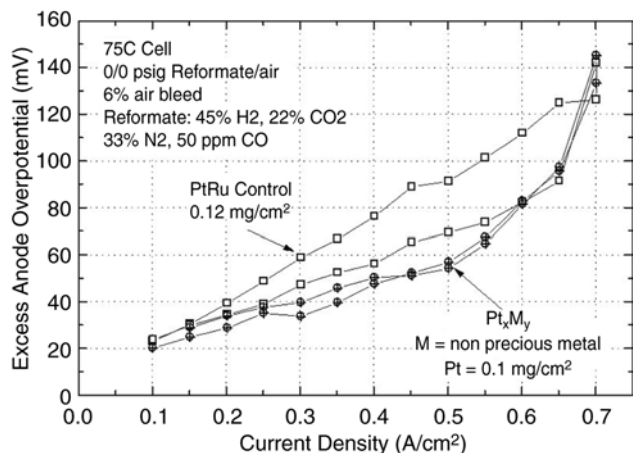


Figure 4. Example of a new reformat-tolerant anode catalyst with Ru replaced by a non-precious metal and containing 0.1 mg/cm² of Pt, which outperforms a PtRu control. The excess anode over-potential is effectively the loss in cell voltage compared to pure hydrogen.

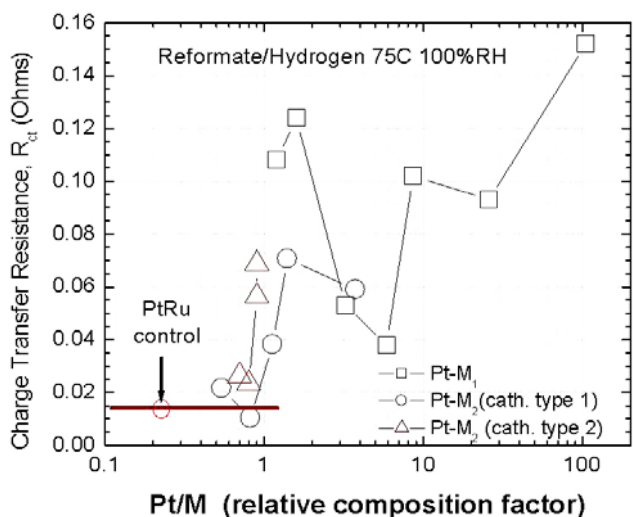


Figure 5. Example of two other new anode catalyst materials, PtM₁ and PtM₂, with non-precious metal replacements for Ru, characterized by electrochemical impedance spectroscopy. The charge transfer resistance is shown for samples with a relative composition factor varying over two orders of magnitude and compared to the baseline PtRu anode catalyst.

reformat for two other Pt-based binaries containing non-precious metals as the second component. It is plotted versus a relative composition factor, which is varied over two orders of magnitude, and shows that there is a range of composition in which the performance approaches that of the PtRu baseline control.

Effective air bleed utilization is critical for reformat tolerance with low catalyst loadings on the CCM. Additional catalyst added at other places in the MEA (reconfigured anode [RCA]) is known to facilitate the chemical oxidation of CO. Using non-precious metals to improve this air bleed effectiveness is desired to meet the overall low precious metal targets. Figure 6 shows the best results to-date for an RCA containing a small amount of a catalyst by using a nonprecious metal. By using the AOP technique, this RCA catalyst outperforms the MEA having no RCA or an RCA based on PtRu.

The performance efficiency results in Figure 2 are directly related to the cathode-specific activity, since for every ~13 mV gain in the polarization curve, the efficiency increases 1%. This activity, in turn, is directly related to the catalyst surface area, which is related to the surface area of the support. During this reporting period, significant work has gone into measuring the surface areas of the nanostructured thin film catalysts by using advanced electrochemical techniques. It is now extremely well documented that our baseline catalysts have mass specific surface areas of about 7 m²/g and effective surface roughness factors of 12–15 cm²/cm². However, the activity per unit of real surface area is six times that for conventional carbon particle supported Pt. This phenomenon is illustrated in Figure 7, where the polarization curves from two nominally identical MEAs, one containing the nanostructured catalysts and one containing conventional carbon-supported catalysts, have been replotted by normalizing to the real

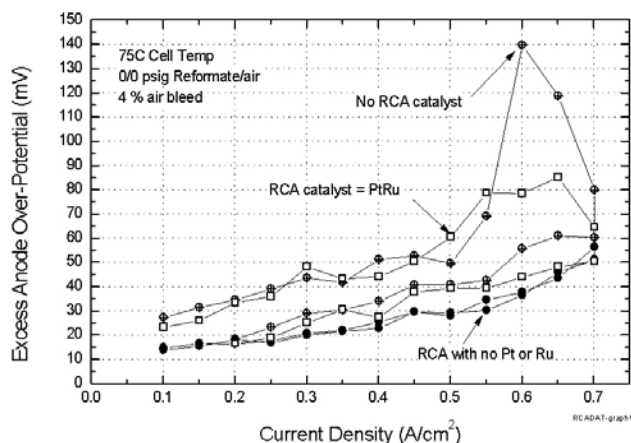


Figure 6. Example of improving air bleed utilization by using nonprecious catalysts elsewhere in the RCA to outperform PtRu.

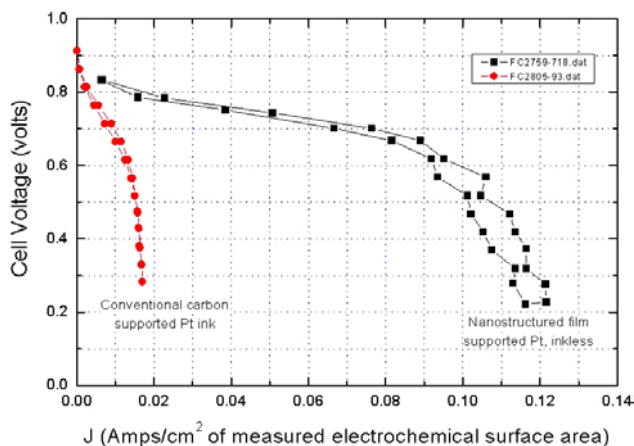


Figure 7. Example of the sixfold increased catalyst activity of the nanostructured film thin-layer catalysts compared to conventional carbon particle-supported dispersed catalysts. For MEAs having the same Pt mass loadings, membranes, and gas diffusion layers, the V(J) polarization curves overlap when J is expressed in terms of A/cm^2 of planar area. When current is normalized to the measured electrochemically active surface area of each catalyst type, the increased activity is revealed.

electrochemically active surface area. Investigation of approaches to increase the surface area of the nanostructured supports over the baseline values has been an important task activity, and results this period have identified several pathways consistent with the established manufacturing process.

Extensive studies were conducted of different electrode backing materials, coatings, and coating configurations. The studies included MEA fuel cell polarization tests with constant PEM and catalysts, under highly controlled temperature, pressure, gas composition, and humidification conditions. The results have highlighted the fact that different configurations provide optimum performance under different conditions. Figure 8 illustrates the dramatic improvement obtained in high-current-density performance under pressurized conditions achieved this year by development of matched electrode backings. Anode and cathode EB optimization studies were also conducted, and performance correlated with three types of flow field design. The EB materials and configurations demonstrating the

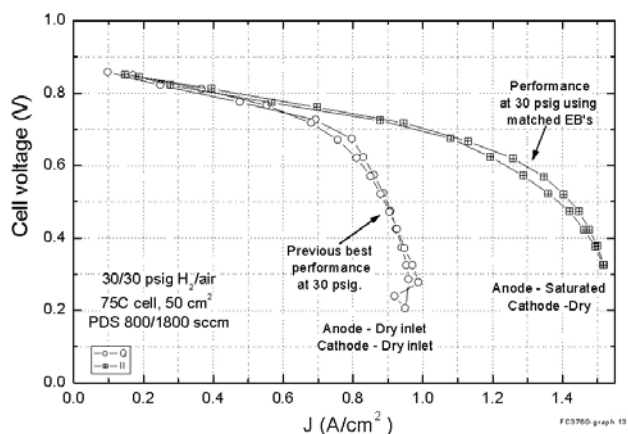


Figure 8. Improvement in pressurized air performance achieved by improved matching of the electrode backings for improved water management with the nanostructured CCM.

highest potential for meeting contract goals were selected for optimization.

Processes and equipment for making membranes and EB media were evaluated, and those having the highest potential for meeting the volume and quality goals were selected for optimization. Optimization of these processes and those previously selected for making catalysts and catalyst-coated membranes is being done on pilot-scale equipment. Each step has been demonstrated in a continuous (roll-goods) mode that is capable of being scaled up to large volumes. Modifications to the pilot plant equipment are being made as the need is identified through optimization experiments. On-line measurement techniques have been identified and are being implemented for use in the catalyst, membrane, and CCM fabrication, as well as EB coating processes. The goal of these on-line measurement techniques is to provide a handle for monitoring and improving quality. Figure 9 illustrates the uniformity of fuel cell performance obtained from MEAs made from different lots of continuously fabricated PEM, different lots of nanostructured catalysts fabricated both continuously and in batch mode, and different lots of EB media. The uniformity of the polarization curves reflects the reproducibility of all the CCM components.

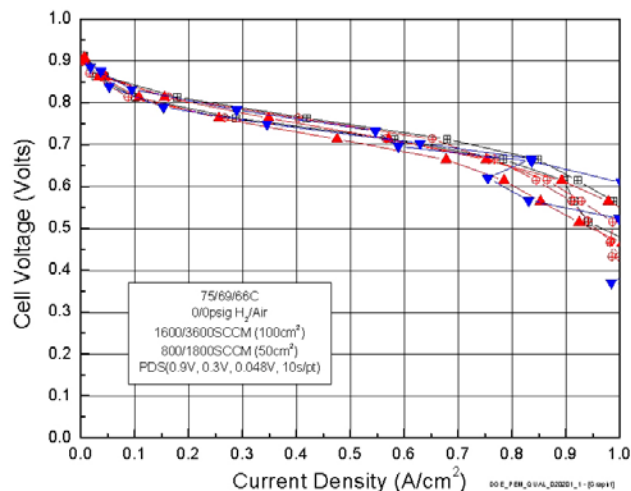


Figure 9. Demonstration of the uniformity of MEAs obtained with different fabrication methods and material lots.

Conclusions

Significant progress is being made in all aspects of the objectives of developing high-performance,

matching PEM fuel cell components and pilot manufacturing processes. Results to-date indicate that (1) the component optimization tasks have the potential for meeting the original contract performance and precious metal loading targets and (2) the selected fabrication processes have the potential for meeting the volume and quality objectives. Future work includes continued optimization of the catalyst, EB, and flow field constructions and the processes for making them. The final MEA and flow field parameters will be defined near the end of Phase 1 for the 10-kW stack build of Phase 2.

Reference

1. Romesh Kumar, E. Danial Doss, Rajesh Ahluwalia, Howard Geyer, and Michael Krumpelt, “Fuel Cell Systems Analysis, FY 2000 Progress Report for Fuel Cell Power Systems,” page 21.

B. Design and Installation of a Pilot Plant for High-Volume Electrode Production

James Arps

Southwest Research Institute

P.O. Drawer 28510

San Antonio, TX 78228-0510

(210) 522-6588, fax: (210) 522-6220, e-mail: jarps@swri.org

DOE Program Manager: JoAnn Milliken

(202) 586-2480, fax: (202) 586-9811, e-mail: JoAnn.Milliken@ee.doe.gov

ANL Technical Advisor: James Miller

(630) 252-4539, fax: (630) 972-4537, e-mail: millerj@cmt.anl.gov

Contractor: Southwest Research Institute, San Antonio, Texas

Contract No. DE-FC02-00EE50625, Period of Performance December 1, 2000–May 1, 2002

Subcontractors: General Motors, Warren, MI; W.L. Gore and Associates, Elkton, MD

Objectives

- Demonstrate proofs of concept for the large-scale preparation of high-performance electrodes for membrane electrode assemblies (MEAs) and assess electrode and MEA architecture against Partnership for a New Generation of Vehicles (PNGV) cost targets.
- Design, build, and install equipment for a high-volume pilot plant capable of catalyzing 100,000 square meters of electrode material per shift per year.
- Complete process development and qualification of the pilot plant.
- Benchmark MEAs fabricated at Southwest Research Institute (SwRI) against commercially available products.
- Incorporate MEAs into a 50-kW fuel cell stack built by General Motors (GM) and deliver stack to Argonne National Laboratory for testing and evaluation.

OAAT R&D Plan: Task 13; Barrier B

Approach

- Prepare MEAs by using ultra-low-load (<0.10 mg/cm² Pt) electrodes and test under hydrogen-air and reformate-air operating conditions.
- Determine the impact of large-scale catalyzation methods on MEA performance, if any, and develop approaches to minimize the effects.
- Establish *in-situ* process control methods for catalyst deposition and demonstrate high-efficiency metal recovery approaches.
- Finalize equipment design and construct pilot plant.
- Fabricate sufficient ultra-low-load MEAs from catalyzed electrode material for incorporation into 50-kW stack.

Accomplishments

- Conducted numerous small-cell (50 cm²) tests of SwRI-prepared and baseline MEAs with simulated reformate under DOE hydrogen-air test conditions.

- Confirmed that performance of pilot-batch ($\sim 10 \text{ m}^2$) continuous roll material is equivalent to that of small-batch (0.2 m^2) manufactured material. Prepared and evaluated 5–10- m^2 continuous lengths of cathode alloy electrode material.
- Incorporated continuously manufactured CARBEL™ CL gas diffusion materials from W.L. Gore & Associates, Inc. (Gore), into MEA architecture.
- Delivered several small-scale Pt and PtRu MEAs to GM for initial testing and evaluation.
- Delivered ~ 12 full-scale (800 cm^2) MEAs to GM and completed initial series of short stack tests.
- Completed cost analysis for electrode catalyzation method and assessed impact on overall MEA cost.
- Selected manufacturer for pilot manufacturing system and initiated construction.

Future Work

- Continue efforts to optimize anode catalysts for improved CO tolerance.
- Conduct additional short-stack tests at GM.
- Complete construction, acceptance testing, and installation of pilot system at SwRI.
- Catalyze anode and cathode materials at target production rates and demonstrate performance equivalent to that of laboratory and pre-pilot materials.
- Validate catalyst utilization and recovery methods of at least 95% efficiency.
- Fabricate MEAs for 50-kW stack.

Introduction

Progress in the adoption of polymer electrolyte membrane (PEM) fuel cell technology in the automotive area will depend to a large extent on the economics of catalyst utilization, the MEA production system, and the resultant performance in a fuel cell system. Recent cost analyses have suggested that MEAs can constitute up to 80% of the cost of a fuel cell stack. Hence, improvements in the inherent performance of MEAs, while substantially reducing the catalyst content per unit area, will contribute significantly to lowering the cost of producing fuel-cell-generated power. Therefore, the development of manufacturing concepts permitting the continuous and high-speed catalyzation of electrodes should have a significant beneficial impact on the cost of the MEAs and the dollars per kilowatt of power produced by the fuel cell.

Until recently, most MEAs were produced in time-consuming, batch-type processes. This situation has existed because of generally low-volume purchases of MEAs and the large variety of MEA sizes and configurations required by the various fuel cell systems manufacturers. In effect, the industry is in a “chicken and egg” situation in which low prices are desired for fuel cell components, such as the MEA, to commercialize

fuel cells and attain high volumes, yet component suppliers need high volumes to attain low prices. Without a large present market, the investment risk is considerable and may be beyond the means of any industrial entity.

High-volume, continuous operations capable of producing subcomponents (such as electrodes) should dramatically reduce the cost of the finished product. Southwest Research Institute is investigating this premise by developing large-area, vacuum-based electrode substrate coating technologies to reduce the overall material content of the finished part. Specifically, “ultra-low” precious-metal-loaded electrodes with loadings of 0.10 mg/cm^2 or less have been fabricated by using state-of-the-art polymer electrolyte membranes and electrode substrates procured from Gore. The best-performing MEAs will be delivered to GM, which will construct and supply a 50-kW fuel cell stack to Argonne National Laboratory.

Approach

Significant progress has been made in the past year in addressing key challenges relating to optimizing power density under representative operating conditions. Thousands of linear feet of intermediate electrode material have been supplied by Gore. This material has, in turn, been used at

SwRI to produce catalyzed electrodes with platinum loadings in the range of 0.05–0.10 mg/cm². Figure 1 compares the performance of a standard “baseline” MEA having nominal loading of 0.1 mg/cm² of Pt per electrode with an MEA using SwRI technology and a loading of 0.05mg/cm² of Pt per electrode under conditions of low fuel stoichiometry and relatively high inlet gas and cell temperature. Although both MEAs utilize 25-μm GORE-SELECT™ membranes, the baseline sample employs a commonly used gas diffusion media (GDM), while the SwRI sample uses CARBEL™ GDM. We believe the synergistic effects of higher catalyst utilization and catalyst activity, coupled with improved gas distribution, result in significantly higher performance over the entire voltage range.

Pilot quantities of catalyzed electrode material, up to several hundred square feet per run, have been prepared at SwRI and in off-site demonstrations by using near-full-scale manufacturing equipment not fully optimized for our process requirements. Small-scale (25–100 cm² active area) and full-scale (800 cm² active area) MEAs have been fabricated by using prepared electrode materials, with selected examples provided to GM. A sample MEA prepared for GM is shown in Figure 2. In addition to ongoing hardware development and testing for the final stack deliverable, GM has conducted single-cell and short-stack testing and evaluation of MEAs fabricated at SwRI. The effects of pressure, temperature, stoichiometry, and humidification on cell-to-cell performance, as well as short-term durability, have been investigated. In initial tests, SwRI MEAs



Figure 2. An 800-cm² active area MEA fabricated at SwRI.

exhibited better beginning-of-life performance than baseline MEAs for both single cells and a large-scale stack at high-pressure, well-humidified conditions.

SwRI’s in-house small-cell testing has generally confirmed that material produced by pilot-scale processing exhibits performance equivalent to that of material produced by using laboratory-scale equipment. Cathode alloy catalysts have also been evaluated and appear to hold promise for the further reduction of platinum content. MEAs using PtRu anode catalysts have been tested on reformat with acceptable results. As shown in Figure 3, a commercially available MEA using a Nafion 112® membrane with a catalyst loading of 0.4 mg/cm² of Pt on the cathode and a similar loading of PtRu on the anode is compared with a

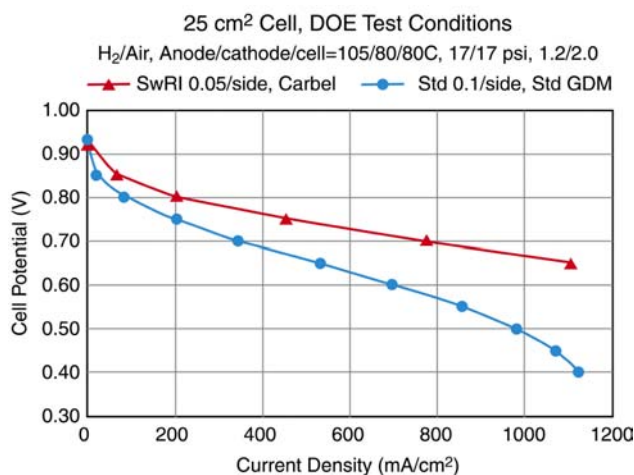


Figure 1. Performance comparison of baseline and experimental SwRI MEAs.

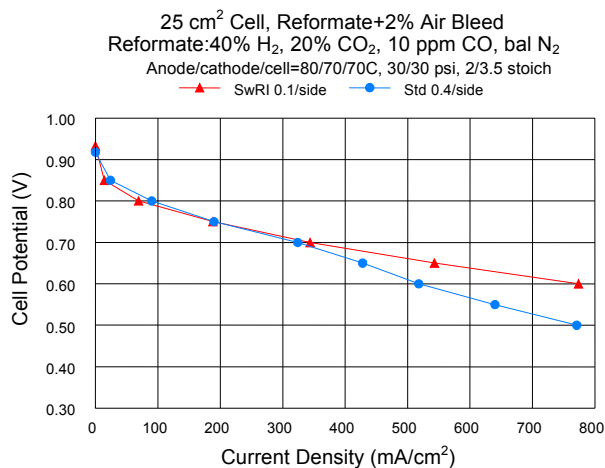


Figure 3. Comparison of SwRI and commercially available MEAs using simulated reformat.

SwRI-fabricated MEA using a 25- μm GORE-SELECT™ membrane and approximately 0.1 mg/cm² of PtRu and Pt on the anode and cathode, respectively. Both MEAs use the same commercially available cloth GDM.

Finally, design and specification of the pilot manufacturing line has been completed, and, with approval from DOE, construction began in late 2000. The system, once completed, will accommodate intermediate electrode materials in roll form up to 30 cm in width and up to several hundred meters in length. A photograph of a system resembling the equipment to be installed is shown in Figure 4. The system is currently scheduled for delivery and initial prove out at SwRI in October of 2001.



Figure 4. Pilot manufacturing line to be installed at SwRI.

Conclusions

SwRI has been tasked with developing a high-volume pilot line for the catalyzation of practical quantities of electrode material for use in transportation applications. The MEAs produced under this project should demonstrate sufficiently low catalyst loadings and high material throughput toward meeting PNGV's projected MEA costs of \$10/kW. While significant progress has been made in adapting the SwRI catalyst deposition technology in the fabrication of reformate-tolerant PtRu anodes, further work is required to increase CO tolerance above 10 ppm and eliminate the need for air-bleed. SwRI will continue to provide GM with test MEAs using various anode and cathode catalyst compositions and loadings for testing under conditions of interest. The best formulations will be produced as full-scale MEAs and assembled into 15–20-cell stacks. Baseline samples are being provided by Gore for use in benchmarking performance. Once the pilot system is delivered and installed at SwRI, pilot-production runs will be carried out by using established optimized anode and cathode recipes to validate and confirm that electrode catalyzation rates, catalyst utilization, and production yields are consistent with program targets.

C. Development of a \$10/kW Bipolar Separator Plate

Leonard G. Marianowski

Gas Technology Institute (GTI)

1700 South Mount Prospect Road

Des Plaines, IL 60018

(847) 768-0559, fax: (847) 768-0916, e-mail: len.marianowski@gastechnology.org

DOE Program Manager: Donna Lee Ho

(202) 586-8000, fax: (202) 586-9811, e-mail: donna.ho@ee.doe.gov

ANL Technical Advisor: Walter Podolski

(630) 252-7558, fax: (630) 972-4430, e-mail: podolski@cmt.anl.gov

DOE Contractor: Gas Technology Institute, Des Plaines, Illinois

Prime Contract No. DE-FC02-97EE50477, November 1998–October 2001

Subcontractors: Avery-Dennison-Stimsonite Corporation, Niles, IL 60714; Superior Graphite Corporation, Chicago, IL 60638; and Honeywell Inc., Torrance, CA 90504

Note: The Institute of Gas Technology (IGT) combined with the Gas Research Institute (GRI) in June 2000 to form the Gas Technology Institute (GTI).

Objectives

- Develop a low-cost molded graphite bipolar separator plate for polymer electrolyte membrane (PEM) fuel cells.
- Evaluate the performance and endurance of the GTI molded graphite bipolar separator plate in fuel cell stacks.
- Build a pilot-production molding line of 5-plates/h capacity to evaluate mass production of molded plates.

OAAT R&D Plan: Task 13; Barrier B

Approach

- Select, blend, and optimize inexpensive raw materials for necessary electrical, chemical, and physical properties of bipolar separator plates for a \$10/kW-manufactured target cost.
- Design, build, and operate the 5-plates/h pilot production molding line at PEM Plates, LLC (a joint venture between GTI and Stimsonite).
- Produce molded bipolar plates from the pilot line for the GTI and Honeywell fuel cell stack tests.
- Assemble fuel cell stacks at GTI to establish the functional performance and endurance of molded plates in stack environments.
- Honeywell, Inc., will assemble and test molded plates from PEM Plates in Honeywell's fuel cell stacks for comparison with a similar stack assembled with standard graphite plates.

Accomplishments

- Met or exceeded DOE-specified electrical, chemical, and physical property targets with an optimized blend of components in out-of-cell laboratory tests and single cell tests.
- Demonstrated fuel cell performance within 5% of state-of-the-art machined graphite fuel cells in side-by-side tests.
- Built a 5-plate/h pilot molding production line facility and related equipment; produced plates for testing at GTI and Honeywell and sent samples to several developers of fuel cell stacks.

- GTI demonstrated the operational functionality of the molded plates in multi-cell fuel cell stacks for heat management, sealing, stacking stability, and water management.
- Operated for over 2,300 h the first 20-cell GTI fuel cell stack using plates produced by PEM Plates with excellent plate performance. Extended life tests of molded plates were accomplished by reuse in subsequent fuel cell stacks, and those plates exceeded 5,000 h operation with no degradation.
- GTI tested the molded bipolar plate performance in multiple fuel cell stacks of 4, 7, 20, 52, and currently 70 cells in both continuous and intermittent operation modes.
- Confirmed the excellent properties of molded plate samples, as reported by several of the major fuel cell developers.
- Attempted to mold the sets of separator plates for the Honeywell fuel cell stack, but these attempts were not successful.
- Attempted to achieve \$10/kW cost target. Target is within reach, with separator plate materials cost at \$4/kW; however, manufacturing costs at \$6/kW depend on the details and complexity of the actual bipolar plate design.

Future Directions

- Design and build the higher-capacity pre-commercial molding line incorporating process improvements.
- Complete licensing discussions with commercial molders and fuel cell stack developers to supply GTI molded bipolar separator plates.

Introduction

The U.S. Department of Energy (DOE) sponsored a program with GTI to develop a molded composite graphite bipolar plate that would be inexpensive and perform as well as machined state-of-the-art graphitized bipolar plates. GTI identified and tested moldable blends of graphites, resins, and various additives and produced a molded composite graphite bipolar separator plate that is equivalent in function and performance to state-of-the-art machined graphite plates. These plates were tested in this DOE program, as well as in several parallel programs at GTI.

Applications for patents for the blended components and the process have been submitted, and PEM Plates, LLC, was formed to commercialize the production of the molded graphite bipolar separator plates. In the past year, PEM Plates, without commitments of orders and a higher-capacity second-generation molding machine, could not sustain its efforts. Consequently, PEM Plates was absorbed into GTI to continue the development of a second-generation machine and process improvements.

Material and production costs for commercial quantities of the plates are estimated to be within \$10/kW; however, the manufacturing cost portion will depend on the complexity of the design of the

bipolar plates and the fuel cell stack. A variety of different designs of anode and cathode gas-flow channels with water cooling channels have been molded (i.e., molded directly to net shapes with no post-molding finishing or machining steps). No significant geometrical or shape limitations have been encountered; however, complexity in the flow field design does dictate the achievable level of tolerances of very thin plates. On the other hand, because the molded composition plates exhibit a degree of inherent flexibility with sufficient strength, thinner plates are possible compared to plates machined from much stiffer graphitized carbon.

Results

Molded Bipolar Plate Tests

The molded graphite plates have been tested over the past three years at GTI under several parallel programs, and other fuel cell stack developers have evaluated samples. As presented previously, electrical, chemical, and physical properties were measured in numerous out-of-cell tests. Extensive single-cell tests of the plates have shown consistent performance in excess of 5,000 h. The molded plates have been successfully scaled up from laboratory-size active areas of 60 cm² to the

full-size DOE-vehicular-specification active area of 300 cm². Figure 1 presents the comparison of the hydrogen-air performance at atmospheric pressure of a single cell with molded graphite flow field plates to a cell with an identically machined flow field in POCO graphite plates. The performance with the molded plates is within 5% of the POCO plates at a typical current density of 400 mA/cm². However, at the higher currents, the performance of the molded plate is better because the inherent hydrophilic nature of the GTI composition aids the removal of product water, especially at high current densities.

Tests of the molded plates in a well-instrumented 300 cm² 20-cell stack with water-cooling were conducted for over 2,300 continuous hours, as shown in Figure 2. These tests demonstrated the endurance of the plates with active thermal management in the 300-cm²-size stacks with the use of water-cooling. Stack testing was

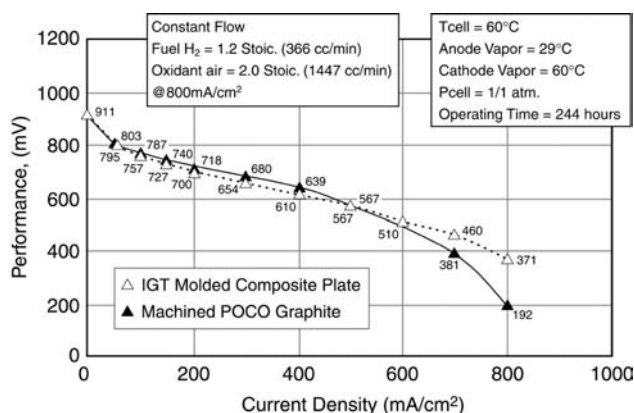


Figure 1. Comparison of molded graphite cell to machined graphite cell.

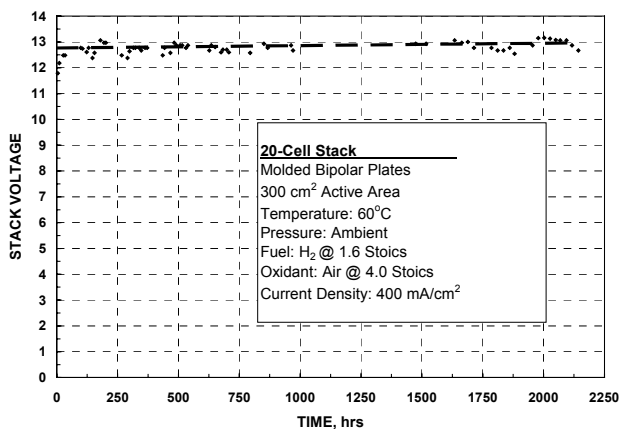


Figure 2. Life test of GTI 20-cell molded bipolar plate fuel cell stack.

conducted mostly in a continuous operation mode of 24 h/day and 7 days/week, but some tests were also conducted in daily cycles of 8 h on and 16 h off, with the molded stack plates cooling and reheating each day. In both test mode environments, the molded plates maintained their integrity, and the fuel cell stack performed equivalently to stacks made with machined graphite plates. Post-test chemical analysis and physical measurements indicated a stable plate composition with no change in measured properties.

Results of tests of the molded plates operating in fuel cells at various pressures (from one to three atmospheres) showed the typical performance gain, including successful gas sealing and water-cooling. Figure 3 shows a variety of multicell stacks built with 7–70 cells and tested at GTI in a variety of programs.

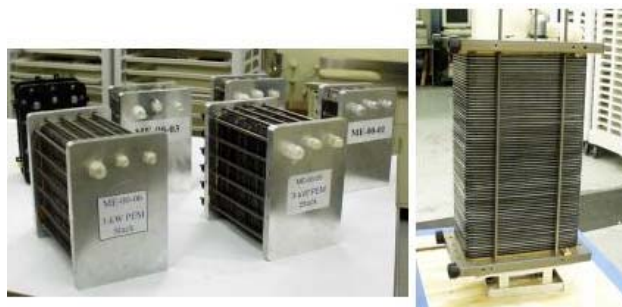


Figure 3. Fuel cell stacks with 7, 20, 52, and 70 cells.

Measurements of Specific Plate Properties

The DOE-specified requirements for conductivity, corrosion, and permeability have been met or exceeded, as shown in Table 1. In addition, other property assessments of the molded plates that are important in the operation and structure of a fuel cell stack were made by GTI. These included measurements and investigations of crush strength, strength within stacks, and strength during handling; elastic and permanent creep; water uptake; chemical leachability; cyclic immersion in boiling water followed by freezing; proof of noncombustibility; recyclability of components; and potential of reuse of components into new plates or other products.

The values of conductivity were measured by using the ASTM C-661 method, and the target values were typically exceeded by a factor of three to eight, depending on plate density. Conductivity and surface resistance measurements were always

Table 1. Molded plate properties: DOE-target values plus GTI measurements.

Plate Property	Measured Value
DOE Specified Properties	
Conductivity	300+ S/cm, about 80% of POCO™ graphite value
DOE Target: > 100 S/cm	
Corrosion	< 5 $\mu\text{A}/\text{cm}^2$
DOE Target: < 16 $\mu\text{A}/\text{cm}^2$	
H ₂ Permeability	<< $2 \times 10^{-6} \text{ cm}^3/\text{cm}^2\text{-s}$ (dry, nonporous plates)
DOE Target: < $2 \times 10^{-6} \text{ cm}^3/\text{cm}^2\text{-s}$	
Additional Properties Measured by GTI	
H ₂ Bubble Pressure	> 15 psig (wet, porous plates)
Crush Strength	> 3,000 psi
Flexibility	3–6% deflection at midspan
Total Creep	~1% elastic deformation at 200 psi and 100°C
Flexural Strength	6,420 psi (820 std. dev.)
Combustibility	0 (in propane flame)

compared with measurements of POCO graphite plates used as a standard.

The corrosion rate target of less than 16 $\mu\text{A}/\text{cm}^2$ was also satisfied. Corrosion was evaluated in hydrogen, air, and oxygen atmospheres in a dilute sulfuric acid solution with 2 ppm fluoride by using ASTM G5 method at 90°C and pH~4. The GTI molded-composite blend exhibited total corrosion rates below 5 $\mu\text{A}/\text{cm}^2$. Hydrogen permeability was measured as a function of plate density, related to molding pressure. Plates can be molded either more or less dense than POCO graphite, thereby controlling the porosity. The hydrogen permeability rate measured for the dense, nonporous plates was << $2 \times 10^{-6} \text{ cm}^3/\text{cm}^2\text{-s}$ at 90°C and 207 kPa (30 psig), which is always below the DOE-specified value of $2 \times 10^{-6} \text{ cm}^3/\text{cm}^2\text{-s}$.

Additional measurements were made of the plate crush strength, plate flexural strength, plate mid-span flexibility, and plate creep characteristics. The molded plates are expected to withstand an anticipated holding force of 200 psi pressure in the

fuel cell stack, including stacking dimensional nonuniformities induced by gasketing or assembly methods, plus a myriad of handling and packaging actions from the production line to stack assembly. The measured strength values shown in Table 1 yield a good safety margin. The strength and slight flexibility of the molded composite plates advantageously allow the stacks to be more durable. The plates have retained their electrical and physical properties after being subjected to immersion in boiling water followed by freeze-thaw cycles. Maximum loss of weight in any of the tests has been on the order of 0.5%.

Molded Plate Production and Cost Estimates

Since PEM Plates was absorbed back into GTI, discussions with potential licensee-molders and fuel cell developers have progressed. The knowledge from molding the composite plates in the 5-plates/h pilot line (plus the experience of commercial molders in the design of a second generation molding machine) indicates that production rates of hundreds of plates per hour are nearing reality. As determined previously, for carload quantities, raw material costs will be \$4/kW or less. Production costs are expected to be about \$6/kW, but this cost strongly depends upon the complexity of the plate design.

Capital and operating costs were revisited for the second-generation machines to produce hundreds of plates per hour. Annual production quantities of about 100 MW of fuel cells are needed to achieve production costs below \$6/kW for reasonable separator plate designs. This quantity of plates is equivalent to about 2,000 cars per year with 50-kW fuel cell engines.

Conclusions

After identifying a unique blend of component materials for a molded graphite bipolar separator plate for PEM fuel cells, development of a rapid molding process began with a pilot production line. Thousands of plates have been molded and thousands of hours of fuel cell stack tests have been

conducted, yielding performance practically equivalent to state-of-the-art machined graphite plates. In commercial production quantities, the estimated costs of molded separator plates are about \$10/kW. However, more needs to be done to reach commercial production:

- A second-generation molding machine needs to be validated for production rates of hundreds of plates per hour;
- Successful molding trials must be demonstrated for several stack developer plate designs; and
- Stack performance, endurance, and quality verification testing is needed by stack developers.

D. Carbon Composite Bipolar Plates

T.M. Besmann (primary contract), J.W. Klett, and J.J. Henry, Jr.
Surface Processing and Mechanics Group and Carbon and Insulating Materials Group
Oak Ridge National Laboratory
P.O. Box 2008, MS 6063, Bldg. 4515
Oak Ridge, TN 37831-6063
(865) 574-6852, fax: (865) 574-6918, e-mail: besmannm@ornl.gov

DOE Program Manager: JoAnn Milliken
(202) 586-2480, fax: (202) 586-9811, e-mail: JoAnn.Milliken@ee.doe.gov

Contractor: Oak Ridge National Laboratory, Oak Ridge, Tennessee
Prime Contract No. DE-AC05-00OR22725

Objectives

- Develop a slurry-molded carbon fiber material with a carbon-chemical-vapor-infiltrated sealed surface as a bipolar plate.
- Collaborate with potential manufacturers to test and manufacture the resulting components.

OAAT R&D Plan: Task 13; Barrier B

Approach

- Fabricate fibrous component preforms for the bipolar plate by using slurry molding techniques with carbon fibers of appropriate lengths.
- Fabricate hermetic plates using a final seal with chemical-vapor-infiltrated carbon.
- Develop commercial-scale components for evaluation.

Accomplishments

- Demonstrated ability to mold two-sided prototypical 100-cm² active area plate.
- Demonstrated good polarization behavior in a cell.
- Measured thermal diffusivity (0.0290 cm²/s) and determined thermal conductivity (1.37 W/m•K).
- Provided two-sided specimens to industry for evaluation.
- Licensed technology to Porvair Fuel Cell Technology.

Future Directions

- Develop bipolar plate material/configuration to meet various users' unique requirements.
 - Transfer technology and assist in scale-up with Porvair.
-

Introduction

During FY 2001, the Oak Ridge National Laboratory (ORNL) carbon composite bipolar plate effort has achieved several programmatic goals: molding two-sided preforms, measuring thermal diffusivity, and licensing the technology. We produced two-sided components measuring 2.5 mm in thickness with 100-cm² active area. Sample components are being tested and evaluated at Plug Power, Honeywell, Ballard, and International Fuel Cells. We demonstrated previously that projected costs would meet program goals, that the material properties met program requirements, and that the component had the substantial advantage of weighing almost 50% less than competing materials.

Approach

Fibrous component preforms for the bipolar plate are prepared by using slurry molding techniques with 100- μ m carbon fibers (e.g., Fortafil) in water containing phenolic resin. The approach involves a vacuum molding process that produces a low-density preform material. A phenolic binder is used to provide green strength and assist in providing geometric stability after an initial cure. We fabricated a set of brass molds with channels measuring 0.78 mm (31 mil) deep and wide. The molds are used to impress channels and other features into the preform material. The surface of the preform is sealed by using a chemical vapor infiltration (CVI) technique in which carbon is deposited on the near-surface fibers sufficient to make the surface hermetic. The CVI technique involves placing the preforms in a furnace that is heated to 1,300–1,500°C and allowing methane (under reduced pressure) to flow over the component. The hydrocarbon reacts and deposits carbon on the exposed fibers of the preform, and when sufficient deposition has occurred, the surface becomes sealed. Thus, the infiltrated carbon provides both an impermeable surface and the necessary electrical conductivity so that power can be efficiently obtained from the cell. Processing times are in the range of 4 h.

Results

ORNL produced 100-cm² active area bipolar plates with flow field patterns and other necessary features molded into both sides by using brass molds

of the Los Alamos National Laboratory (LANL) design (Figure 1). Slurry-molded preforms measuring 2.5 mm in thickness were produced for fabrication into two-sided bipolar plates. The preforms were placed between the brass molds, and the assembly was placed in a heated press. The mold was uniformly compressed to 10 kPa (14 psi) at 200°C and held briefly to both impress the features and cure the phenolic resin. The molded preforms released readily from the mold (a common release agent was used), and the features were precisely reproduced in the preform. The plates were subsequently sealed by using the CVI process.

A xenon flash diffusivity technique was used to measure the thermal diffusivity of the composite at room temperature. A xenon flash lamp provided a heating pulse to the specimen's front surface. An infrared detector was employed to record the back surface temperature rise after the pulse. We calculated the thermal diffusivity of the specimen by using the analysis described in ASTM Designation E1461 (1992) "*Standard Test Method for Thermal Diffusivity of Solids by Flash Method.*" Measurements of the through-thickness thermal properties of the plate material were performed by using a square sample cut from the plate with a thickness of 2.461 mm. Five measurements were taken, yielding an average thermal diffusivity $\alpha = 0.0290$ cm²/s, S.D. = 0.0004 (assuming that the specific heat of graphite yields a thermal conductivity of 1.37 W/m•K). This value is low because of the significant porosity in the material. High thermal diffusivity is desirable to facilitate heat removal from the stack.

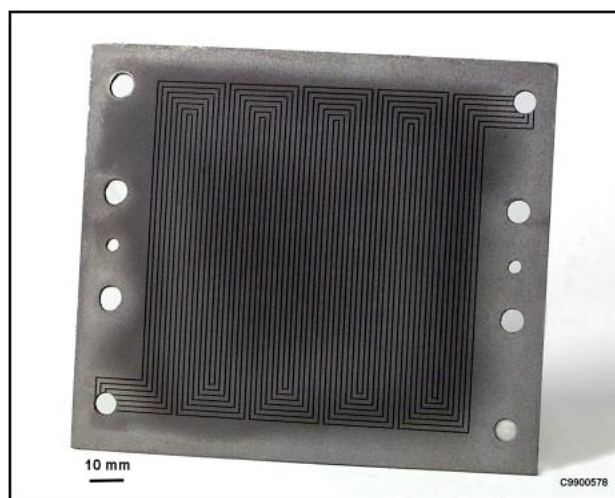


Figure 1. Completed carbon composite bipolar plate.

Polished cross-sections revealed the structure of the carbon composite bipolar plate. Figure 2 shows the flow field in the plate, revealing the sealed surface of the porous material. The relatively poor tolerances on the mold appear to have caused some disruptions in the surface of the plate. However, higher-precision molds used by a fuel cell manufacturer evaluating this technology have demonstrated preparation of high-tolerance components.

The 100-cm²-active-area, two-sided bipolar plate prepared at ORNL was tested in a fuel cell at LANL. Figure 3 illustrates the measured resistivity and cell voltage behavior. The plate performed well in a cell; however, LANL reports using high flow rates to compensate for leakage from the seals along the edges. This problem can be easily remedied by use of an adhesive seal.

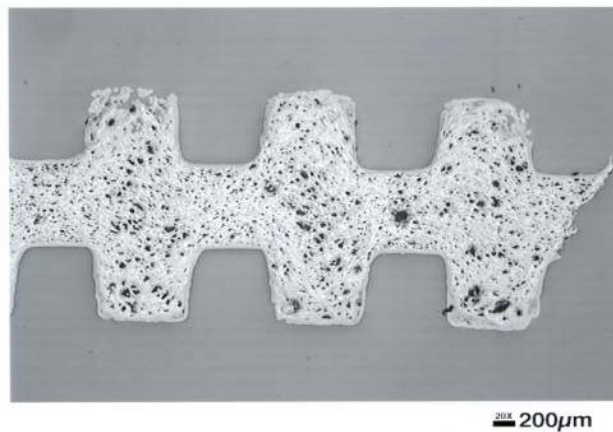


Figure 2. Optical micrograph of a polished cross-section of a carbon composite bipolar plate.

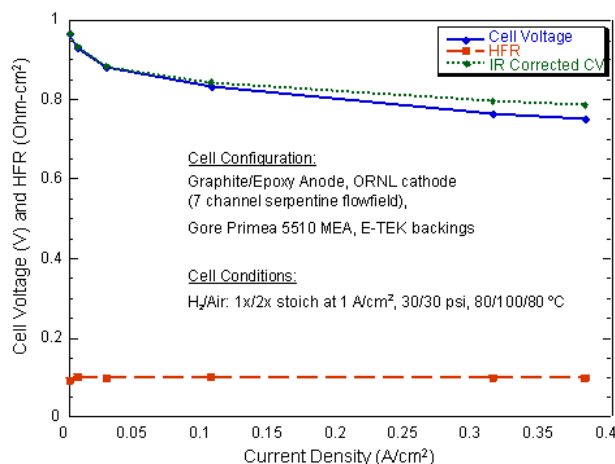


Figure 3. Resistivity and cell voltage from testing at LANL reveals good properties and behavior.

Conclusions/Future Work

During this period, ORNL (1) demonstrated the fabrication of molded two-sided bipolar plates and their infiltration with carbon and (2) measured thermal properties and cell behavior. While the through-thickness thermal conductivity was low, the cell behavior was good. The technology has been licensed to Porvair Fuel Cell Technology, and several fuel cell manufacturers are evaluating sample plates. Table 1 provides a comparison of DOE targets and the materials developed.

Table 1. Material property targets and values.

Property	DOE Target	POCO Graphite	Carbon Composite
Bulk conductivity (S/cm)	>100		200–300
Surface resistivity (Ω/cm)		8	12
Hydrogen permeability (cm ³ /cm ² -s)	<2 × 10 ⁻⁶	Meets target	Meets target
Corrosion rate (μA/cm ²)	<16	80	6
High-volume production cost (\$/kW)	<10	40	5.50

Future work will concentrate on developing carbon composite bipolar plates with unique properties to meet the requirements of several fuel cell manufacturers. It will also involve assisting Porvair in scaling up the technology for production.

FY2001 Publication/Presentation

- T.M. Besmann, J.W. Klett, J.J. Henry, Jr., and E. Lara-Curzio, “Carbon/Carbon Composite Bipolar Plate for Proton Exchange Membrane Fuel Cells,” *J. Electrochem. Soc.* 147 (11) 2000.

Patents Issued

- Bipolar Plate/Diffuser for a Proton Exchange Membrane Fuel Cell*, issued on March 14, 2000, as U.S. Patent # 6,037,073.
- Bipolar Plate/Diffuser for a Proton Exchange Membrane Fuel Cell*, issued January 9, 2001, as U.S. Patent # 6,171,720.

E. Cost-Effective Surface Modification for Metallic Bipolar Plates

M.P. Brady and L.D. Chitwood

MS 6115, Oak Ridge National Laboratory

P.O. Box 2008, Oak Ridge, TN 37831-6115

(865) 574-5153, fax: (865) 241-0215, e-mail: bradymp@ornl.gov

DOE Program Manager: JoAnn Milliken

(202) 586-2480, fax: (202) 586-9811, e-mail: JoAnn.Milliken@ee.doe.gov

ORNL Technical Advisor: David Stinton

(865) 574-4556, fax: (865) 574-6918, e-mail: Stintondp@ornl.gov

Objectives

Develop a low-cost metallic bipolar plate alloy that will form an electrically conductive and corrosion-resistant TiN surface layer during thermal nitriding to enable use in a polymer electrolyte membrane (PEM) fuel cell environment.

OAAT R&D Plan: Task 13; Barrier B

Approach

- Conduct a study of the nitridation behavior of a series of inexpensive Ni-Ti- and Fe-Ti-based alloys that can meet DOE bipolar plate performance and cost goals.
- Identify a combination of Ti content, ternary and higher-order alloying addition(s), and nitridation reaction conditions that result in the formation of an adherent, dense TiN surface layer.
- Immerse nitrided alloy coupons in a 5% HF acid solution, measure weight loss, and conduct cross-section electron microscopy evaluation to screen for the presence of defects in the nitride layer. Characterize nitride layer microstructure and composition by x-ray diffraction and electron probe microanalysis. Use this information in a feedback loop to modify alloy chemistry and nitridation processing conditions to optimize the corrosion protection effectiveness of the nitride surface layer.
- Measure electrical conductivity of select nitrided alloys by D.C. four-point probe.
- Evaluate corrosion behavior of select nitrided alloys in simulated PEM fuel cell environments (in collaboration with K. Weisbrod and C. Zawodzinski of Los Alamos National Laboratory [LANL]).

Accomplishments

- Evaluated the nitriding behavior of a series of developmental Ni-Ti- and Fe-Ti-based alloys with ternary and quaternary alloying additions. Identified alloy chemistries/nitriding conditions that led to the formation of adherent TiN-based surface layers with good corrosion resistance in short-term, 5% HF acid immersion screenings.
- Demonstrated capability of a new, industrial-scale, high-density infrared processing technique to nitride model Fe-Ti and Ti alloys in seconds, compared with hours or days, by conventional nitriding techniques determined in collaboration with C. Blue and V.K. Sikka of Oak Ridge National Laboratory (ORNL).
- Delivered a series of model and developmental alloys to LANL for corrosion testing in simulated PEM fuel cell environments. Established, by using a model refractory alloy, that a nitrided surface can exhibit sufficient corrosion resistance, without significant Nafion[®] membrane contamination, in a PEM fuel cell environment.
- Revealed through testing at LANL that the first generation of developmental nitrided Ni-Ti- and Fe-Ti-based alloys exhibited inadequate corrosion resistance. Post-exposure analysis suggested that the corrosion

susceptibility was related to poor nitride coverage at alloy grain boundaries. Preliminary evaluation of the first alloy of a second generation of Ni-Ti-based alloys designed to eliminate this problem indicated a corrosion current density on the order of $1-2 \times 10^{-6}$ A/cm² at 0.98 V versus SCE in pH 3 sulfuric acid at room-temperature. This result is close to meeting DOE's corrosion-resistance goals.

Future Directions

- Optimize composition/nitridation conditions for the second generation of Ni-Ti- and Fe-Ti-based alloys to eliminate corrosion susceptibility resulting from poor nitride coverage at alloy grain boundary sites. A go/no go decision will be made regarding the ability of these nitrided alloys and this approach to meet DOE bipolar plate corrosion-resistance goals.
- Down select alloy composition and explore scale-up issues with commercial alloy producers.
- Implement process optimization study for inexpensive, rapid nitridation by using high-density infrared processing.
- Supply nitrided bipolar plates to Los Alamos National Laboratory and fuel cell manufacturers for in-cell performance evaluation.

Introduction

The bipolar plate is one of the most expensive components in PEM fuel cells. Thin metallic bipolar plates offer the potential for significantly lower cost than the currently used machined graphite bipolar plates, and they may offer reduced weight/volume and better performance than developmental carbon fiber and graphite bipolar plates currently under consideration. However, inadequate corrosion resistance can lead to high electrical resistance and/or contaminate the PEM. Metal nitrides (e.g., TiN) offer electrical conductivities an order of magnitude greater than that of graphite and are highly corrosion resistant. Unfortunately, conventional coating methods leave "pin-hole" defects in the nitride layers that result in accelerated local corrosion and unacceptable performance.

Approach

The goal of this effort is to develop a Ti-containing bipolar plate alloy that will form an electrically conductive and corrosion-resistant TiN surface layer during thermal (gas) nitriding. There are three advantages to this approach. First, because the nitriding is performed at elevated temperatures, pin-hole defects are not expected because thermodynamic and kinetic factors favor complete conversion of the metal surface to nitride. Second, thermal nitridation is an inexpensive, well-established industrial technique. Third, the alloy can be formed into final shape by inexpensive metal-forming techniques, such as stamping, before

thermal nitridation. The key issues are nitride layer cracking, adherence, and morphology (discrete internal precipitates versus continuous external scales), which can be controlled through proper selection of alloy composition and nitridation conditions.

Existing commercial alloys were typically designed to form oxide layers for corrosion protection and do not thermally nitride to form a corrosion-resistant surface layer. Therefore, this effort is focused on designing a new family of alloys specifically to form a corrosion-resistant TiN surface. As shown in Figure 1 for a series of model Ti-based alloys studied under this program, alloy composition can significantly influence the corrosion resistance of the resultant nitride surface layer.



Figure 1. Nitrided model Ti-alloy coupons after 20 h immersion in 5% HF, illustrating that alloy composition can significantly influence the corrosion resistance of the resultant TiN-based surface layer.

Results

Results to date strongly support proof of principle for thermal nitridation to protect a metallic bipolar plate. A model, thermally nitrided refractory alloy, Tribacor 532N (Nb-30Ti-20W wt. %), exhibited a corrosion current density of only 6.1×10^{-7} A/cm² at 0.98 V versus normal hydrogen electrode (NHE) and stable behavior for 700 h under 1 A/cm² in the LANL corrosion test cell (data of K. Weisbrod, pH 3 sulfuric acid, 2 ppm F⁻, 80°C); the same alloy exhibited essentially no Nafion[®] membrane contamination (~1% active sites affected) after a 300-h immersion screening in pH 2 and pH 6 sulfuric acid (with air or hydrogen) (data of C. Zawodzinski, LANL). These results establish that a nitrided surface can perform well in a PEM fuel cell environment. The key challenge is whether such corrosion-resistant nitride zones can be produced from an alloy that is sufficiently inexpensive to meet DOE bipolar plate cost goals (refractory alloys, such as Tribacor 532N, are too costly for transportation-related applications).

Efforts have focused on the development of inexpensive Ni-(5-15)Ti and Fe-(5-15)Ti wt.%-based alloys that can meet the DOE cost goals. As shown in Figure 2, composition/processing conditions to form an adherent TiN surface layer on Ni-Ti- and Fe-Ti-based alloys have been identified. Bulk electrical conductivities were in the range of $1-2 \times 10^4 \Omega^{-1}\text{cm}^{-1}$ after nitriding, which surpasses the DOE electrical conductivity target by two orders of magnitude.

Corrosion testing at LANL in simulated PEM fuel cell environments indicated insufficient corrosion resistance in the first generation of the Ni-Ti- and Fe-Ti-based alloys. Post-exposure analysis suggested that the susceptibility was related to preferential nitridation at alloy grain boundaries, which was exacerbated by alloy grain growth during the nitridation treatment. A worst-case example of this phenomenon is shown in Figure 3 for nitrided Fe-35Ni-8Ti, a composition that was borderline for external TiN surface layer formation. Although the TiN layers shown in Figure 2 are of much higher quality, there are similar, occasional small local regions of preferential grain boundary nitridation, which degrade the continuity and corrosion protection effectiveness of the TiN surface layer.

A combination of process and alloy optimization is being pursued to eliminate this problem. A heat

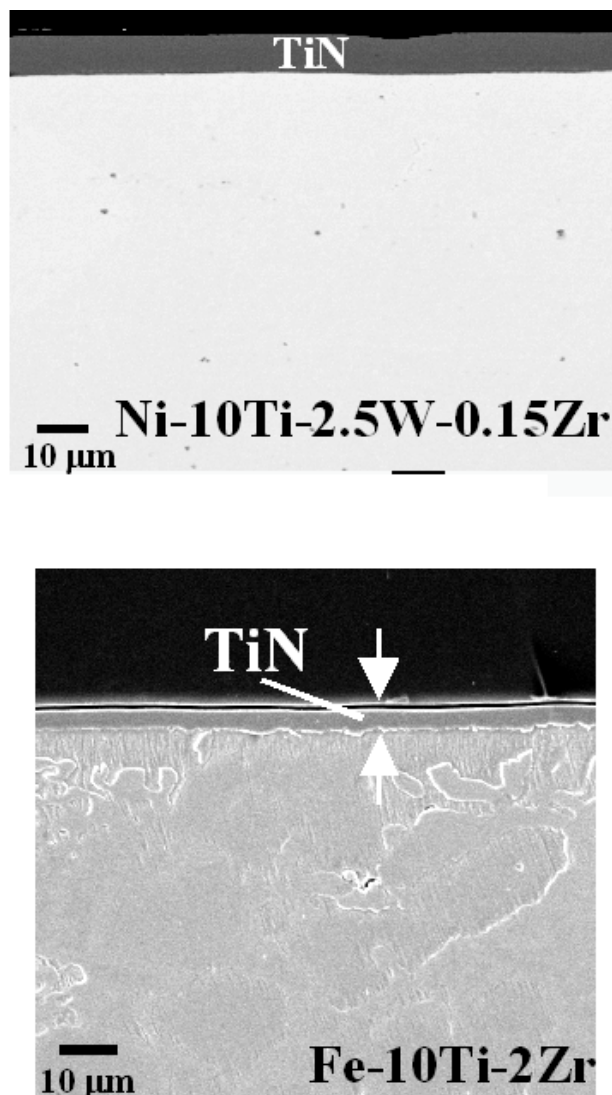


Figure 2. Cross-section electron micrographs of nitrided Ni-Ti- and Fe-Ti-based alloys (wt.%) showing external TiN surface layer formation.

treatment step before nitridation has been added to coarsen the alloy grain structure so that appreciable grain growth during the nitridation treatment does not occur. A promising alloying addition to modify the nitrogen permeability of the alloy to minimize preferential grain boundary nitridation has also recently been identified. Preliminary results have yielded corrosion current densities in the range of $1-2 \times 10^{-6}$ A/cm² at 0.98 V vs. saturated calomel electrode (SCE) in pH 3 sulfuric acid at room temperature, which are close to the DOE bipolar plate corrosion resistance goal.

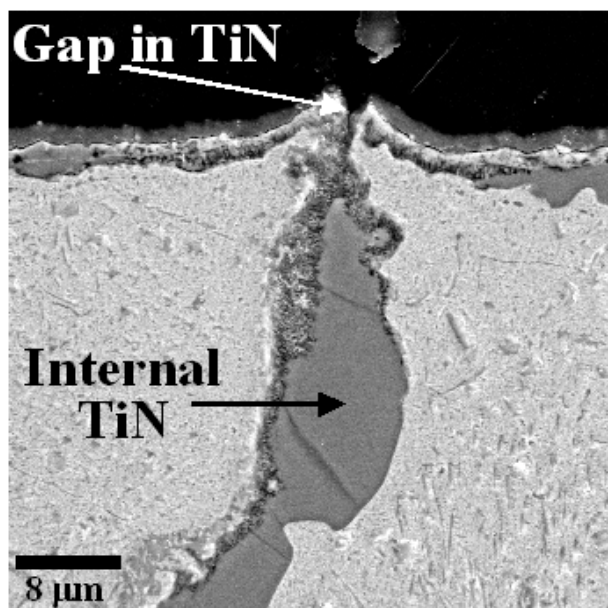
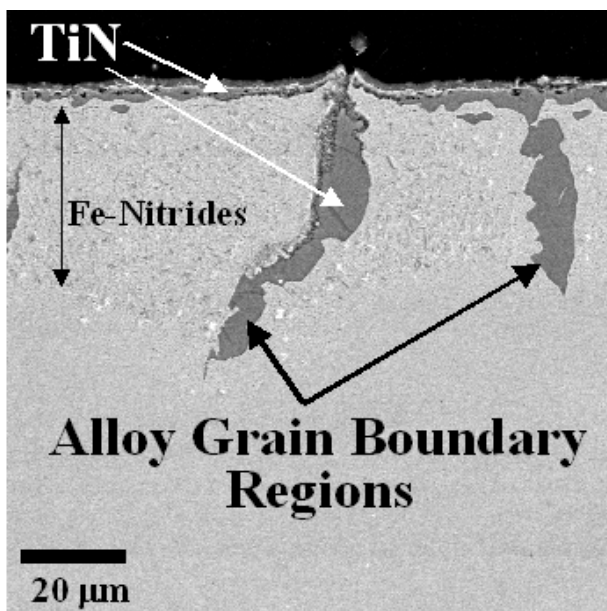


Figure 3. Cross-section electron micrographs of nitrided Fe-35Ni-8Ti wt.% highlighting preferential nitridation and gaps at alloy grain boundary sites. (Worst-case example shown to illustrate effect.)

Alternative nitriding approaches are also under investigation. High-density infrared processing ([http://www.ms.ornl.gov/sections/mpst/process/craig blue/default.htm](http://www.ms.ornl.gov/sections/mpst/process/craig%20blue/default.htm)) is of particular interest because of the rapid heating rates ($> 400^{\circ}\text{C/s}$) and applicability to continuous processing (collaboration with C. Blue and V.K. Sikka, ORNL) (Figure 4).



Figure 4. High-density infrared processing lamp (picture courtesy of Craig Blue).

Preliminary screening showed that model Ti- and Fe-Ti-based alloys could be nitrided in seconds by rapid infrared heating to just under their melting points in a nitrogen-containing atmosphere (conventional nitriding is done at lower temperatures and typically takes hours or days). Although conventional thermal nitriding is commercially available and relatively inexpensive, the use of infrared processing has great potential to further reduce cost and increase throughput volume for the industrial-scale production/nitriding of metallic bipolar plates.

Conclusions/Future Work

Good progress has been made in developing Ni-Ti- and Fe-Ti-based alloys to form a corrosion-resistant nitride surface layer with the potential to meet DOE cost goals. However, issues remain regarding inadequate nitride coverage and protection at alloy grain boundary sites. Efforts are focused on optimization of alloy composition/nitridation conditions to eliminate this susceptibility. A go/no go decision will be made regarding the ability of these nitrided alloys and this approach to meet DOE bipolar plate corrosion resistance goals, and a down select will be made regarding alloy composition. Work will then focus on scale-up issues with commercial alloy producers and delivery of nitrided bipolar plates to LANL and fuel cell manufacturers for in-cell performance evaluation.

F. High-Temperature Membranes

Thomas A. Zawodzinski (primary contact), Francisco Uribe, Wayne Smith, Michael Eikerling, Lawrence Pratt, Antonio Redondo, Tom Springer, Judith Valerio, David Vernon, Don McMurry, and Guido Bender

Los Alamos National Laboratory

Electronic and Electrochemical Materials and Device Research Group

Los Alamos, NM 87545

(505) 667-0925, fax: (505) 665-4292, e-mail: zawod@lanl.gov

DOE Program Manager: JoAnn Milliken

(202) 586-2480, fax: (202) 586-9811, e-mail: JoAnn.Milliken@ee.doe.gov

Objectives

- To develop new membranes and membrane electrode assemblies (MEAs) for operation at temperatures of 120–150°C.

OAAT R&D Plan: Task 13; Barrier B

Approach

- Simultaneously carry out R&D on:
 - Physical chemistry of polymer electrolytes,
 - New polymeric electrolytes,
 - New approaches to proton transport in polymer electrolytes, and
 - Development of MEAs based on new polymer electrolytes.
- Evaluate the following types of polymers:
 - Poly(styrene sulfonic acid) side chains grafted to a TFE/perfluoropropylene copolymer and
 - Polyarylene ether sulfones with varying degrees of sulfonation.

Accomplishments

Physical Chemistry

- Began to collect data on transport in membranes.
- Performed computational studies of different acid moieties.

New Membranes

- Tested new materials for operation at 120°C.
- Initiated synthesis of new polymers with higher acidity.

MEAs

- Fabricated MEAs for one class of materials.
- Revisited high-temperature behavior of Nafion[®]-based MEAs.

Industrial and Other Collaborative Interactions

- Worked directly with university partner in developing and testing high-temperature membranes.
- Assisted DOE industry partners in MEA development for high-temperature membranes.
- Assisted university partners in membrane characterization.

- Started High-Temperature Polymer Membrane Working Group.

Future Directions

Physical Chemistry

- Substantially increase available data on transport in membranes.
- Apply computational tools more extensively.
- Experiment with elevated temperature operation/alternative hydration methods.

New Membranes

- Prepare new materials for operation above 120°C.
- Develop new means of facilitating proton transport in high-temperature MEAs.
- MEA fabrication for stiffer membranes.
- Study oxygen reduction reaction (ORR) in high-temperature conduction media.

Industrial and Other Collaborative Interactions

- Work directly with membrane supplier in developing high-temperature membranes.
- Assist DOE industry partners in MEA development for high-temperature membranes.
- Assist university partners in membrane characterization.
- Lead High-Temperature Polymer Membrane Working Group.

Introduction

The need for improved and less-expensive membranes has long been recognized as a key factor impacting the commercial introduction of polymer electrolyte membrane fuel cells (PEMFCs). More recently, it was realized that it is desirable to operate at temperatures exceeding the currently typical 80°C. Operation at higher temperature would facilitate stack and system thermal management, increase CO tolerance, and improve electrode kinetics. This is a very challenging task. We view the polymer electrolyte development effort as a long-term problem and have structured the work described below accordingly. Also, we include work that will lead to increased insight to guide the overall effort.

Although much synthetic work is under way in industrial, government, and academic laboratories, it is unclear whether the range of that work is sufficiently broad to solve the problem with high-temperature membranes. The problem requires work on all aspects of MEA components. Most efforts address the need for improved thermal stability but fail to address the requirement of maintaining conditions conducive to proton conduction in the polymeric medium. Furthermore, most proposed

solutions pay scant attention to several serious points of impact on the composite electrode behavior. At this point, we do not know which of several approaches is most promising. Thus, we will implement (1) a full-fledged effort to explore approaches involving polymer synthesis and development, as well as implementation of new “carrier” media to replace the function of water in Nafion[®], and (2) a study of proton transfer dynamics. We will also leverage our work from BES-Chemical Sciences activities related to understanding fundamentals of the proton transfer and transport processes. We will use our fairly well developed theoretical approaches to explore specific possibilities for new acid group types or for acid-base interactions that could lead to progress in proton transfer media.

We also must address the formation of MEAs from any new polymers, including any critical additives. We must develop a detailed understanding of the materials aspects of MEA formation so that we can approach the processing of MEAs. The ORR activity within MEAs containing different additives or other mechanisms of proton transfer must be understood as well.

Results

Physical Chemistry

Critical factors for the use of these membranes in virtually every application include the membrane conductivity and the electro-osmotic drag coefficient (E_D). To measure electroosmotic drag, we adopted the method discussed by Ren et al. (1997). This method essentially uses a careful mass balance in a potentiostated cell exposed to methanol. From the water collected from the cathode effluent at various current densities, we can separate the effects of reaction, diffusion, and electro-osmotic drag on water transport. At high current densities, a plot of water flux across the membrane versus current density becomes linear, as electro-osmotic drag dominates over diffusion. Although this method employs methanol in the measurement, it is not strictly a "DMFC" method.

Experimental results including conductivity and electro-osmotic drag coefficients derived from the data are shown in Table 1 for a number of experimental polymers, as well as for Nafion 117[®]. Columns 2 through 5 show data taken from tests carried out in a fuel cell configuration, while proton conductivity reported in the last column was measured on an immersed free-standing film. The selectivity (ratio of conductivity to methanol permeation rate), columns 4 and 5, reflects the trade-off between changes in conductivity and methanol permeation rate and is a measure of the effectiveness of a given membrane in the DMFC application.

The BPS series of polymers is a class of polyarylene ether sulfones with varying degrees of

sulfonation. The number following the BPS prefix specifies the degree of sulfonation. For example, BPS-40 corresponds to a polymer in which 40% of the monomer has been sulfonated. Ion Clad consists of poly(styrene sulfonic acid) side chains grafted to a TFE/perfluoropropylene copolymer and was obtained from Pall Corporation (id R-4010). Ion Clad's IEC is 1.5 meq/g.

These membranes initially showed good performance and a low electro-osmotic drag coefficient (1.1). However, over the course of five days of testing, the experimentally determined electro-osmotic drag coefficient had gradually increased to 2.5, possibly because of degradation of the polystyrene portion of the polymer.

The following important observations can be made by reviewing Table 1:

- High conductivities can be obtained, even with aromatic sulfonate membranes under conditions of high degrees of sulfonation.
- Significantly lower electro-osmotic drag coefficients are observed for most of the aromatic sulfonates.
- The conductivity derived from measurements taken in the fuel cell configuration is lower than that obtained from free-standing films.
- Methanol permeation is much lower for the aromatic sulfonates.
- The lower methanol permeation rate does not always translate to a lower selectivity.
- The conductivity and drag coefficient of the BPS polymers increases with increasing level of sulfonation while the selectivity decreases.

Table 1. Membrane properties.

Membrane	MeOH Perm (60°C) $\times 10^6$ (cm ² /s)	Conductivity mS/cm	Selectivity 10^{-6} mS s/cm ³	Relative Selectivity	Electro- Osmotic Drag Coefficient E_D	Proton Conductivity (mS/cm)
Nafion 117 [®]	2.83	84.67	29.96	1.00	~3.6	110
BPS-40	0.61	38.48	62.65	2.09	~1.5	80
BPS-45	0.83	28.22	33.85	1.13	~1.9	
BPS-50	0.88	40.22	45.95	1.53	~2.5	100
BPS-60	2.23	52.29	23.49	0.78	~3.0	170
Ion Clad	0.58	25.93	44.67	1.49	1.1–2.5	

The one anomaly is that the conductivity of the BPS-45 membrane does not lie between BPS-40 and BPS-50 because the test membrane is much thinner than the other membranes. Therefore, when the interfacial resistances associated with the MEA are normalized for membrane thickness, the BPS-45 membrane has a conductivity much lower than what would have been observed had a thicker membrane been used.

To rationalize the data, we must consider several factors. These include the polymer water content, acid group type, and polymer microstructure. The water content of the BPS-40 and BPS-60 polymers is similar and, on a per-sulfonate basis, is lower than that of Nafion[®]. The higher conductivity is probably most sensibly rationalized as being due to the high ion-exchange capacity of the BPS polymers. The effect of polymer microstructure is presently unclear, and efforts to address this aspect are ongoing.

We focus here on the influence of acid group structure on these effects. A key determinant of electroosmotic fluxes is the tightness of water binding to sulfonate moieties. In Figure 1, we compare the computed Density Functional Theory (DFT) structure of water complexes with sulfonic acids attached via perfluorinated and aromatic moieties. Clearly, the less-acidic toluene sulfonic acid has a more tightly packed water solvation

sphere. This is a consequence of the less-delocalized negative charge on the anionic conjugate base. The higher charge density on the sulfonate more strongly interacts with neighboring water molecules, creating the observed structure.

Because the electro-osmotic drag coefficient is related to the ease of “tugging” a water molecule along with the moving proton, the formation of the tighter solvation shell clearly will resist displacement. Note that this is an overly simplistic discussion of the phenomena underpinning electro-osmosis. It is highly likely that structural factors, notably pore structure, will play a key role in determining the actual drag coefficient.

Similar calculations can be used to provide substantial insight into the conduction and water transport properties of polymers with different acid groups. For example, we found that the bis (trifluoromethanesulfonyl) imide acid undergoes acid dissociation at roughly the same water content as most other acid groups. However, in this case, the transition of the hydronium ion thus formed to an outer sphere position occurs upon dissociation, with three water molecules present. All sulfonic acids studied to date required six waters to bring about this transition. This phenomenon accounts for the higher conductivity at low water content observed for imide-based polymers by the Clemson group.

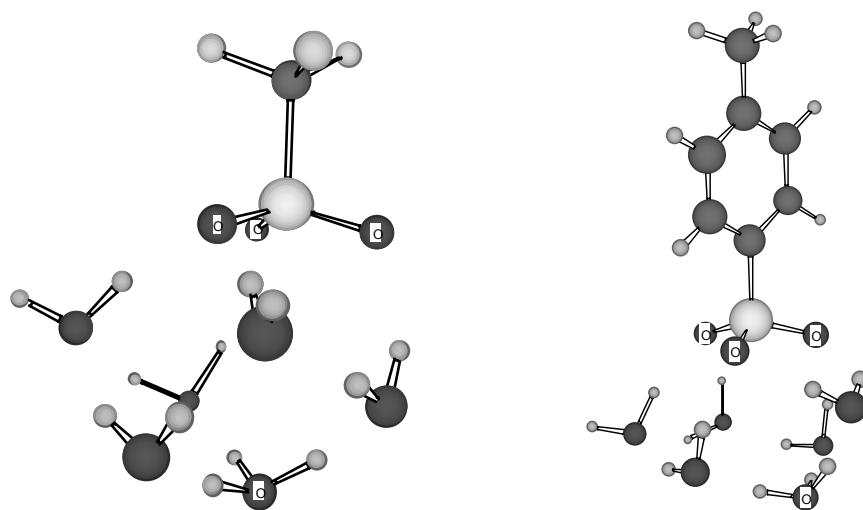


Figure 1. Computed structures of model acid hydrates, indicating tightness of binding of water of solvation to anion. Left: Trifluoromethane sulfonic acid hexahydrate; Right: p-toluene sulfonic acid hexahydrate; Hydronium oxygen to sulfonate oxygen distances: left: 0.4235 nm; right: 0.3914 nm.

New Membranes

A series of poly-sulfonated sulfones was synthesized for use as proton exchange membranes (PEMs) in fuel cells by the McGrath group at Virginia Polytechnic Institute and State University. These materials are designated BPS-XX. These copolymers are unique because they were synthesized by direct polymerization of sulfonated monomers, unlike previous efforts in which the homopolymers were post-sulfonated. This approach allows control of the exact location of the ion-conductive sulfonic acid moiety on the aryl rings. The polymers are formed by a step-growth mechanism, which requires very pure reactants. The sulfonic acid sites are meta to the sulfone in the final product. In contrast, in the post-sulfonated analog, sulfonation occurs on the activated ether rings along the polymer backbone rather arbitrarily. One distinct advantage of pre-sulfonation is that the sulfonic acid sites are on the deactivated positions in the ring once the polymer is formed. Placing the sulfonic acid on these sites may afford a more stable acid group. The sulfonic acid moiety in these polymers is unchanged after aging 30 min in air at 220°C. When well hydrated, these materials have conductivity approaching that of Nafion (see below).

We are developing additional new membranes, as well as membranes with different proton carrier materials.

Membrane-Electrode Assemblies

Because of the physical properties of new polymer electrolyte membranes, it is typically a difficult challenge to make MEAs that exhibit satisfactory performance. We have successfully catalyzed the Virginia Polytechnic Institute and State University membranes, but the performance still lags our expectations. We expect to apply approaches developed for the Virginia Polytechnic Institute and State University polymers and other high-temperature polymers (obtained from industry) methods to new polymers.

Industrial and Other Collaborative Interactions

We have developed a series of collaborative efforts with industry, other national laboratories, and universities to achieve the targets for high-temperature polymer membranes. To facilitate this effort, we started the High-Temperature Polymer Membrane Working Group, which has met twice to date. Biannual meetings are planned to assess progress.

To facilitate the development of new materials, we have also initiated a series of projects on high-temperature membranes at universities. Participants include Virginia Polytechnic Institute and State University, the University of Connecticut, Penn State, Case Western Reserve University, and the University of Wisconsin. Each participant has a different approach to the problem, ranging from new polymers to inorganic membranes. These universities typically supply materials to Los Alamos National Laboratory for testing.

Conclusions

The development of new polymer electrolytes for operation at elevated temperature is under way. However, this is a long-term project. Replacement of water is the most difficult problem, but adequate stability and cathode activity are not trivial objectives to achieve. We have started to address this problem this year. Fundamental work, including computational and experimental studies of new acid-functionalized materials, can be useful. The first polymers geared for temperatures in excess of 100°C are emerging, and testing is showing that, although promising, there are definite shortcomings. Work continues to make viable new materials.

Reference

- X.M. Ren, W. Hendersom, and S. Gottesfeld, 1997. *J. Electrochem Soc.* 144, L267.

G. Metallized Bacterial Cellulose Membranes in Fuel Cells

Hugh O'Neill, Barbara R. Evans, and Jonathan Woodward (primary contact)

Chemical Technology Division

Oak Ridge National Laboratory

P.O. Box 2008

Oak Ridge, TN 37831-6194

(865) 574-6826, fax: (865) 574-1275, e-mail: oop@ornl.gov

DOE Program Manager: JoAnn Milliken

(202) 586-2480, fax: (202) 586-9811, e-mail: JoAnn.Milliken@ee.doe.gov

ORNL Technical Advisor: David Stinton

(865) 574-4556, fax: (865) 574-6918, e-mail: stintondp@ornl.gov

Objectives

- Develop an inexpensive, renewable, thermally stable cellulosic biomaterial for polymer electrolyte membrane fuel cells (PEMFCs).
- Construct and demonstrate the high-temperature operation of a membrane electrode assembly (MEA).
- Characterize the properties of the MEA and determine power densities.
- Optimize the power density of the MEA by *in-vitro* and *in-vivo* membrane modification methods.

OAAT R&D Plan: Task 13; Barriers A, B

Approach

- Development of an in-house facility for bacterial cellulose generation.
- Deposition of metals suitable as catalysts in cellulose matrix.
- Synthesis of ion-conducting membrane by:
 - a) Infusion of electrolytes into the structure followed by dehydration,
 - b) Chemical modification of the hydroxyl ($-OH$) groups on the fibrils with sulfonate ($-SO_3^{2-}$) groups to enhance H^+ conductivity, and
 - c) Modification of the membrane during synthesis with chemically altered glucose precursors.
- Characterization of the native and modified cellulose matrix properties with emphasis on reduced catalyst loading, increased thermal stability, and enhanced ion-conducting properties.
- Testing of the MEA to demonstrate low-hydrogen-gas (H_2) crossover, high-carbon-monoxide (CO) tolerance, high power density, and low cost.

Accomplishments

- Made initial discovery: the spontaneous deposition of palladium in commercially available bacterial cellulose.
- Demonstrated that in-house facility for cellulose production by *Gluconacetobacter hansenii* is operational.
- Demonstrated the deposition of palladium, gold, and silver by *G. hansenii* cellulose.
- Determined thermal stability and H_2 crossover characteristics of native cellulose.
- Modified membrane with sulfonic acid groups.

Future Directions

- Determine the acid stability of the membranes under fuel cell operating conditions.
- Generate proton-conductive membranes with high-temperature stability.
- Develop current collectors.
- Test MEA in collaboration with fuel cell developer.
- Incorporate MEA into fuel cell stack in collaboration with fuel cell developer.

Introduction

In current PEMFC technology, perfluorosulfonic acid-based membranes (e.g., Nafion[®]) have long been the standard. The most notable drawbacks of this type of membrane are their limited stability at temperatures greater than 100°C, dependence on H₂O for conduction, and relatively high cost. Operating temperatures greater than 120°C are considered necessary for catalytic efficiency and protection of the catalyst against carbon monoxide poisoning.

The present concept proposes a cellulose matrix secreted by bacteria as a suitable material for PEMFC technology development (Figure 1a, 1b). Each component of the membrane electrode assembly (MEA) (catalyst and electrolyte membrane) is constructed by using bacterial cellulose, underlining the multifunctional nature of this material. In addition, the novel fabrication and processing methods of the components highlight the innovative approach to MEA assembly proposed by

this concept. The main impact, at the system level, of a cellulose-based PEM fuel cell is that it will operate at temperatures $\geq 130^\circ\text{C}$, circumventing the problems associated with Nafion[®]-based PEMFCs.

The initial discovery that led to the idea that this material may be useful for PEMFCs was the observation that bacterial cellulose samples incubated in a solution of ammonium hexachloropalladate turned black as a result of the deposition of palladium (Pd) in the cellulose under ambient conditions (Figure 2a). The precipitated metal formed a homogeneous matrix of finely divided metal particles dispersed evenly throughout the pellicule. When dehydrated, the metallic bacterial cellulose dried to a thin membrane (Figure 2b) and, in the presence of a suitable electron donor, catalyzed the evolution of H₂ in aqueous solution. These observations indicated that this material would act as a catalyst for the anodic oxidation of H₂ and corresponding cathodic reduction of O₂ in an MEA.

A hybrid material acting as the current collector and catalyst layer will be synthesized by the



a. Growth of bacterial cellulose in glucose-rich medium at 25°C.



b. Processed bacterial cellulose after treatment with 1% NaOH and Na-acetate (pH 4.5).

Figure 1. Cultivation and processing of bacterial cellulose.



a. Hydrated bacterial cellulose after incubation in ammonium hexachloropalladate.



b. Dried palladated bacterial cellulose.

Figure 2. Treatment of bacterial cellulose with ammonium hexachloropalladate.

incorporation of electrically conductive material, such as carbon felt or paper, into the cellulose during bacterial growth, followed by deposition of the metal within the resulting matrix. A proton-conductive membrane will be generated by chemical modification of the cellulose to introduce the appropriate reactive groups. The MEA components will be assembled by using a simple cold-pressing procedure, resulting in high interfacial contact and compatibility between the layers.

Approach

An in-house facility for bacterial cellulose generation has been established. The properties of the bacterial cellulose are identical to those of the commercial product used in the initial experiments. The initial research goals are focused on development of the electrolyte layer of the PEMFC.

Three different approaches for the fabrication of an ion-conducting membrane are under investigation:

- (1) Over two hundred years of chemical modification of cellulose has led to products ranging from textiles to thermoplastics. Similar techniques will be exploited to synthesize a cellulose-based membrane with a proton-conducting ability that rivals that of Nafion[®] but operates at higher temperatures (130°C).
- (2) In its hydrated native state, bacterial cellulose holds over 100 times its own weight in H₂O. An electrolyte membrane will be made by dehydration of the material after infusion of electrolytes into the structure. Potential reagents

that will be tested are solid acids, such as CsHSO₄.

- (3) Modification of the membrane *in-vivo* by introduction of chemically reactive groups (SO₃²⁻) into the cellulose structure by addition of glucose analogs to the medium during cultivation will be demonstrated.

Development of the catalyst layer is also under way. The mechanism of palladium deposition is being investigated. This research will give insight into methods to deposit other metals, such as platinum. Future research will focus on the development of current collectors and assembly and testing of the MEA.

Results

As a proof-of-principle experiment, an MEA was constructed by sequentially drying a layer of bacterial cellulose that was infused with 1 M potassium chloride between two layers of palladated bacterial cellulose (Figure 3). Platinum (Pt) wires were used as current collectors. Suitable controls were carried out to demonstrate that the Pt wires were not responsible for the anodic oxidation of H₂. An output of 84.3 μW/cm² (192 μA and 0.48 V) was demonstrated by using H₂ generated from a simple acid-displacement reaction. These results are preliminary and serve only to prove the hypothesis that an MEA made with bacterial cellulose exhibits fuel cell behavior (Figure 4). The experiment was carried out at room temperature and ambient

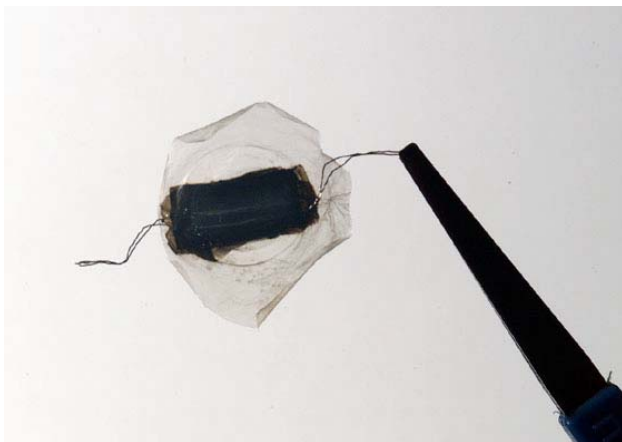


Figure 3. Membrane electrode assembly.

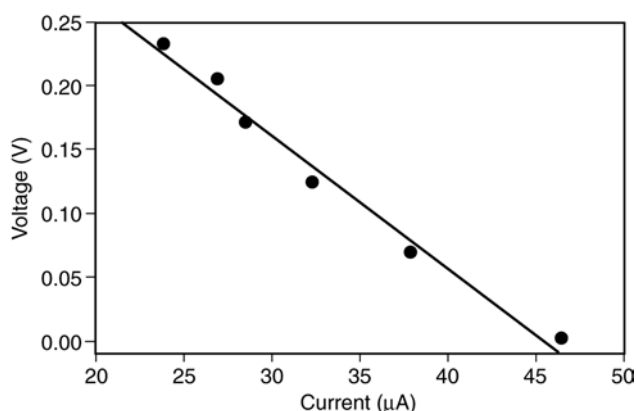


Figure 4. Voltage versus current curve for cellulose-based MEA. The resistance was increased in 2-k Ω increments from 1 to 11 k Ω . The experiment was carried out at 26°C and 1 atm by using a 4% H₂ stream at 40 mL/min.

pressure. Optimization of the reaction in terms of temperature, pressure, and humidity would certainly increase the performance.

Bacterial cellulose has the desired physical and chemical properties for PEMFC technology. The hydrated bacterial cellulose dries to a thin membrane 34 μm in thickness, as measured by scanning electron microscopy. The dried membrane does not rehydrate; no swelling of the dried membrane was evident after boiling for 30 min in H₂O. The thermal properties of the dried material were compared with those of Nafion 117[®]. Thermogravimetric analysis profiles of the bacterial cellulose and Nafion 117[®] are shown in Figure 5. The profile for dry bacterial cellulose indicated that it loses H₂O up to approximately 100°C, above which there is no weight loss to 130°C. In the dry state, decomposition

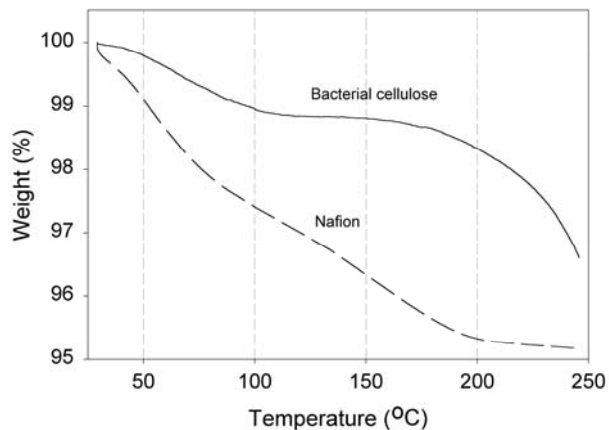


Figure 5. Comparison of the thermogravimetric analysis profiles of bacterial cellulose and Nafion 117[®] (solid line, cellulose; dashed line, Nafion[®]).

occurs above this temperature. However, under humid conditions, it is likely that the thermal stability would be increased. In contrast, the profile for dry Nafion 117[®] showed that it continually loses weight over the temperature range measured. This demonstrates the favorable temperature stability characteristics of bacterial cellulose compared to Nafion 117[®]. In addition, the H₂ crossover characteristics of bacterial cellulose and Nafion 117[®] indicate that bacterial cellulose is approximately 40% less permeable to H₂ than Nafion 117[®] (Figure 6). It is mechanically stable to tearing and can be folded repeatedly without damage.

Preliminary data have been obtained for the chemical modification of bacterial cellulose with sulfonate groups. The ion-exchange capacity of the membrane is approximately 1.1–1.2 mequiv/g cellulose. However, the structural integrity of the membrane was adversely affected. Further studies are under way to investigate this observation.

Conclusions

Although the project has only recently obtained funding and the results are preliminary, bacterial cellulose does offer favorable characteristics for PEMFC technology. The operation of a bacterial cellulose-based MEA was demonstrated, albeit at low efficiency. Efforts are directed to increase efficiency by developing electrolyte layer, catalyst layer, and current collectors. In the context of the

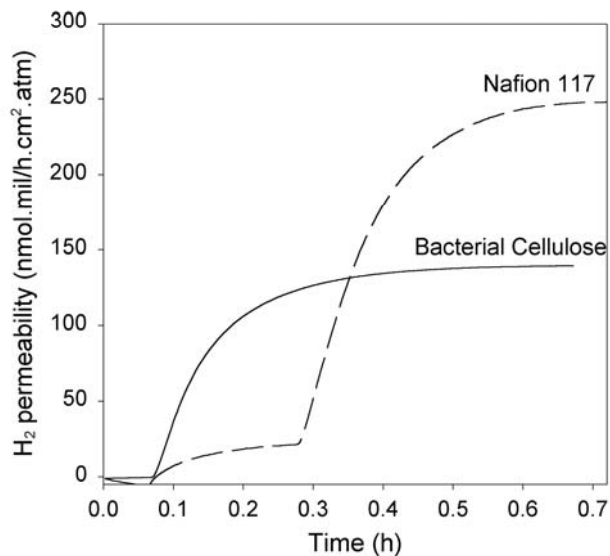


Figure 6. Comparison of the crossover characteristics of bacterial cellulose and Nafion 117[®] (solid line, cellulose; dashed line, Nafion[®]). The experiment was carried out in 4% H₂/96% Ar at 46 psi and 25°C.

program, the synthesis of a bacterial cellulose membrane with ion-conducting ability is the most important goal for the overall success of the project. low efficiency.

Publication/Presentation

1. Hugh O'Neill, Barbara R. Evans, and Jonathan Woodward, "Metallized Bacterial Cellulose Membranes in Fuel Cells," presented at 2001 National Laboratory R&D Meeting DOE Fuel Cells for Transportation Program, Oak Ridge, TN.

Invention Disclosure

Barbara R. Evans, Hugh O'Neill, Valerie P. Malyvanh, and Jonathan Woodward, 2001, "Metallization of Bacterial Cellulose for Electrical and Electronic Device Manufacture," ID 0869, S-96, 631.

H. Carbon Foam for Fuel Cell Humidification

J.W. Klett (primary contact), April McMillan, Lynn Klett, and Nidia Gallego

Carbon and Insulation Materials Technology Group

Oak Ridge National Laboratory

P.O. Box 2008, MS 6087, Bldg. 4508

Oak Ridge, TN 37831-6087

(865) 574-5220, fax: (865) 576-8424, e-mail: klettjw@ornl.gov

DOE Program Managers: JoAnn Milliken and Patrick Davis

(202) 586-2480, fax: (202) 586-9811, e-mail: JoAnn.Milliken@ee.doe.gov

(202) 586-8061, fax: (202) 586-9811; e-mail: patrick.davis@ee.doe.gov

ORNL Technical Advisor: David Stinton

(865) 574-4556, fax: (865) 574-6918, e-mail: stintondp@ornl.gov

Contractor: Oak Ridge National Laboratory, Oak Ridge, Tennessee

Prime Contract No.: DE-AC05-96OR22464

Objective

- Determine if graphite foams can be used in humidification systems to enhance the humidification of the fuel cell inlet air.
- Demonstrate the ability to combine cooling of power electronics and fuel cell coolant with humidification of the inlet air.

OAAT R&D Plan: Task 13; Barriers B, C

Approach

- Design and construct a humidification test cell to use different foam structures to effect evaporation of water.
- Perform tests to characterize the humidification potential of the foam and develop optimized designs that minimize pumping power yet maximize humidification.

Accomplishments

- Demonstrated that foam could successfully humidify dry inlet air to 87% saturation at 60°C by using a simulated power electronic device.

Future Directions

- Collaborate with fuel cell manufacturer and an original equipment manufacturer (OEM) to commercialize the technology.
 - Determine whether the heat exchange process for humidification can be used to capture wastewater from the fuel cell exhaust.
 - Develop a full-scale prototype humidifier for fuel cell applications.
-

Introduction

The efficiency of the automotive polymer electrolyte membrane (PEM) fuel cell depends on many factors, one of which is the humidification of the inlet air. If the inlet air is not sufficiently humid (saturated), then the stack can develop dry spots in the membrane, and efficiency and voltage will drop. Therefore, it is necessary to ensure that humid inlet air at the proper elevated temperature is supplied to the stack. Current methods involve using a spray nozzle to atomize water droplets onto a cloth or wire mesh substrate. As the inlet air passes over the cloth, it gains moisture and becomes more humid; however, since the air is not preheated, the actual level of humidification (percent humidity) drops as the air is heated in the fuel cell. If heat could be supplied to the water efficiently, the system would become independent of the ambient conditions, the inlet air could become more humid at the proper temperatures, and the overall stack could maintain a high level of efficiency. Graphite foam has been demonstrated to be very efficient in heat transfer in previous work with power electronic heat sinks and automotive radiators. Using the carbon foam in the PEM fuel cell may solve the inlet air humidification problems. This unique graphite foam (Figure 1) has a density between 0.2 and 0.6 g/cm³ and a bulk thermal conductivity between 40 and 187 W/m•K. The ligaments of the foam exhibit a thermal

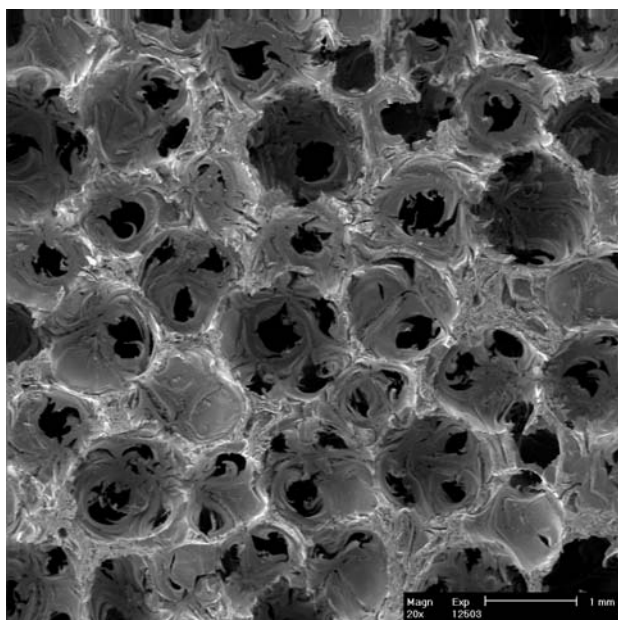


Figure 1. Oak Ridge National Laboratory's (ORNL's) graphite foam.

conductivity higher than that of artificial diamond. Additionally, in combination with a very accessible surface area ($> 4 \text{ m}^2/\text{g}$), the overall heat transfer coefficients of foam-based heat exchangers can be up to two orders of magnitude greater than those of conventional heat exchangers (in some designs).

The high thermal conductivity, combined with a very high specific surface area ($>4 \text{ m}^2/\text{g}$), permits the graphite foam to use waste heat from power electronics, cooling fluids, and exhaust gases to vaporize water on the pore surfaces more efficiently than in previous work, thus enhancing humidification. The high conductivity of the foam will also permit heating of the inlet air, thereby supplying hot, humid inlet air to the fuel cell stack, regardless of the ambient conditions. As a further benefit, the evaporative cooling effect (humidification) in this chamber can be used as a cooling mechanism for power electronics or other heat sources.

Approach

To characterize the behavior of the foam as a humidifier, a test chamber (Figure 2) was modified to quantify its ability to saturate air with water. As shown in Figure 2, the foam is mounted to an aluminum plate (usually by brazing) and placed in a cavity where the cooling fluid flows. The system is designed with no gap around the foam, thereby forcing the fluid to pass through the pores of the foam. The system is sealed with o-rings, and pressure taps are inserted into the chamber to measure the pressure drop of the system. A tube was inserted into the chamber to supply water directly to the foam, so it saturates the foam completely. As the air is forced through the foam, it forces the water over the surfaces of the foam, leading to efficient

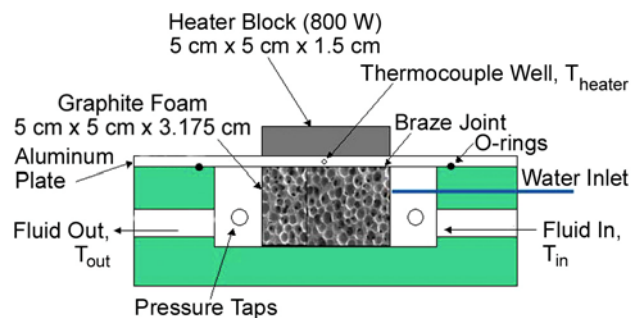


Figure 2. Schematic of the humidification chamber.

evaporation. The heat from the heaters is transferred to the foam ligaments and then to the water on the surfaces of the foam. As the water evaporates, it removes significant amounts of heat while simultaneously saturating the air. A simulated power inverter (cartridge heaters in a 5-cm × 5-cm × 2-cm aluminum block) is mounted to the aluminum plate and is capable of generating up to 800 W (32 W/cm²).

The simulation was performed by first characterizing the foam block with just dry air at 20°C and 10% relative humidity with various power densities. Next, water was added to the carbon foam at flow rates of 10 cm³/min and 20 cm³/min. The outlet air temperature was monitored, and by performing a mass balance on the water, the relative humidity was then calculated. Also, the pressure drop through the system was monitored. The results of these tests are presented in Figure 3 and Table 1.

As seen in Table 1, the graphite foam reduced the electronic temperatures with dry air alone. However, when the water was added to the foam for evaporation, the electronic temperature dropped. Because the latent heat of vaporization of water is several orders of magnitude greater than the sensible heat capacity of water and air, only small amounts of water are needed to effect a large absorption in energy. As seen in Table 1, the relative humidity of the outlet air (inlet to the fuel cell) can be modified easily by changing the amount of water added to the foam. Saturated inlet air should be relatively easy to achieve at temperatures of 60°C by changing the volume of water added to the system and the power density of the electronics. However, the problem will be to balance the heat rejection from the power electronics or the coolant with the volume of inlet air and water needed to humidify the inlet air.

To scale this up to a full-scale automotive fuel cell, over 500 pounds per hour of saturated inlet air

will be required at temperatures of approximately 60–80°C. Actual requirements will change with OEM and are proprietary. Values used are for illustration only. Assuming the ambient air is 25°C with 10% relative humidity, the enthalpy of the ambient air is roughly 30 kJ/kg of dry air. At a fuel cell inlet condition of 60°C and saturated (100% relative humidity), the enthalpy is 461 kJ/kg of dry air. Therefore, to saturate the ambient air, over 430 kJ/kg of dry air must be supplied to heat the air, along with 152 g of water per kilogram of dry air. This corresponds to roughly 3.75 kg of dry air/min, or 4.5 m³/min (160 standard cubic feet per minute) of ambient air and nearly 27 kW of power. As the expected power dissipation of the power electronics will be approximately 30 kW of power, this would be sufficient to perform the proper humidification of the inlet air by using the graphite foam. However, the largest problem will be the supply of water for the humidification — roughly 566 g/min of water (1.24 lb/min, or 0.15 gal/min, or 9 gal/h). Because a typical current vehicle can travel four hours on a tank of gas, it would use 36 gal of water between fuel refills. While this amount is achievable, it is not practical.

Conclusions

Graphite foam is an excellent base for humidification of fuel cell inlet air. While it has been demonstrated to be able to humidify inlet air to near-saturation levels, several problems exist. First, the volume of water needed is enormous, and it is anticipated that the water will have to be captured in the exit stream of the fuel cell. Therefore, it may be more efficient to use the hot exit gases from the fuel cell to provide the heat rather than the power electronics. By cooling the exit stream while humidifying the inlet air, the dew point of the exit gas can easily be reached and water will condense, thereby allowing the water to be recycled.

Table 1. Results of humidification tests at a power density of 19 W/cm².

Water Flow Rate (cm ³ /min)	Air Flow Rate (kg/min)	$\frac{g_{water}}{kg \text{ dry air}}$ (g/kg)	Electronic Temperature (°C)	Outlet Air Temperature (°C)	RH% outlet Air	RH% @60°C	RH% @80°C
0	0.17	1.44	162	103	<0.5	1.17	0.5
10	0.17	58.6	151	73	24	43.5	18.3
20	0.17	115.7	136	58	87	79	33

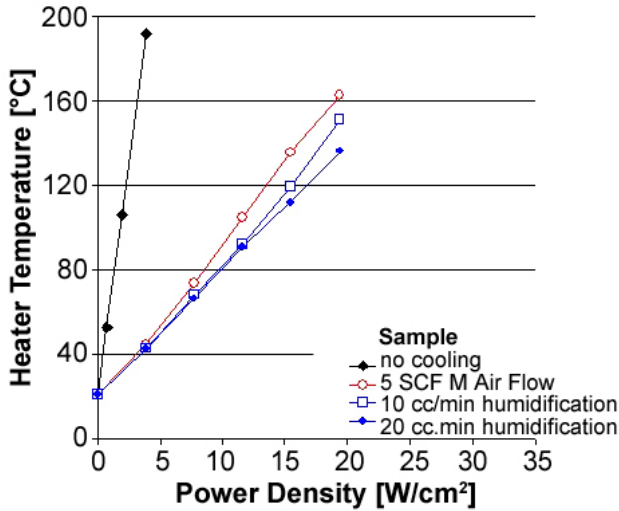


Figure 3. Heater temperatures as a function of power density for various water flow rates for humidification.

Second, while the fuel cell inlet air will be required to operate at several atmospheres above ambient for proper fuel cell application, this pressure will be sufficient to force the air through the foam. Although the pressure drop of the foam is significant, it is believed that, by design optimization, humidification of the air can be achieved while maintaining low pressure drop through the foam (i.e., pin-fin arrangements, blind holes, and corrugation). Future work will explore these options and determine the best methods of using the foam for humidification while maintaining the lowest pressure drop.

Other future work of this program will be to collaborate with an OEM and a fuel cell manufacturer to develop a prototype humidifier and test it in a real system. Because the water balance on the system will be the most difficult task to overcome, several different designs will be desired to optimally achieve the humidification while recovering excess water from the fuel cell.

I. Electrodes for PEM Operation on Reformate/Air

Thomas A. Zawodzinski (primary contact), Francisco Uribe, Wayne Smith, Tom Springer, Judith Valerio, David Vernon, Tommy Rockward, Don McMurry, Guido Bender, Mike Hickner*, Eric Brosha, Bruce Orler, and Chris Adams

Electronic and Electrochemical Materials and Device Research Group

Los Alamos National Laboratory

Los Alamos, NM 87545

(505) 667-0925, fax: (505) 665-4292, e-mail: zawod@lanl.gov

* Virginia Polytechnic Institute and State University (Virginia Tech)

DOE Program Manager: JoAnn Milliken

(202) 586-2480, fax: (202) 586-9811, e-mail: JoAnn.Milliken@ee.doe.gov

Objective

To achieve maximum performance in polymer electrolyte membrane fuel cells (PEMFCs) under conditions appropriate for reformate/air operation and with methods that allow cost and efficiency targets to be met for transportation.

OAAT R&D Plan: Task 13; Barrier A

Approach

- Simultaneously achieve the following cell characteristics:
 - Highest possible performance at 0.8 V,
 - Minimum air injection for CO cleanup,
 - Minimum catalyst loading, and
 - Minimum losses due to dilution at high fuel utilization.

These cell characteristics will be accomplished through applied R&D to (1) develop an understanding of electrocatalysis and transport issues related to cathode performance and (2) use this understanding to guide the development, testing, and demonstration of improved electrodes.

Accomplishments

Cathode Performance: Cell performance at 0.8 V and 0.85 V was studied. Performance improvements, relative to that obtained at steady state in cells using Pt, were obtained with different alloy catalysts and by using low-duty-cycle pulsing of the cell voltage to lower voltages.

- Demonstrated stable operation of cell, yielding 0.1 A/cm² at ~0.85 V (on H₂), by using 0.4 mg Pt on the cathode and 0.4 A/cm² at 0.8 V (on reformate).
- Initiated studies of electrode structure-property relationships.
- Continued studies of a series of alloy catalysts.

Impurity Tolerance: Reduction in precious metal loading (to 0.1 mg/cm²) confirmed.

- Reconfigured matrix electrode assembly tolerates 100 ppm CO in reformate with only 0.1 mg/cm² of catalyst (with air bleed).
- Extensive studies of other impurities reveals extremely high sensitivity to hydrogen sulfide poisoning.

Future Directions

Cathode Work: Overall goal is to increase achievable current density at ~0.8 V.

- Improve cathode catalysts.
- Vary catalyst layer and backing compositions to improve hydration.
- Perform extensive studies of materials properties of cathodes.
- Develop catalyst layer with controlled nanostructures.

Anode Work: Overall goal is to minimize effects of dilution and CO.

- Improve anode catalysts, reconfigure anodes, and improve effectiveness of air injection for ever-higher CO tolerance.
- Improve catalyst layer composition to further minimize dilution effects and increase fuel utilization.

Practical Studies of Critical Impact

- Address matrix electrode assembly durability issues: accelerated life test protocols, “brute force” testing, and materials evolution modeling.
- Probe break-in effects by using segmented cell.
- Develop new matrix electrode assembly fabrication approaches.

Diagnostics

- Complete segmented cell development, make design/specs available to companies, and implement additional probes for local temperature (among other tasks).
- Increase attention to diagnosing long-term performance limitations.

Industrial Interactions

- Carry out extensive, direct interaction with industrial partners to implement best strategies in stacks.
- Continue matrix electrode assembly development with outside parties.
- Implement Web site to allow rapid updating of DOE partners on current work; receive “instant feedback.”

Introduction

The requirements for overall polymer electrolyte membrane fuel cell (PEMFC) performance include operation under conditions of maximum fuel utilization efficiency, as well as the best possible performance using gasoline-derived reformate. These requirements are tightly coupled because the former entails higher cell voltages (and thus some focus on the PEMFC cathode), while higher cell voltages also may provide some “relief” in the context of the stringency of the CO tolerance requirements. As the targets for CO tolerance have been met or exceeded, the focus of this project has shifted to increased emphasis on achieving improved cathode performance at higher cell voltage while meeting difficult cost targets. Thus, decreased Pt loading is essential. This is primarily a problem related to cathode performance. We seek to address these needs by (1) developing an understanding of

electrocatalysis and transport issues related to cathode performance and (2) using this understanding to guide the development, testing, and demonstration of improved electrodes.

A few issues still need to be investigated in terms of anodes. We are testing the single cells under steady-state and transient exposure to various levels of CO, especially focusing on conditions appropriate for off-design conditions of the fuel processor, such as during system start-up. This latter work exploits the ever-increasing levels of CO tolerance we are able to achieve.

Approach

The first goal is to achieve 100 h of stable cell operation with neat H₂ at 0.85 V, 0.1 A/cm² at 80°C, and 30-psig cathode/anode pressure with a modified cathode. Catalyst loading will be between 0.2 and

0.4 mg/cm². Figure 1 shows that the voltage achieved is 0.84 V.

The second goal is to achieve 100 h of stable cell operation with neat H₂ at 0.8 V, 0.4 A/cm² at 80°C, and 30 psig cathode/anode pressure with a modified cathode. Catalyst loading will be <0.3 mg/cm². Tests are in progress.

Results

Cathode Performance

To meet efficiency requirements for operation on reformed gasoline, cathode performance must be improved at high cell voltages. Operation at high cell voltages necessarily implies operating with little water production at the cathode. We previously showed that dry conditions lead to poorer oxygen reduction reaction (ORR) kinetics and that there is a decline in steady-state current with time after changing cell voltage from 0.6 V to 0.8 V. We tried to overcome this problem by “pulsing” the cell to lower voltages. The results of such an operation mode, with a 1% duty cycle at the lower cell voltage, are also shown in Figure 1. Clearly, the application of such a pulse provided improved steady-state performance. The nature of the improvement was studied, and we found that it is more likely that oxide formation occurs, blocking sites for oxygen adsorption. Indeed, cyclic voltammograms, shown in Figure 2, indicate the formation of oxide occurs at different potentials for different alloys, accounting for their different

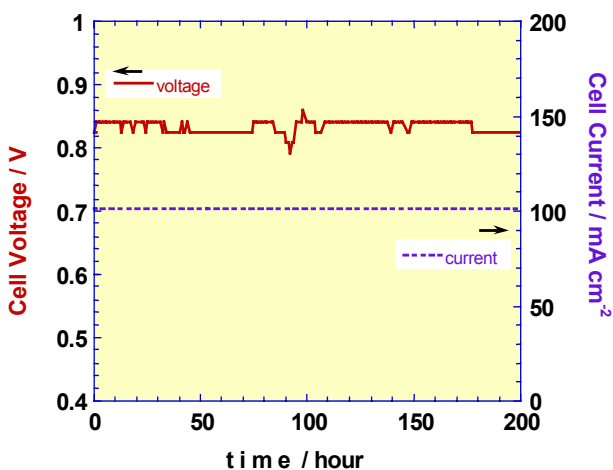


Figure 1. Cell voltage as a function of time at a constant current of 100 mA/cm², with current pulsing (H₂ fuel).

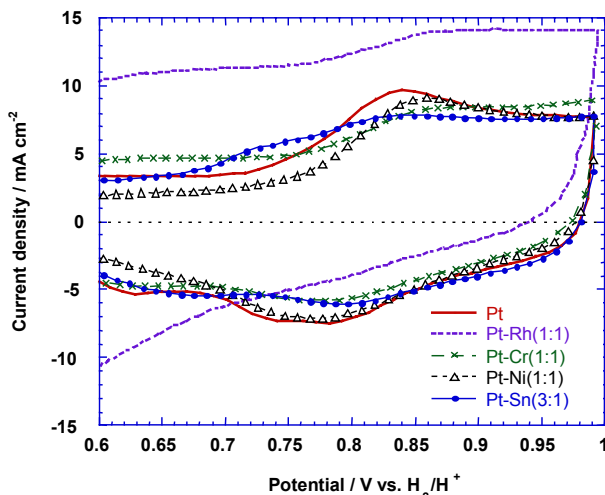


Figure 2. Cyclic voltammograms of electrodes employing various alloy catalysts. Note the shifted peak for Pt-Ni and Pt-Cr.

activity levels. We believe that the alloying elements (such as Cr or Ni) may “sacrificially” scavenge oxide from the Pt.

We have also begun investigating the performance on reformat. As expected, we achieved a sustained current density somewhat lower than the target of 0.4 A/cm² @0.8 V; we achieved, instead, roughly 0.35 A/cm² @0.8 V. This result is shown in Figure 3.

Last year, we found that, given our catalyst layer preparation method, there appears to be a limit to how much catalyst is actually accessed; our current estimate is that this is less than 40%. To achieve the

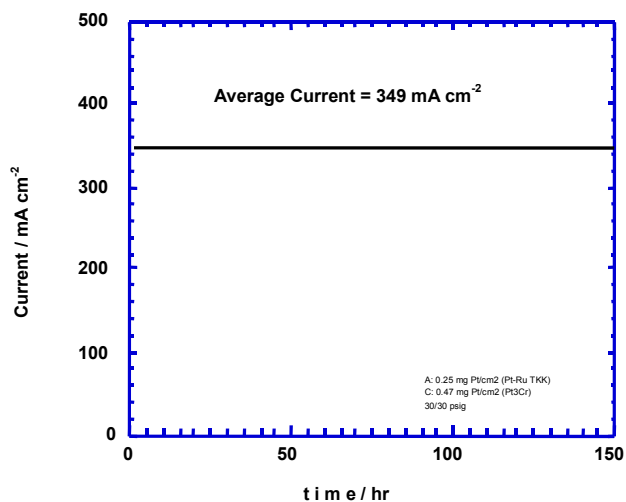


Figure 3. Cell current as a function of time at a constant voltage of 0.8 V, with current pulsing (reformat feed).

goal of higher utilization, we deemed it necessary to first understand the relationship between electrode microstructure and electrochemical activity. We are carrying out a series of studies, including modulated differential scanning calorimetry (DSC), to probe the state of ionomer in the catalyst layer, extensive microscopy to look at catalyst-polymer interactions, various atomic force microscopy (AFM) studies to assess the strength and morphology of electrodes using different additives, and other relevant studies.

Anode Performance

We have continued to progress toward the simultaneous goals of enhanced CO tolerance with minimum air injection and minimum catalyst loading. We have repeatedly demonstrated that we can simultaneously lower catalyst loading to 0.1 mg/cm^2 and achieve complete tolerance to 100 ppm CO with air bleed (Figure 4).

Segmented Cell

We also wish to highlight substantial progress in the development of a key diagnostic tool, our segmented cell. This tool is being adopted by industry. We have made radical changes to eliminate problems with electrical cross-talk between segments and to enable the accurate determination

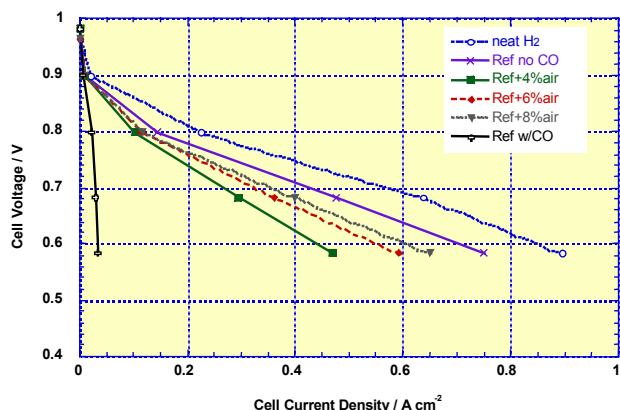


Figure 4. Recovery of cell performance with air bleed for a cell using only 0.1 mg/cm^2 anode precious metal loading.

of high-frequency resistance in each segment. To do this, we have developed a cell with a series of Hall probes of local current. This cell is now providing data of unprecedented quality. Furthermore, there are essentially no differences between a normal cell and the segmented cell in terms of construction details, and thus the performance of the cell is more typical.

A picture of one side of such a cell is shown in Figure 5. Gas flows into, for example, the top left corner, along the serpentine path and out the bottom right corner. A series of data probing the behavior of different parts of the cell is shown in Figure 6. These data indicate that segments near the cell inlets (segments 1–3) and outlets (segments 8–10) have the poorest high-frequency resistance and performance. Such data will prove invaluable in studying the durability of matrix electrode assemblies.

One additional area studied in this effort is the effect of additional impurities — other than CO — arising from the reformat feed. One impurity of some interest is H_2S , which may be formed in small quantities. We are systematically studying the impact of ever-lower amounts of this compound on cell lifetime. In Figure 7, we show the effect of as

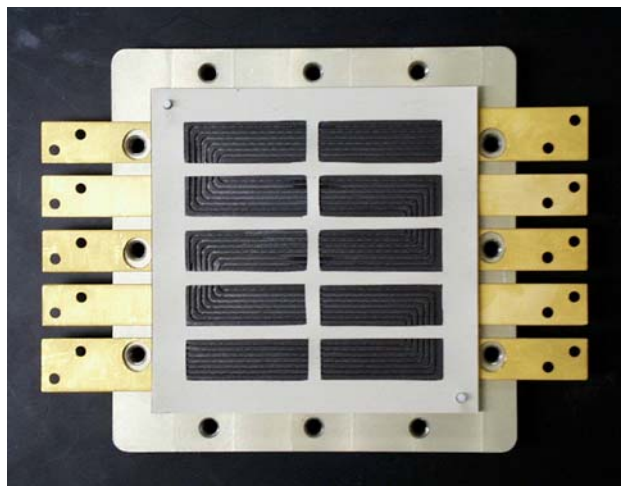


Figure 5. Segmented cell.

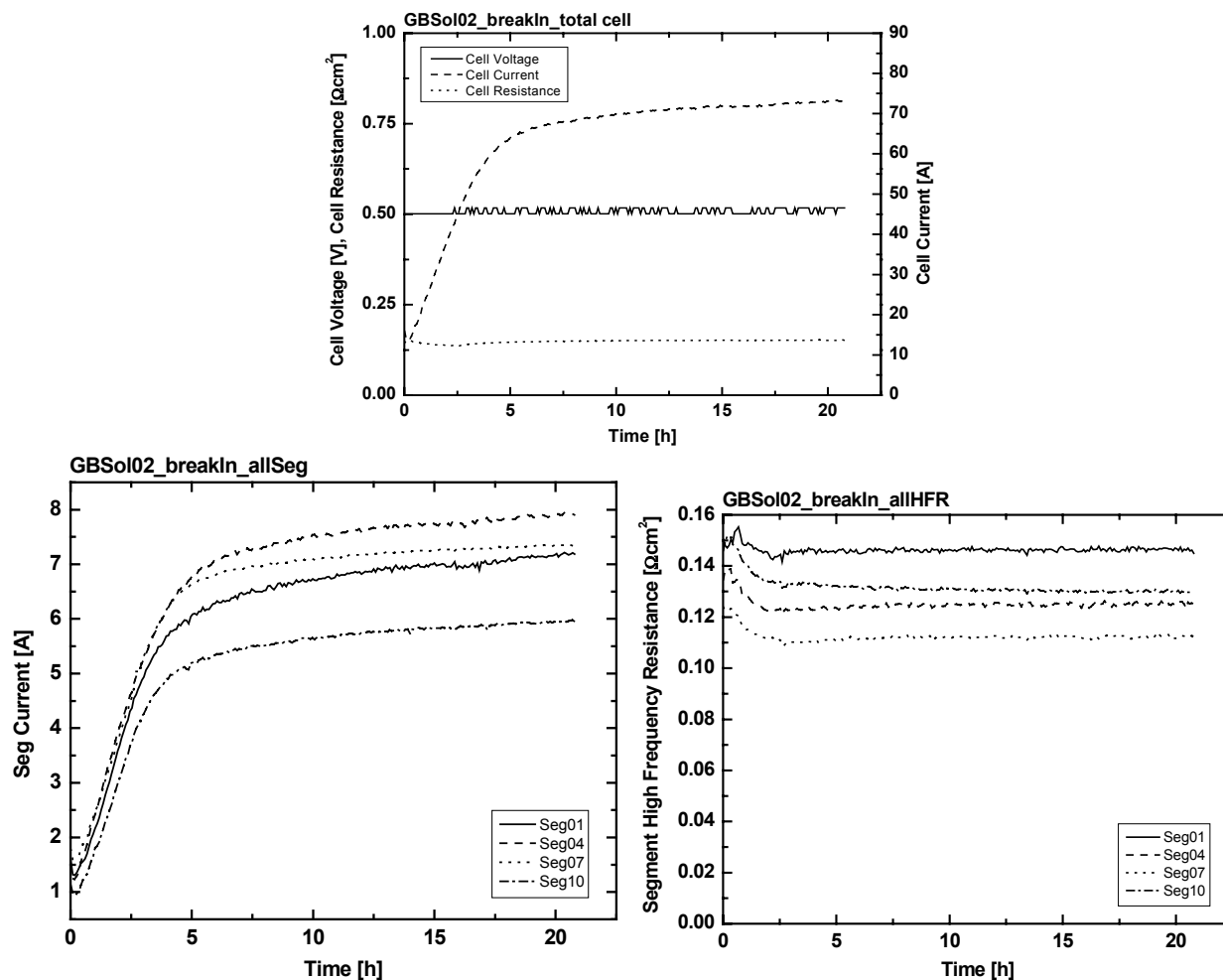


Figure 6. The time evolution of the total cell current and resistance during break in (top), the time evolution of individual segment currents (bottom, left), and the time evolution of individual segment high-frequency resistance (bottom, right).

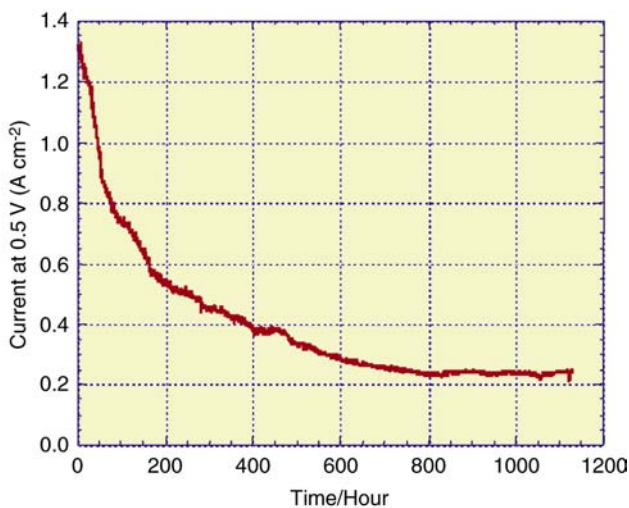


Figure 7. Effect of 200 ppb hydrogen sulfide in hydrogen on cell performance over time.

little as 200 ppb on cell performance. Clearly, there is a dramatic negative effect on performance. This highlights the need for complete removal of H₂S from the anode stream.

Conclusions

We have extensively tested both cathode and anode properties in PEMFC single cells. Highlights of that effort are listed below:

Cathode

- Approached milestones (100 mA/cm²@0.85 V on H₂, 400 mA/cm²@0.8 V on reformat),
- Began developing database of structure/property relationships,
- Began developing new materials-oriented tools for improved understanding of limiting factors

in matrix-electrode assembly performance and lifetime.

- Extensively improved segmented cell diagnostics.

Anode

- Conducted extensive work with other impurities, including H₂S and NH₃.
- Demonstrated repeatable results with as low as 0.1 mg/cm² precious metal loading, and
- Continued work under cold-start conditions.

J. New Electrocatalysts for Fuel Cells

P.N. Ross (primary contact), N.M. Marković, T.J. Schmidt, and V. Stamenković

Materials Sciences Division

Lawrence Berkeley National Laboratory

University of California

Berkeley, CA 94720

(510) 486-6226, fax (510) 486-5530, e-mail: pnross@lbl.gov

DOE Program Manager: JoAnn Milliken

(202) 586-2480, fax: (202) 586-9811, e-mail: JoAnn.Milliken@ee.doe.gov

Objective

Conduct research on the kinetics and mechanism of electrode reactions in low-temperature fuel cells. Develop new electrocatalysts by using a materials-by-design approach.

OAAT R&D Plan: Task 13; Barrier A

Approach

- Study the kinetics of fuel cell electrode reactions on well-characterized model electrodes and high-surface-area fuel cell electrocatalysts by using modern electroanalytical methods.
- Study the mechanisms of the reactions by using state-of-the-art *in-situ* spectroscopes.
- Use ultra-high vacuum (UHV) methods of surface preparation and surface analyses to form tailored surfaces. Synthesize nanoclusters to have the tailored surface.
- Characterize the microstructure of the nanoclusters by high-resolution electron microscopy.
- Transfer technology to catalysts developers/vendors.

Accomplishments

- Optimized the oxygen reduction activity/stability on Pt₃Ni and Pt₃Co bulk alloys and high-surface-area catalysts.
- Determined the effect of Pt particle size on the oxygen reduction reaction (ORR).
- Elucidated the reaction mechanism of CO₂ effects on Pt-Ru and Pt-Mo alloy surfaces.
- Elucidated the reaction mechanism of the “cleansing” of CO adsorbed on Pt and Pt-based alloy surfaces by oxygen (air) bleeding.
- Interacted with fuel cell developers to provide better understanding of oxygen-reduction kinetics.

Future Directions

Cathode side:

- Develop and optimize a new class of non-Pt model catalysts. Synthesize and test new non-Pt high-surface-area catalysts at fuel cell conditions.
- Characterize and test high-surface-area Pt-Fe catalysts.
- Create “skin” nanostructures of Pt on non-noble substrates and determine activity and stability as novel low-Pt air cathode electrocatalyst. Select the most promising substrate for synthesis as high-surface-area catalyst.

Anode side:

- Characterize structure/kinetics of Pd-based bimetallic nanoparticles.
- Determine CO-tolerance of tailored electrodes consisting of thin films (1–10 monolayers) of Pd on the close-packed single crystal surfaces of Ta, Re, and W.

Introduction

Lawrence Berkley National Laboratory's (LBNL's) activities during the past year are reported in two task areas: (1) creating, characterizing, and optimizing air cathode catalysts and (2) elucidating the reaction mechanisms of CO₂ "poisoning" and "cleansing" by air bleeding with Pt-Ru and Pt-Mo alloy catalysts.

Results**1. Optimizing PtNi and PtCo alloy air cathode electrocatalysts.**

For phosphoric acid fuel cells (PAFCs), Pt-alloy cathode catalysts (e.g., PtNi, PtCo, PtCr, PtFe) were found to improve the performance of gas diffusion air cathodes. Recent work on polymer electrolyte membrane fuel cell (PEMFC) cathode catalysts indicated similar effects, but the magnitude of these effects is still unclear. For the unambiguous determination of the intrinsic catalytic activity of PtNi and PtCo, we used the rotating ring-disk electrode (RRDE) method with model bulk alloys and the thin-film RRDE method for the carbon supported fuel cell catalysts. By using these techniques, the intrinsic catalytic activity of electrocatalysts can be assessed in the absence of mass transport resistance that occurs in membrane electrode assemblies. Hydrogen adsorption pseudocapacitance was used to titrate the number of Pt surface atoms and to estimate the surface composition of the alloy catalysts, on the basis that hydrogen is adsorbed only on Pt sites.

Figure 1 summarizes the kinetic currents for the ORR on the supported PtNi and PtCo catalysts in 0.1 M HClO₄ at 333 K. Pure Pt is also shown as a reference. These graphs clearly show that the kinetics of the ORR are dependent on the nature of the alloying component (e.g., Pt < PtNi < PtCo) and the surface composition (Pt₃Co < PtCo). A small activity enhancement (per platinum surface atom) of ca. 1.5 is observed for the 25 at% Ni and Co catalysts. A more significant increase in catalytic

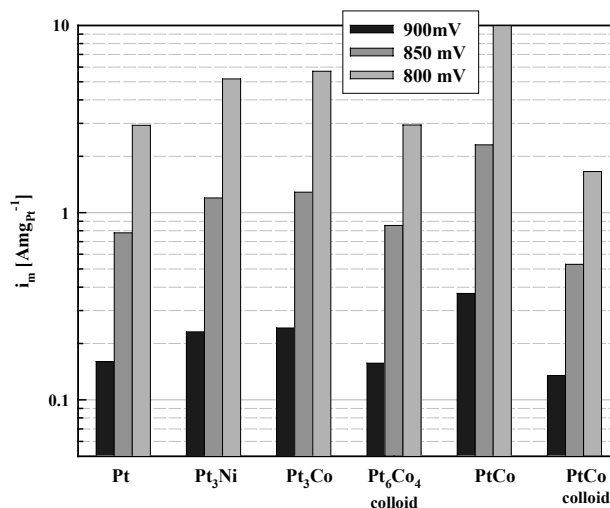


Figure 1. Summary of the activities for PtNi and PtCo catalysts at fuel cell relevant conditions.

activity, a factor of 2–3, is obtained for the 50 at% Co. The 50% Ni catalyst was less active than the Pt standard and unstable at technologically relevant potentials and at 333 K.

The graph of Figure 1 also shows that the PtCo catalysts prepared via colloidal precursors are less active than catalysts prepared by a classical proprietary method. Ring current collection measurements for production of peroxide during the ORR indicated no significant difference between the Pt and Pt-alloy catalysts. Together with the observed Tafel slopes (90–110 mV/dec) and activation energies (20–25 kJ/mol), it was concluded that the kinetic enhancement is contained in the pre-exponential factor. This implies that the most important effect of alloying is modification of the coverage of the Pt sites by nonreactive oxygenated species.

To achieve further improvements in air electrode performance by using Pt-based catalysts, we also studied what is known as a "particle size effect": a change in the structure and/or electronic properties of Pt particles supported on carbon as the diameter is reduced from 10 to 1 nm. The results show that, in the absence of specific adsorption (such as in the Nafion[®] polymer electrolyte), there is no particle

size effect, at least for particle diameters > 4 nm. The best performance of the air cathode should be achieved with highly dispersed Pt clusters (e.g., one should synthesize Pt particles with the maximum number of Pt surface atoms per unit mass of Pt).

On the basis of these advances, it appears possible to reduce the Pt loading on the air electrode from the present levels of ca. 0.3 mg/cm² to 0.15 mg/cm² without sacrificing performance.

2. Insight into the CO₂ and air-bleed effects on PtMo and PtRu alloys

By utilizing the thin-film RRDE method at fuel-cell-relevant temperatures and gas mixtures, an original electrochemical protocol was used to determine the differences in activity between the best PtRu and PtMo catalysts, as shown in Figure 2. The following were evaluated, in the sequence listed here: The current density measured for pure H₂, which was used as the benchmark for the maximum possible activity, was compared to the current obtained with 75%H₂/25%N₂ mixtures, which were used to test the effect of dilution. After this test, the following were evaluated, in the sequence listed here: the effect of CO in hydrogen, the effect of CO₂ in hydrogen, the effect of CO concentration in 75%H₂/25%CO₂, and finally the recovery achieved by air-bleeding mixtures.

There are two main characteristics that mark catalytic behavior of PtRu and PtMo catalysts. The first characteristic is that the reduction of CO₂ on a PtRu electrode has only a modest effect on anode

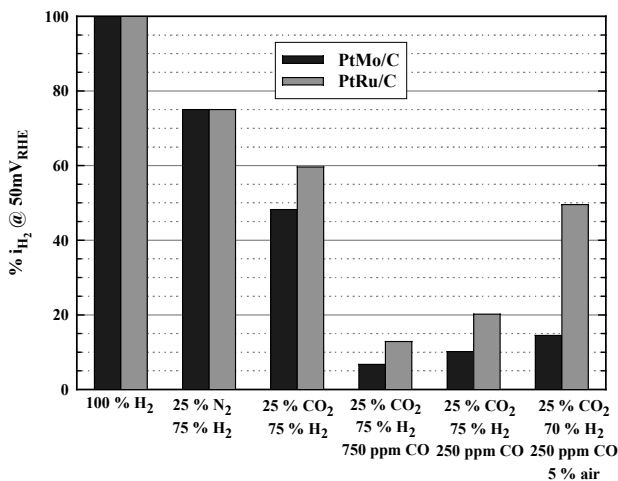


Figure 2. Summary of the activities at 50 mV for PtRu and PtMo catalysts at fuel-cell-relevant conditions.

performance. In contrast, a large deactivation, equivalent to ca. 50 ppm of CO, was observed on the PtMo catalysts in the presence of CO₂. It is not clear why CO₂ has different effects on catalytic properties of PtRu and PtMo, even for the same surface compositions. The second characteristic is that, in the presence of CO, the air-bleeding has a negligible effect on the catalytic properties of PtMo catalyst. Activity of the PtRu catalyst is, however, completely corrected by bleeding of 5% air into the CO-contaminated hydrogen. The difference is attributed to the fundamental properties of Ru versus Mo. Both Mo and Ru serve to nucleate OH on the surface from water dissociation, but only Ru adsorbs CO and catalyzes CO oxidation (i.e., “cleanses” the surface).

New commercially available catalysts having a greater Ru content than used at present should enable the precious metal content in anodes to be reduced by about 50%.

Conclusions

Use of Pt-Co alloy catalysts with optimized particle size should enable Pt loadings on the air cathode to be reduced by about a factor of two from current practice with standard pure Pt catalysts.

New commercially available Pt-Ru alloy catalysts having a greater Ru content than used at present should enable the precious metal content in anodes to be reduced by about 50%.

Publications

- N.M. Marković and P.N. Ross, “Electrocatalysis by Design: From the Tailored Surface to a Commercial Catalyst,” review article, *Electroch. Acta*, **45** (2000):4101–4115.
- V. Stamenković, N.M. Marković, and P.N. Ross, “Structure-relationships in Electrocatalysis: Oxygen Reduction and Hydrogen Oxidation Reactions in Solution Containing Chloride Ions,” *J. Electroanal. Chem.* **500** (2001):43.
- T.J. Schmidt, B.N. Grgur, N.M. Marković, and P.N. Ross, “Oscillatory Behavior in the Electrochemical Oxidation of Formic Acid: Rotation and Temperature Effects,” *J. Electroanal. Chem.* **500** (2001) 43.
- C. Saravanan, N.M. Marković, M.H. Gordon, and P.N. Ross, “Stripping and Bulk CO Oxidation at the Pt-electrode Interface: Dynamic Monte Carlo Simulations,” *J. Chem. Phys.* **114** (2001):6404–6412.

K. Low-Platinum and Platinum-Free Catalysts for Oxygen Reduction at PEMFC Cathodes

Karen Swider-Lyons (primary contact), Gregory B. Cotten, and Jason A. Stanley

Naval Research Laboratory

Code 6171

4555 Overlook Ave., SW

Washington, D.C. 20375-5342

(202) 404-3314, fax: (202) 767-3321, email: karen.lyons@nrl.navy.mil

Wojtek Dmowski and Takeshi Egami

Department of Materials Science and Engineering

University of Pennsylvania

3231 Walnut Street

Philadelphia, PA 19104

DOE Program Manager: JoAnn Milliken

(202) 586-2480, fax: (202) 586-9811, e-mail: JoAnn.Milliken@ee.doe.gov

Contractor: Naval Research Laboratory

Prime Contract No. DE-A101-00EE50639

Objective

- Decrease or eliminate the noble metal content of oxygen reduction reaction (ORR) catalysts by developing advanced hydrous oxide catalysts designed for rapid transport of protons, water, electrons, and oxygen.
- Develop target catalysts that offer high catalytic activity and low cost.

OAAT R&D Plan: Task 13; Barrier B

Approach

- Hydrous oxides are prepared as nanocomposites of various transition metal and rare earth oxides. The electrocatalytic activity of the materials is screened in half-cell measurements at the Naval Research Laboratory (NRL).
- The local structure of the amorphous catalysts is characterized from 0.2 to 2 nm via pair-density function analysis of x-ray diffraction patterns. X-ray diffraction is performed by the University of Pennsylvania at the National Synchrotron Light Source (NSLS) at Brookhaven National Laboratory.
- Structural characterization of active catalysts by the University of Pennsylvania will be used to determine structure-property relationships and activity mechanisms and guide the design of next-generation catalysts.
- Catalysts that exhibit high activity and corrosion resistance in half-cell measurements are tested in polymer electrolyte membrane fuel cells (PEMFCs) at Los Alamos National Laboratory (LANL).

Accomplishments

- We found that half-cell measurements on catalysts of a platinum (Pt) -doped iron phase have approximately 20 times the activity of 10% Pt/vulcan carbon (VC) per weight percent (wt%) Pt.

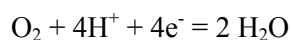
Future Directions

- Correlate the half-cell results to actual PEMFC performance in tests at LANL.
- Ascertain corrosion resistance of catalysts in half-cell and full-cell measurements.
- Investigate other Pt-doped phases (non-iron phases).
- Develop Pt-free catalysts by using transition-metal oxide mixtures that mimic Pt performance.

Introduction

State-of-the-art PEMFCs contain high loadings of Pt, making the fuel cells costly and subject to market fluctuations in the availability of the noble metal. By using little or no Pt in fuel cell cathodes, we can drastically reduce the cost of the fuel cells and imports of noble metals.

The catalytic activity of the ORR at the fuel cell cathode is known to be relatively slow, presumably because it is a four-electron mechanism:



For this reaction to proceed unencumbered, the catalyst site must also have a supply of oxygen, protons, and electrons, and it must be able to transport water away from the cathode. The reaction becomes limited when the transport of any of these four species slows.

Hydrous ruthenium oxide (RuO_xH_y) is an example of a material that has both high proton and electron transport. Pair-density function analysis of the x-ray diffraction pattern (PDF-XRD) of “amorphous” RuO_xH_y indicates that the most catalytically active material comprises ordered regions from 0.5 to 1.5 nm that are intertwined with unordered regions. By using the PDF-XRD data, in addition to magnetic measurements, we surmised that the high electrochemical and catalytic activity of RuO_xH_y is caused by its inherent nanocomposite structure: ordered regions for electron transport and hydrous regions for proton transport [1]. The naturally forming structure of RuO_xH_y is used in this program as an inspiration for designing new catalytically active materials.

Approach

This new program targets the discovery of low-Pt and Pt-free catalysts by developing new “amorphous” and/or nanocomposite ORR catalysts. The criteria for selection of the materials are that

they must be able to attract and transport (1) oxygen gas, (2) protons, (3) electrons, and (4) water.

Transition-metal oxides are selected for testing on the basis of their potential to meet these criteria. All catalysts are oxide based, because hydrous oxides are good proton and water conductors, and they often have high resistance to corrosion. Most metals, including Pt, are prone to corrosion at the operating conditions required for the PEMFC cathode. Oxides are less prone to poisoning, and some mixed-oxide catalysts also have the ability to mimic Pt.

Catalyst powders are prepared from aqueous solutions in ambient conditions and then annealed at various temperatures to adjust their water contents. The water content of the final materials is determined via thermal analysis. The activity of the catalysts for the ORR is screened by using a rotating-disk electrode (RDE) method [2]. The catalysts are mixed with VC and a 5 wt% Nafion[®] solution to make a conductive ink that is applied to the RDE and dried. The final RDE is tested in 0.1 M H_2SO_4 under both argon (Ar) and O_2 flows to determine the effect of O_2 on the catalyst. The catalysts are cycled at 5 mV/s between -0.01 and 1.3 V versus normal hydrogen electrode (NHE) at 60°C using rotation rates ranging from 1,000 to 1,750 rpm. The activity of the new transition metal catalysts is estimated by comparison with a standard RDE of 10 wt% Pt/VC catalyst (Alfa). Tafel plots are calculated from the RDE data as described in the literature.

Additional characterization is carried out at NRL by using thermal analysis and x-ray photoelectron spectroscopy (XPS).

The catalyst structures will be resolved by the University of Pennsylvania via PDF-XRD. X-ray diffraction is carried out at the National Synchrotron Light Source at Brookhaven National Laboratory. The PDF-XRD analysis will show the defect structure of the oxides and whether the Pt in the catalyst structures is present as small clusters or is dissolved in the oxide structure. This information

will be used to design the next generation of low-Pt catalysts and ultimately to design Pt-free catalysts. The catalysts will be tested at the DOE fuel cell testing facility at LANL for characterization under fuel-cell operating conditions.

Results

The difference in the cyclic voltammogram (anodic sweep) of 10% Pt/VC is shown in Figure 1. A greater negative current is measured under O_2 flow than under Ar flow because of the reduction of oxygen on the Pt catalysts. The difference between the O_2 and Ar curves reflects the current of the ORR. Several hydrous oxides have been doped with 0.5–5% Pt per mole of metal in the oxide. The actual Pt content of these materials is not yet known; it is too low to be detected by means of XPS. The cyclic voltammetry of the Fe phase changes dramatically when more than 0.5 wt% Pt is added, and it begins to resemble pure Pt when cycled in Ar. The Pt-doped Fe phase also behaves similarly to the 10% Pt/VC catalyst when cycled under O_2 . The data for a ~5% wt% Pt- Fe_x phase mixed with 80 wt% VC [20:80 (~5% Pt- Fe_x):VC] are shown in Figure 2. When normalized for Pt content, the 20:80 (~5% Pt- Fe_x):VC has almost 20 times the activity of the 10% Pt:VC, as shown in Figure 3. The Tafel plots of the

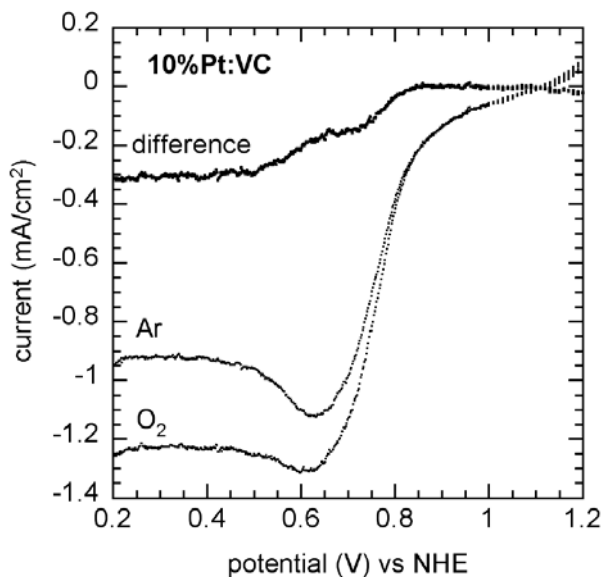


Figure 1. Anodic sweep of cyclic voltammogram of 10% Pt/VC in Ar and O_2 and the difference in the current caused by the ORR. Conditions: sweep rate = 5 mV/s; electrolyte: 0.1 M H_2SO_4 ; rotation rate = 1,250 rpm; temperature = 60°C.

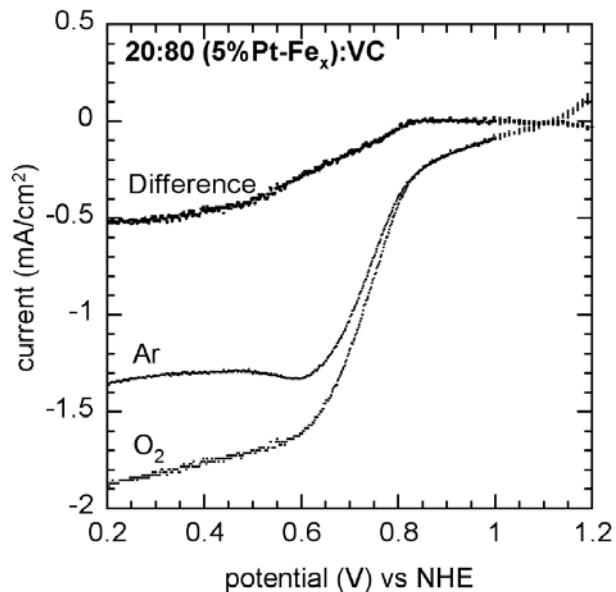


Figure 2. Anodic sweep of cyclic voltammogram of 20% (~5% Pt- Fe_x):VC in Ar and O_2 and the difference in the current caused by the ORR. Conditions: sweep rate = 5 mV/s; electrolyte: 0.1 M H_2SO_4 ; rotation rate = 1,250 rpm; temperature = 60°C.

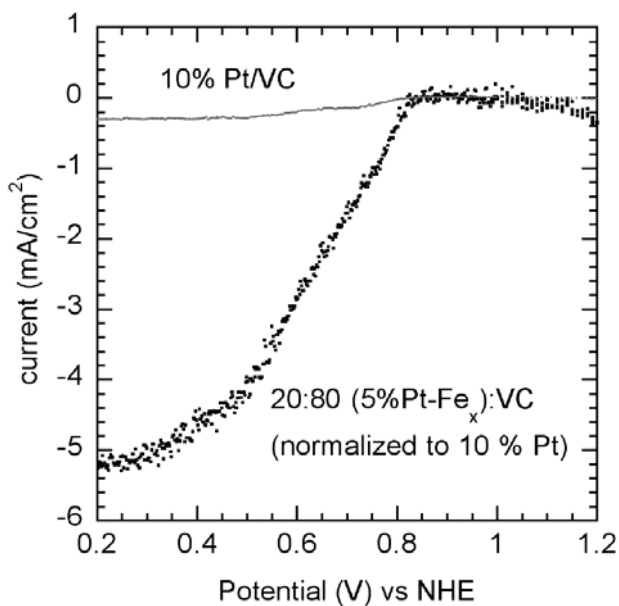


Figure 3. Normalized comparison of current from ORR of 10% Pt:VC and 20% (~5%Pt- Fe_x):VC using data from Figures 1 and 2.

ORR for the catalysts reflect the same trends shown in Figures 1 through 3.

Conclusions

The ORR activity of Pt is greatly enhanced by dissolving it in a matrix that is a good proton and water conductor. PDF-XRD structural measurements will be used to discern the state of the Pt in the Fe phase. Upcoming testing of the catalysts in LANL PEMFCs will indicate their actual activity and corrosion stability. The decreased Pt in the PEMFC will result in a significant decrease in the

cost of PEMFCs. Other transition-metal oxide systems containing little or no Pt will continue to be developed.

References

1. K. E. Swider-Lyons, K.M. Bussmann, D.L. Griscom, C.T. Love, D. R. Rolison, W. Dmowski, and T. Egami, in *Solid State Ionic Devices II – Ceramic Sensors*, Electrochemical Society Meeting, October 2000, in press.
2. S. Lj. Gojkovic, S.K. Zecevic, and R.F. Savinell, *J. Electrochem. Soc.* **145** (1998) 3713.

L. Low-Platinum-Loading Catalysts for Fuel Cells

Radoslav Adzic (primary contact), S.R. Brankovic, and J.X. Wang

Brookhaven National Laboratory, Bldg. 555

Upton, NY 11973-5000

(631) 344-4522; fax: (631) 344-5815, e-mail: adzic@bnl.gov

DOE Program Manager: JoAnn Milliken

(202) 586-2480, fax: (202) 586-9811, e-mail: JoAnn.Milliken@ee.doe.gov

Contractor: Brookhaven National Laboratory, Upton, NY

Prime Contract No. DE-AC02-98CH10886

Objective

- Conduct research on a new method to prepare Pt-Ru catalysts that involves spontaneous deposition of Pt on Ru nanoparticles.
- Develop a new catalyst with a considerably lower Pt loading and improved CO tolerance compared with the commercial Pt-Ru catalysts.

OAAT R&D Plan: Task 13; Barriers A and B

Approach

- Conduct proof-of-principle research with spontaneous deposition of Pt on an Ru(0001) electrode.
- Demonstrate spontaneous deposition of Pt on carbon-supported Ru nanoparticles.
- Determine the catalytic properties of the new catalyst for H₂ and H₂ + CO oxidation.
- Explain the catalytic activity and function of the new catalyst.

Accomplishments

- Developed a new method for the preparation of Pt-Ru and similar bimetallic catalysts that involves a spontaneous deposition of Pt submonolayers on metallic Ru nanoparticles.
- Prepared electrocatalysts with at least three times lower Pt loading and a higher CO tolerance than the commercial Pt-Ru alloy catalyst.
- Documented the following results:
 - All Pt atoms are on the surface of the Ru nanoparticles; thus, submonolayer amounts of Pt provide a high activity.
 - The mass-specific activity for H₂ oxidation is about 2–3 A/mg of Pt, which is approximately 300% better than state-of-the-art data.
 - *In-situ* infrared (IR) data indicate lower CO bonding strength to Pt in this catalyst than to the Pt-Ru alloy catalysts, which provides a tentative explanation of its improved CO tolerance.
- Submitted a patent application for the new catalysts.

Future Directions

- Further optimize the catalysts prepared by spontaneous deposition of Pt. Characterize the catalyst by means of electrochemical, high-resolution transmission electron microscopy (HRTEM), and extended x-ray absorption fine structure (EXAFS) techniques.

- Test the catalyst in a membrane electrode assembly and investigate means to reduce or replace Ru in the catalyst with non-noble metals.

Introduction

In June 2001, we commenced a project sponsored by DOE's Office of Transportation Technologies (OTT) to explore methods to decrease the Pt loading in Pt-Ru catalysts for H₂/CO oxidation in polymer electrolyte membrane fuel cells (PEMFCs). Despite considerable advances in the development of these electrocatalysts, their activity and CO tolerance are still unsatisfactory, and their Pt loading is too high. These are major obstacles to large-scale application of PEMFCs.

In this report, we describe a breakthrough that can help eliminate these obstacles: a new method of preparing the Pt-Ru catalysts that involves spontaneous deposition of Pt on Ru nanoparticles. Pt is deposited only at the surface of Ru nanoparticles rather than throughout the Pt-Ru nanoparticles. The method facilitates tuning of the electronic and catalytic properties of Pt-Ru catalysts by controlling the Pt cluster size. In contrast to the Pt-Ru alloy catalysts, this structure has *all the Pt atoms available for the catalytic reaction*, which decreases the Pt loading. We have submitted a patent application for the new catalysts.

Results

Spontaneous Deposition of Pt on Ru

We demonstrated the spontaneous deposition of Pt on Ru by immersing the ultra-high vacuum (UHV)-prepared Ru(0001) in a solution containing Pt ions. This procedure yields submonolayer-to-multilayer Pt deposits, the coverage and morphology of which depend on the Pt ion concentration of the solution and the time of immersion. Figure 1 shows Pt deposits, which have a columnar shape and a relatively uniform size, and 2–6-nm clusters with an average height of 2 monolayers (ML). Spontaneous deposition of Pt on carbon-supported Ru nanoparticles was found to occur on the samples reduced in H₂ atmosphere at ~300°C for 2 h.

Catalytic Activity

Figure 2 shows a comparison of the activity of the Pt-Ru 1:20 electrocatalyst prepared by

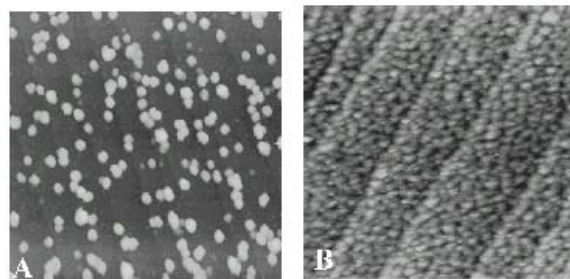


Figure 1. Scanning tunneling microscopy (STM) images: (A) 200 × 200 nm and (B) 100 × 100 nm of spontaneously deposited Pt on Ru(0001) from 0.1 mM and 10 mM H₂PtCl₆ in 0.1 M H₂SO₄, respectively. Images obtained at open circuit potentials; Z ranges (A) 5 nm and (B) 2 nm.

spontaneous deposition and E-TEK's Pt-Ru 1:1 alloy electrocatalyst for the oxidation of H₂ in 0.5 M H₂SO₄. Polarization curves were obtained by using a rotating-disk thin-film electrode at 2,500 rpm. The curves in the upper panel are nearly identical, although the Pt loading differs by a factor of three. Therefore, as shown in the lower panel, the mass-specific activity with respect to Pt for the catalyst obtained by spontaneous deposition of Pt is three times that of the E-TEK Pt-Ru alloy.

Table 1 lists the mass-specific currents for H₂ oxidation as a function of the Pt loading and the Nafion[®] film thickness at 50 mV and 2,500 rpm (normalized by the Pt loading). For E-TEK's Pt-Ru catalysts, the mass-specific current increases several times with the decrease of the Pt loading and Nafion[®] film thickness. For the same 3-μg/cm² Pt loading, the data obtained with different Nafion[®] film thicknesses indicate that the effect of the Nafion[®] film becomes negligible below a thickness of 10 nm. The activities of the catalysts prepared by spontaneous deposition of Pt on Ru for three different Pt:Ru ratios (Table 1, lower part) are about three times those of the E-TEK Pt-Ru alloy. These data indicate that, even for a very low Pt coverage on Ru, its activity for H₂ oxidation is preserved; this activity is required for an active, CO-tolerant catalyst.

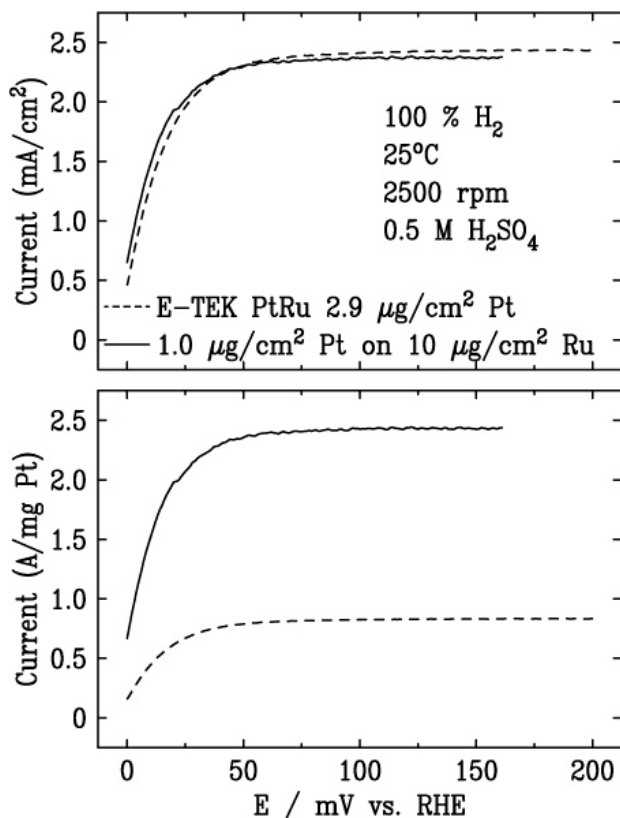


Figure 2. Polarization curves for the catalyst prepared by spontaneous deposition of Pt on Ru nanoparticles on Vulcan XC72 (solid line) and E-TEK’s 20% 1:1 Pt-Ru catalyst (dashed line) for the oxidation of H₂ at 0.05 V in 0.5 M H₂SO₄ at 25 °C. The curves were obtained by using a thin-film rotating electrode at 2,500 rpm (upper panel); mass-specific activities (lower panel).

Figure 3 shows a comparison of the current as a function of time for the oxidation of H₂ (with 100 ppm CO for the Pt-Ru₂₀ electrocatalyst and for E-TEK’s Pt-Ru catalyst and with Pt loadings of 0.95 μg/cm² and 2.93 μg/cm², respectively). The current for the oxidation of pure H₂, which is the same for both catalysts, was used for the normalization. With a very thin (1 nm) Nafion® film and low Pt loading, the loss of activity after 1 h for the spontaneously deposited Pt sample is small (ca. 15%). The loss of activity for the E-TEK Pt-Ru catalyst is much more pronounced (more than 50%). Figure 4 shows the behavior of the two catalysts with 1,000 ppm CO and with a thicker Nafion® film than that shown in Figure 3. A considerably higher CO tolerance is observed for the new catalyst.

Table 1. Mass-specific current (J) at 50 mV and 2,500 rpm for H₂ oxidation in 0.5 M H₂SO₄ at 25°C as a function of Pt loading and Nafion® film thickness for E-TEK’s Pt-Ru electrocatalyst and the electrocatalyst Pt-Ru_x obtained by spontaneous deposition.

Sample	Pt nmol/cm ²	Pt μg/cm ²	D _{Nafion} nm	J A/mg
Pt-Ru	100	19.5	100	0.13
Pt-Ru	25	4.88	50	0.52
Pt-Ru	15	2.93	10	0.82
Pt-Ru	15	2.93	5	0.86
Pt-Ru	15	2.93	1	0.90
Pt-Ru	10	1.95	1	1.05
Pt-Ru ₅	5	0.95	1	2.58
Pt-Ru ₁₀	5	0.95	1	2.48
Pt-Ru ₂₀	5	0.95	1	2.64
Pt-Ru ₂₀	3	0.57	1	3.74

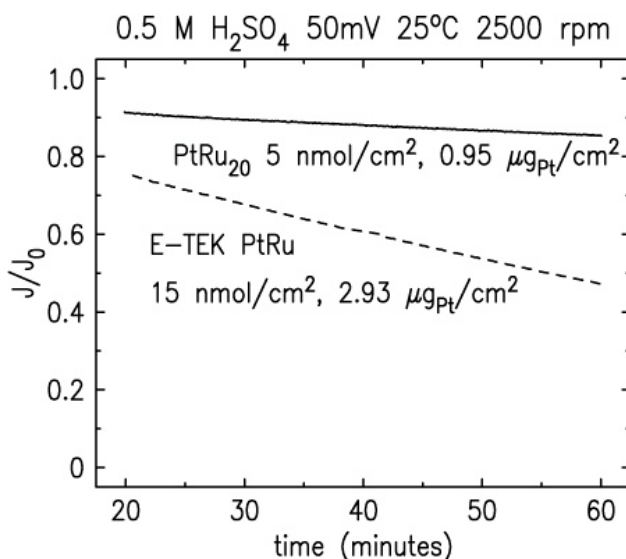


Figure 3. Time dependence of the normalized current for the oxidation of H₂ with 100 ppm CO in 0.5 M H₂SO₄ at 25°C; j₀ is the H₂ oxidation current.

In-Situ Infrared Spectroscopy

Infrared spectra for CO adsorbed on the Ru(0001) surface with a Pt submonolayer as a function of potential reveal two bipolar bands with the potential-dependent frequencies, which change from 2,011 to 2,021 cm⁻¹ and from 2,070 to 2073 cm⁻¹ (Figure 5). The first band is associated with CO adsorbed on Ru(0001), but it is shifted to higher frequencies compared with the band for bare

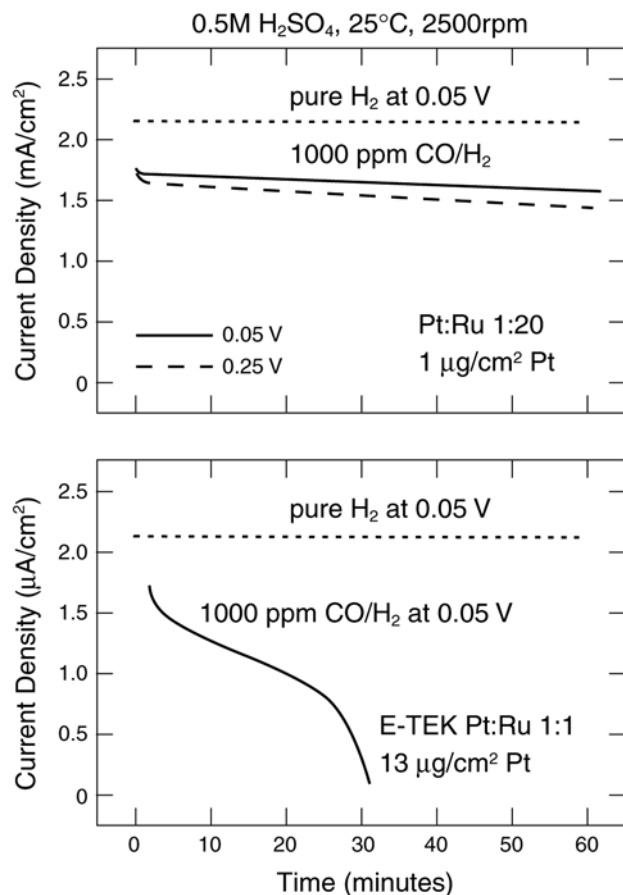


Figure 4. Time dependence of the normalized current for the oxidation of H₂ with 1,000 ppm CO in 0.5 M H₂SO₄ at 25 °C.

Ru(0001) obtained under the same conditions (which is between 2,000 and 2,013 cm⁻¹). The second band is caused by CO adsorption on Pt and is red-shifted in comparison with the band for Pt(111) — between 2,075 and 2,080 cm⁻¹. This finding indicates a decrease in the bond energy of CO to Ru and an increase in the bond energy to Pt. It is, however, important to note that an increase in the band frequency is observed with respect to Ru (2,000–2,020 cm⁻¹). In addition, an increase of the band frequency is observed if the Pt band is compared with a single band for the Pt-Ru (50:50) alloy (2,055–2,065 cm⁻¹), indicating a weaker bond to Pt for this electrocatalyst than for the Pt-Ru alloy.

For the electrocatalysts prepared by spontaneous deposition, the above analysis indicates that, for the Pt islands on Ru, CO coverage is expected to be lower than that for the Pt-Ru alloy. Thus, we tentatively propose that this mechanism is

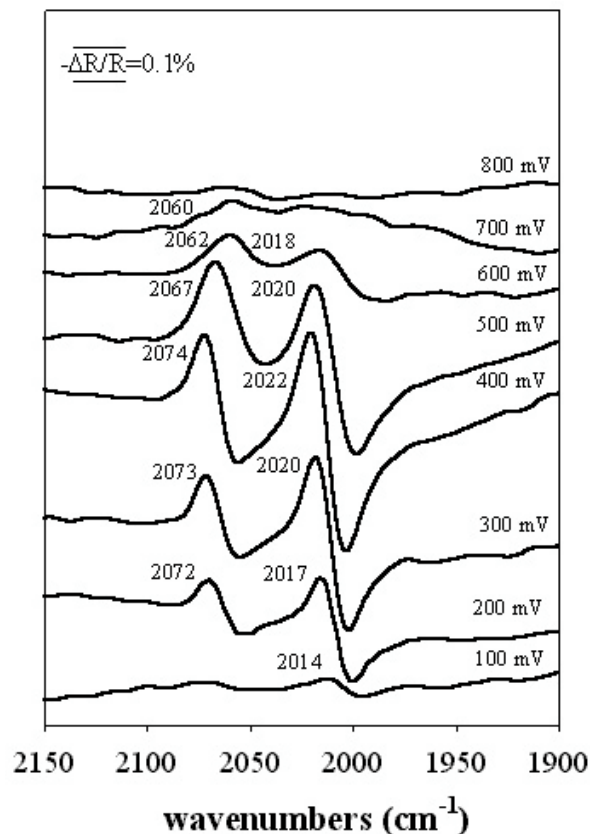


Figure 5. IR spectra for a Ru(0001) electrode with a submonolayer of Pt in a CO-saturated 0.1 M H₂SO₄. The reference spectrum is at 0.075 V; the sample spectra are taken starting from 0.10 V and increased incrementally by 100 mV up to 0.80 V. In total, 8,192 scans were co-added in 16 cycles, 512 scans each; the resolution was 8 cm⁻¹. Spectra were offset for clarity.

responsible for the enhanced CO tolerance of the Pt-Ru electrocatalyst obtained by spontaneous deposition.

Conclusions

The new electrocatalyst has higher mass-specific activity and CO tolerance than commercial electrocatalysts with several times larger Pt loading. The Pt islands on Ru have apparently lower CO coverage than that for the Pt-Ru alloy, which is a tentative explanation of its higher activity. The ability of Ru to oxidize CO is critical, and it seems to be pronounced in this catalyst.

M. Carbon Monoxide Sensors for Reformate-Powered Fuel Cells

Fernando Garzon

MS D429, MST-11 Group

Los Alamos National Laboratory

Los Alamos, New Mexico 87544

(505) 667-6643, fax: (505) 665-4292, e-mail garzon@lanl.gov

DOE Program Manager: Nancy L. Garland

(202) 586-5673, fax: (202) 586-9811, e-mail: nancy.garland@ee.doe.gov

DOE Contractor: Los Alamos National Laboratory, Los Alamos, NM 87544

Objectives

- Develop a high-temperature sensor for measurement of 0.1–2% carbon monoxide in reformate gas for fuel processor control.
- Develop a low-temperature sensor for measuring 10–100-ppm range concentrations for stack poisoning control.

OAAT R&D Plan: Task 3; Barriers D, E, and F

Approach

- Two electrochemical sensor types are being investigated for high- and low-temperature carbon monoxide sensing:
 - A solid oxide electrolyte device is being developed for the high-temperature application.
 - Ytria-doped zirconia oxygen ion conductor is being investigated as the solid electrolyte.
 - Strontium yttrium zirconium oxide proton conductor is also being evaluated as the solid electrolyte.
 - A low-temperature amperometric device, based on carbon monoxide inhibition of hydrogen reduction kinetics using either a perfluorosulfonic acid polymer electrolyte or an inorganic acid electrolyte, is being evaluated.
- LANL will interact with industry or other groups at LANL to test sensors in multicomponent reformate gas environments that simulate typical fuel processor output gases.

Accomplishments

- Developed a zirconium oxide-based high-temperature sensor. The sensor responds well to ppm and percent concentrations of carbon monoxide levels in air.
- Successfully synthesized and characterized strontium zirconate proton-conducting thin-film electrolytes.
- Developed and tested amperometric low-temperature carbon monoxide sensors under a variety of conditions. These devices respond well to carbon monoxide in hydrogen streams.

Future Directions

- Develop strontium zirconate proton-conducting high-temperature devices.
- Optimize low-temperature amperometric devices.
- Evaluate catalyst composition, loading, and particle size effects on sensor performance.
- Investigate alternative electrolytes.

- Study the influence of sensor geometric configuration on sensor performance.
- Test the sensor prototypes in actual reformat gas streams.

Introduction

The detection and measurement of carbon monoxide in high-temperature reformat streams is of vital importance to the successful implementation of fuel cells for transportation. Current sensor technology is designed for operation in ambient air environments and will not function at the low-oxygen partial pressures present in reformat gas. The 2000 Sensor Needs for Fuel Cells Workshop, attended by industry, national laboratory, and university participants, identified CO sensing in hydrogen reformat gas as a critical technology for successful fuel cell system deployment. Much research is being performed to optimize low-cost fuel reformer systems that convert liquid hydrocarbon fuels to hydrogen gas-containing fuel streams for powering fuel cells. The fuel cell anodes where hydrogen is electrochemically oxidized are typically platinum based. It is well known that low concentrations of carbon monoxide (~10–100 ppm) in hydrogen can severely degrade the performance of PEM fuel cells. The performance degradation is due to strong adsorption of carbon monoxide on the electro-active platinum surface sites where hydrogen is normally oxidized.

A necessary goal of fuel reformer systems is the minimization of carbon monoxide in the effluent from the fuel processor subsystem. Many reformer systems use a secondary partial oxidation reactor that selectively oxidizes the carbon monoxide present in reformat streams. In most transportation applications, the reformer and the selective oxidation reactors do not operate continuously under steady-state conditions; large transients may occur that produce relatively large amounts of carbon monoxide. To protect the PEM fuel cells from performance-degrading concentrations of carbon monoxide, it is therefore highly desirable to have a low-cost, real-time carbon monoxide measurement system that provides feedback control to the fuel processing system. Feedback control is also necessary to operate these systems at maximum energy efficiency, as air-bleeding methods are commonly used to reduce the concentrations of carbon monoxide in fuel cell systems. This method, while effective, reduces the energy efficiency of the

fuel cell system and, thus, should be used only for carbon monoxide transients. Fast, continuous measurement of carbon monoxide concentrations in fuel processor streams is thus of great value in reformat-powered PEM fuel cell power plants. We are designing and developing solid-state electrochemical sensors meeting these criteria and demonstrating prototype sensors.

Approach

High-temperature carbon monoxide sensors

Zirconia-based electrochemical oxygen sensors are currently being used by virtually all automobile manufacturers to control the air-fuel ratio of modern gasoline-powered vehicles. They have been hugely successful for improving engine performance and fuel efficiency and for reducing air emissions when coupled to a computer-controlled fuel injection system and a catalytic converter.

Recently, LANL has developed a fundamentally new approach to electrochemical sensors that enables the sensing of gases other than oxygen. Our gas-sensing devices are based on thin-film transition metal oxides (TMOs) deposited on oxygen ion-conducting solid-state electrolytes. The TMOs are central to the operation of the devices: they are electronically conducting and act as the electrodes for our sensors, they are catalytically active and can provide selective catalyzation under appropriate conditions, and they conduct oxygen atoms and act as the source of oxygen for oxidizing reactions. When used with a more catalytically inert counter electrode, an electric potential develops across the oxygen ion conductor because of preferred oxidation of the analyte (species being analyzed) on the catalytic electrode. The magnitude of the voltage is proportional to the concentration of the gas analyte in the sampled gas.

Proton-conducting solid electrolyte ceramics may also be used to produce electrochemical sensors suitable for carbon monoxide detection in hydrogen gas streams. We are currently electrochemically and crystallographically evaluating three specific compounds ($\text{SrZr}_{0.9}\text{Yb}_{0.1}\text{O}_{2.95}$, $\text{SrCe}_{0.95}\text{Yb}_{0.05}\text{O}_{2.975}$, and $\text{BaCe}_{0.9}\text{Yb}_{0.1}\text{O}_{2.95}$) for their suitability as

hydrogen ion solid electrolytes. The strontium zirconate ($\text{SrZr}_{0.9}\text{Yb}_{0.1}\text{O}_{2.95}$) has the maximum stability with respect to alkaline earth-carbonate and hydroxide formation, whereas the barium cerate ($\text{BaCe}_{0.9}\text{Yb}_{0.1}\text{O}_{2.95}$) has the highest protonic conductivity in water or hydrogen-containing atmospheres. These electrolyte materials may prove ideal for the production of potentiometric sensors for the detection of carbon monoxide in hydrogen.

Low-temperature carbon monoxide sensors

Low-temperature carbon monoxide sensors based on the reversible carbon monoxide adsorptive poisoning of hydrogen electro-oxidation are being developed by LANL. It is well known that the adsorption of carbon monoxide onto platinum electrode surfaces inhibits the hydrogen oxidation process. The addition of transition metals (such as ruthenium) to the platinum electrode materials greatly improves the oxidation kinetics. An amperometric sensor that senses the inhibition to hydrogen oxidation can be fabricated from a platinum electrode, a proton conductor, and a platinum-ruthenium alloy electrode. The platinum electrode current density will be influenced by the surface coverage of carbon monoxide on the electrode surface. Reverse biasing the sensor will give an asymmetric response because the oxidation rate for hydrogen on the platinum-ruthenium alloy electrode will not be strongly affected by low levels of carbon monoxide. The alloy electrode thus serves as an internal reference without the need for a separate gas compartment.

Results

High-temperature carbon monoxide sensors

We have successfully fabricated a platinum/yttria-stabilized zirconia/gold electrode device that responds well to carbon monoxide in air. The device was produced by using electron beam deposition of the electrode materials and the solid electrolyte. Figure 1 illustrates the device response to the addition of 500 parts per million carbon monoxide to air. The sensor response to carbon monoxide in hydrogen is slower than that in air. The slow equilibration kinetics of the carbon monoxide-oxide ion reaction on the solid electrolyte in environments of low oxygen partial pressure may be hampering the time response of these devices.

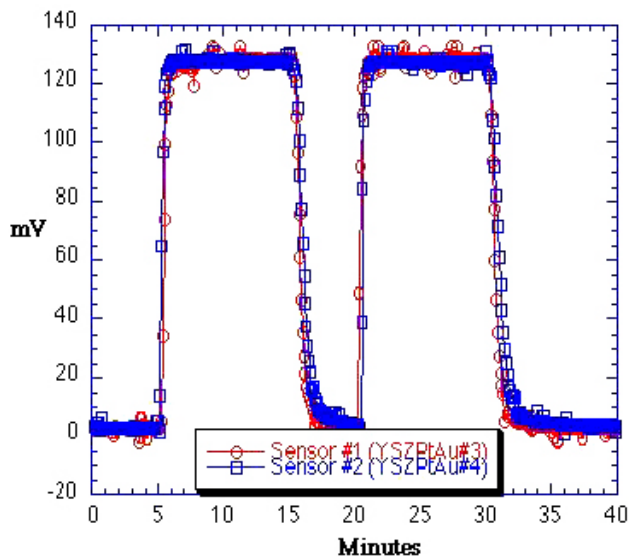


Figure 1. High-temperature sensor response to 500-ppm carbon monoxide in air. The carbon monoxide gas was stepped on, off, on to illustrate sensor response dynamics.

A proton-conducting ceramic may be more suitable for the high hydrogen partial pressure environment. Proton-conducting solid electrolyte thin films of perovskite-phase strontium zirconate were successfully developed this year. Sensor testing based on high-temperature, proton-conducting oxide films will commence next year.

Low-temperature carbon monoxide sensors

Our low-temperature device, a platinum/Nafion[®]/platinum-ruthenium alloy sensor, responded well to varying concentrations of carbon monoxide in a hydrogen gas mixture. The devices were fabricated by using electrode ink deposition methods onto Nafion[®] perfluorosulfonic acid polymer electrolytes. The device was operated in amperometric mode at varying bias potentials and temperatures. Figure 2 displays the device response at 90°C for varying concentrations of carbon monoxide. Figure 3 shows the device behavior at varying temperatures. The current suppression visible in the upper right hand quadrant of the figure occurs as a result of the inhibition of hydrogen oxidation by the carbon monoxide gas adsorption on the platinum surface. This poisoning reaction does not occur on the platinum-ruthenium alloy reference electrode. The inhibition is less pronounced at higher temperature, but the response time of the

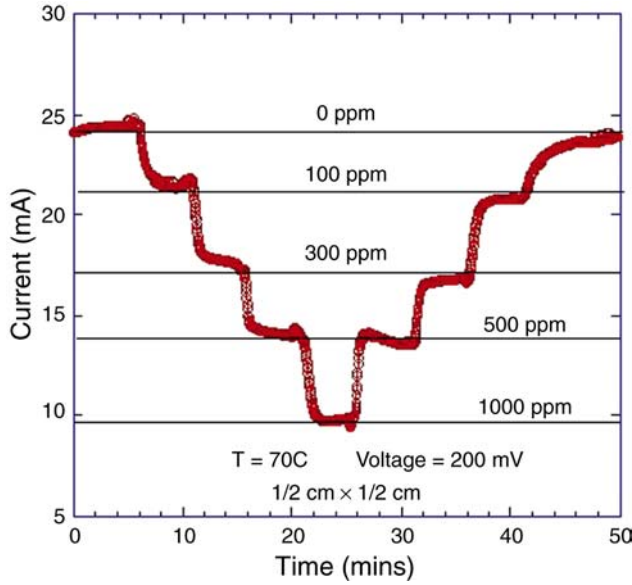


Figure 2. Low-temperature sensor response to varying concentrations of carbon monoxide gas in water-vapor-saturated hydrogen streams at 90°C.

device is faster at the highest test temperature of 90°C.

Conclusions

We have successfully developed high- and low-temperature sensors for carbon monoxide gas. The high-temperature sensors respond best to gas environments with relatively high oxygen partial pressures. We will pursue sensor designs that use high-temperature, proton-conducting solid electrolytes for improved response characteristics in a hydrogen atmosphere. The low-temperature amperometric sensors offer a promising technology for carbon monoxide detection in hydrogen streams. The sensors can detect part-per-million concentrations of carbon monoxide. Further improvements to the low-temperature sensor technology include selecting an electrolyte with a lower conductivity dependence on hydration state, improving response time, and testing for long-term stability in real reformat streams.

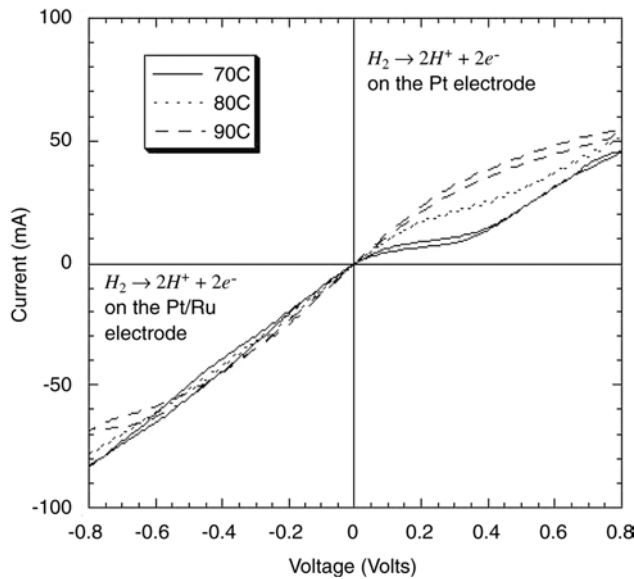


Figure 3. Low-temperature sensor current-voltage characteristics at varying temperatures in an atmosphere of 1,000-ppm carbon monoxide mixed into water vapor saturated hydrogen.

N. Electrochemical Sensors for PEMFC Vehicles

Ai-Quoc Pham

*Lawrence Livermore National Laboratory
Chemistry & Materials Science Directorate
P.O. Box 808, L-350
Livermore, CA 94550
(925) 423-3394, fax: (925) 422-6892, e-mail: pham2@llnl.gov*

*DOE Program Manager: JoAnn Milliken
(202) 586-2480, fax: (202) 586-9811, e-mail: JoAnn.Milliken@ee.doe.gov*

*Contractor: Lawrence Livermore National Laboratory, Livermore, CA
Prime Contract No. W-7405-ENG-48. EE-0502*

Objectives

- Develop sensors for transportation fuel cell systems.
 - Develop a hydrogen safety sensor.
 - Develop a hydrogen sensor for reformat fuel monitoring.
 - Develop a CO sensor for reformat fuel monitoring.

OAAT R&D Plan: Task 13; Barriers A and B

Approach

- Characterize and select various oxygen and proton conducting electrolytes.
- Evaluate the mixed potential response of various n-type oxide electrodes.
- Fabricate and test sensors.
- Develop microsensors with incorporated heater.

Accomplishments

- Built a complete experimental setup for sensor characterization.
- Selected an oxygen ion-conducting electrolyte.
- Evaluated various n-type oxide electrodes and selected the most promising electrode.
- Developed a novel type of sensing electrode (a patent application is in progress).
- Successfully tested first prototype hydrogen sensor. The response time was as fast as 1 s, which meets the DOE target for sensing hydrogen in air.

Future Directions

- Reduce sensor operating temperature.
 - Fabricate microsensor.
 - Provide sensors to DCH Technology for testing.
-

Introduction

Polymer electrolyte membrane fuel cells (PEMFCs) are among the most promising clean power technologies being developed for transportation applications. The introduction of this new transportation technology will mean important changes in car design, as well as incorporation of new features that are not currently required in internal combustion engine automobiles. For example if hydrogen fuel is supplied by an onboard fuel reformer that delivers a hydrogen stream containing several other gases, additional control and monitoring devices are needed to protect and efficiently operate the PEMFCs.

The purpose of this project is to design, develop, and demonstrate solid-state electrochemical sensors for the various controls and monitoring required for PEMFC vehicles. Target hydrogen concentrations are in the range of 0.1 to 10% with response times of 1 s, as defined in the 2000 Sensor Needs for Fuel Cells Workshop. The first year of the project is focused on the development of a hydrogen sensor for safety monitoring. The hydrogen sensor for fuel monitoring will be developed during the second year and the CO sensor during the third year.

Approach

A number of hydrogen and combustible gas sensors are available commercially. However, none of them appear to straightforwardly satisfy all the stringent requirements for automobile applications. In particular, the commercial hydrogen safety sensors suffer from significant long-term drifting and cross-sensitivity. Our approach is to use solid-state electrochemical sensor technology. The robustness and reliability of that technology have been proven in automobile oxygen sensors. Our sensor consists of an oxygen-conducting electrolyte membrane sandwiched between two electrodes — one serving as a reference and one as a working electrode. The working electrode has mixed potential response when exposed to an atmosphere containing hydrogen (i.e., because of the competing oxidation-reduction reactions of hydrogen and oxygen on the electrode surface, the potential of the mixed potential electrode departs from the actual thermodynamic value). The reference electrode, which is designed to reach thermodynamic equilibrium, will thus have a different potential. The potential difference between the two electrodes is

the sensor voltage, which is dependent on the hydrogen concentration. This type of sensor does not require a separate reference gas compartment.

Accomplishments

This project started in January 2001. First, we built a complete test setup to characterize the hydrogen sensors. The experimental setup includes several gas lines with mass flow controllers for gas mixing, a tube furnace for testing sensors at high temperatures, and a potentiostat coupled with an AC electrochemical impedance analyzer for the characterization and monitoring of sensor signals.

Several electrolytes were evaluated. We determined that oxygen ion-conducting electrolytes such as yttria-stabilized-zirconia (YSZ) and samarium-doped ceria were best suited for the present hydrogen safety sensor design. A number of oxide electrodes were then screened for their mixed potential response in the presence of hydrogen. Oxides with n-type conductivity such as zinc oxide (ZnO) were found to have the highest signal amplitude. This result is consistent with the literature data. However, the main drawback of most mixed potential sensors is the slow response, especially during the recovery period (when hydrogen is removed from ambient gas). We developed a novel sensor with very fast response time. Figure 1 shows the sensor response to the presence of 1% hydrogen in ambient air. At an operating temperature of 600°C, the sensor response time was 1 s, which meets the DOE response time

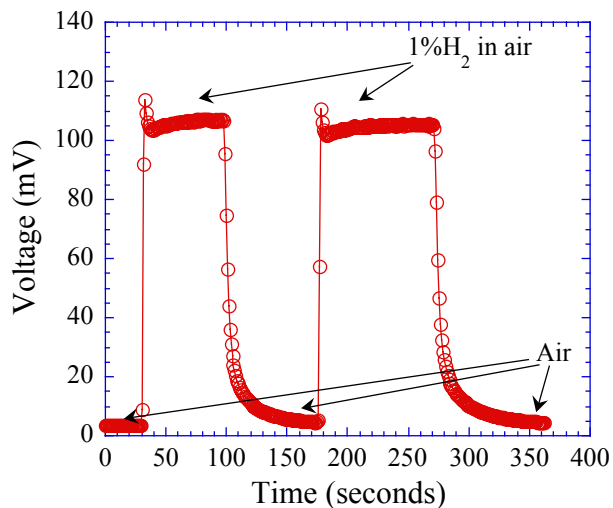


Figure 1. Sensor response to hydrogen at 600°C.

requirement for measuring hydrogen in air, albeit at a temperature above the DOE goal. These types of sensors require operation at constant elevated temperature (above ambient temperature). However, the recovery time when hydrogen was removed was significantly longer (about 200 s). When hydrogen was introduced back into the test chamber, the final sensor signal was always the same, independent of the starting voltage. This finding indicates good signal reproducibility when hydrogen is present. For practical safety application, sensor reproducibility and fast response to the introduction of hydrogen are the most important factors. Figure 1 shows that the sensor signal amplitude was very large (more than 100 mV). Figure 2 shows the plot of sensor voltage

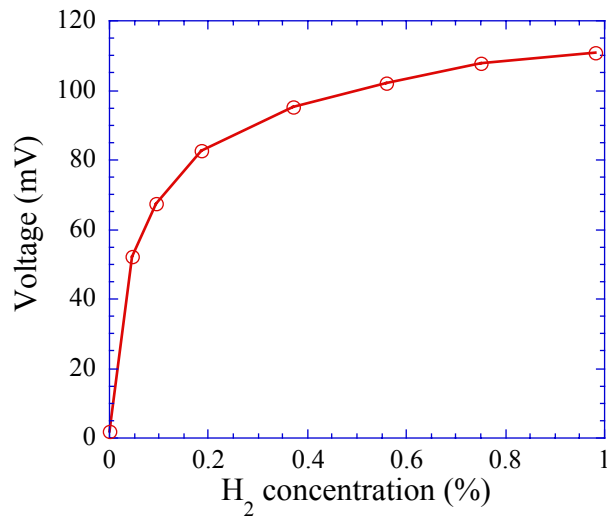


Figure 2. Sensor signal versus hydrogen concentration in air.

versus hydrogen concentration. The sensor has very high sensitivity to hydrogen at concentrations below 0.2 %. The signal tends to level off at higher hydrogen concentrations. Preliminary experiments also indicated that the sensor response was insensitive to humidity in ambient air. No drifting was observed.

Conclusions and Future Work

We have developed a novel hydrogen safety sensor with very promising characteristics. A U.S. patent describing the new concept is being filed.

Further work is needed to demonstrate a commercially viable device. In particular, the current sensor operating temperature (600°C) is too high. We plan to reduce the operating temperature to below 500°C. For practical use, we will develop a self-heated microsensors for reduced power consumption and minimum heat generation.

VI. AIR MANAGEMENT SUBSYSTEMS¹

A. Turbocompressor for PEM Fuel Cells

Mark K. Gee

Honeywell Engines and Systems

2525 W. 190th Street, MS-36-2-93084

Torrance, CA 90504

(310) 512-3606, fax: (310) 512-4998, e-mail: mark.gee@honeywell.com

DOE Program Manager: Patrick Davis

(202) 586-8061, fax: (202) 586-9811, e-mail: patrick.davis@ee.doe.gov

ANL Technical Advisor: Robert Sutton

(630) 252-4321, fax: (630) 252-4176, e-mail: sutton@cmt.anl.gov

Contractor: Honeywell Engines and Systems, Torrance, California

Prime Contract No. DE-FC02-97EE50479, October 1997–July 2000

DE-FC02-99EE50579, October 1999–June 2001

Objectives

- Develop an optimum turbocompressor configuration by working with manufacturers of fuel cell systems and following up on the work currently being performed.
- Develop a vehicle-ready motor controller.
- Make available a turbocompressor/motor controller for integration in a fuel cell system.

OAAT R&D Plan: Task 13; Barrier D

Approach

- Use automotive and aerospace turbomachinery technology to reduce cost and lower weight/volume.
- Use VNT[®] (variable nozzle turbine) inlet geometry to improve performance across the flow range.
- Use a mixed-flow-type compressor to improve low flow performance.
- Use contamination/oil-free and zero-maintenance-compliant foil air bearings.
- Use a high-efficiency, low-cost two-pole toothless motor.
- Use low-cost, sensorless, variable-speed motor-controller-topology design.

Accomplishments

- Demonstrated numerous start/stop cycles with no appreciable wear.
- Demonstrated stable operation at full turbine temperature (150°C).
- Achieved compressor and turbine mapping performance that was close to predicted values.

¹ The DOE draft technical targets for fuel cell system compressor/expanders can be found in Table 5, Appendix B. Because the targets in Appendix B were updated after the reports were written, the reports may not reflect the updated targets.

- Completed power consumption evaluation.
- Demonstrated a modified turbocompressor with the increased turbine inlet temperature (315°C) capability and aerospace-quality variable-speed brassboard motor controller in the DOE/Honeywell fuel-cell-brassboard system.
- Completed trade study of the turbocompressor and other compressor/expander designs; recommended the turbocompressor approach.
- Completed the analysis, design, and fabrication of the turbocompressor with a mixed-flow compressor and VNT®.
- Completed the analysis, design, and fabrication of the vehicle-ready motor controller.
- Initiated testing of the turbocompressor and vehicle-ready motor controller.

Future Directions

- Complete testing of the increased turbine inlet temperature turbocompressor in the DOE/Honeywell fuel cell brassboard system.
- Complete testing of the turbocompressor and vehicle-ready motor controller.

Introduction

The objective of this work is to develop an air-management system to pressurize a light-duty-vehicle fuel cell system. The turbocompressor is a motor-driven compressor/expander that pressurizes the fuel cell system and recovers subsequent energy from the high-pressure exhaust streams. Under contract to the U.S. Department of Energy, Honeywell designed and developed the motor-driven compressor/expander and evaluated performance, weight, and cost projection data. Compared with positive displacement technology, the turbocompressor approach offers high-efficiency and low-cost potential in a compact and lightweight package.

Approach

The turbocompressor design shown in Figures 1 and 2 consists of a compressor impeller, an expander/turbine wheel, and a motor magnet rotor incorporated onto a common shaft operating up to a speed of 110 krpm on compliant foil air bearings. A motor controller drives the motor, which is capable of driving the turbocompressor to the maximum design speed. The air bearings are lubrication-free, in addition to being lightweight, compact, and self-sustaining (meaning that no pressurized air is required for operation). The turbocompressor operates by drawing in ambient air through the motor/bearing cavities, in which the air is then

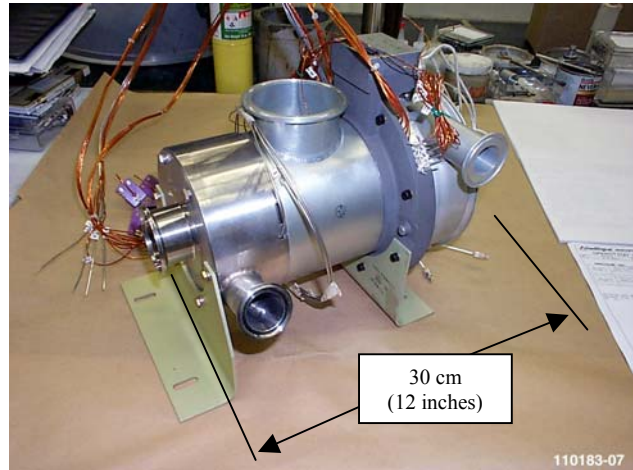


Figure 1. Honeywell fuel cell turbocompressor with mixed-flow compressor and VNT®.

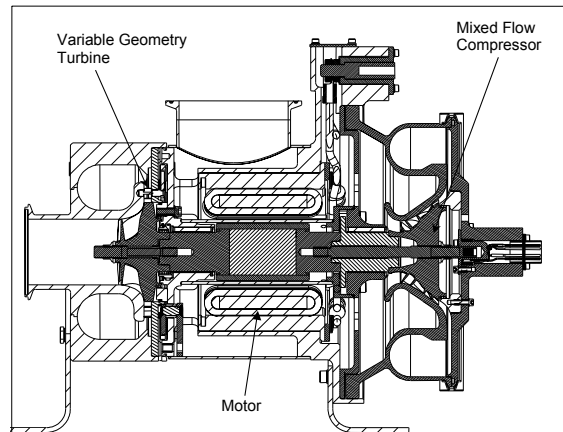


Figure 2. Cross section of fuel cell turbocompressor with mixed-flow compressor and VNT®.

pressurized by the compressor, delivered to the fuel cell stack, and then expanded through the turbine to aid in the overall turbocompressor/fuel-cell-system efficiency.

Results

The current turbocompressor has operated for more than 400 h at varying conditions, with and without motor operation. To date, a maximum speed of 110 krpm has been reached with the motor.

To support the DOE/Honeywell fuel cell brassboard system testing, the turbocompressor was modified to handle increased turbine inlet temperatures. In addition, a modified aerospace-quality controller to replace the commercial unit used previously was assembled and used in the DOE/Honeywell fuel-cell-brassboard system. Testing in the DOE/Honeywell fuel-cell-brassboard system was initiated in late 2000 and is expected to be completed in late 2001.

The turbocompressor and vehicle-ready motor controller outlined in the Variable Geometry for PEM Fuel Cells program awarded in March 1999 have been analyzed, designed, and fabricated and are shown in Figures 1, 2, and 3. Table 1 compares present weight and volume to DOE/PNGV targets. The turbocompressor incorporates a mixed-flow compressor and a VNT[®]. The changes are to improve the low flow performance while maintaining efficiency across the flow range. The vehicle-ready motor controller is smaller and will incorporate sensorless technology; its topology is configured to reduce production cost. Testing of the turbocompressor and integration testing of the motor

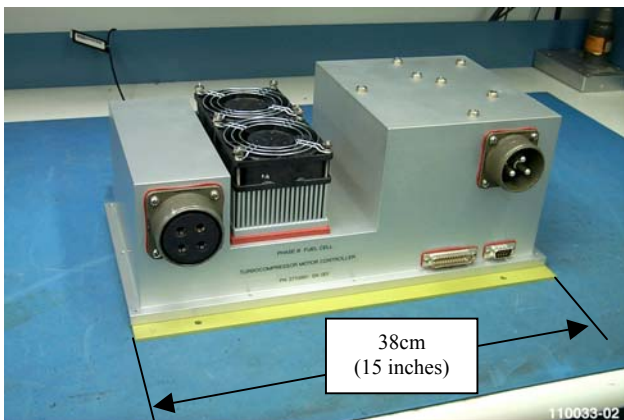


Figure 3. Fuel cell turbocompressor motor controller.

Table 1. Physical parameters of fuel cell turbocompressor.

DOE Parameters	DOE Targets	Honeywell Turbocompressor
Volume	4 L total (w/o heat exchangers)	Turbocompressor: 6 L Controller: 12 L
Weight	3 kg total (w/o heat exchangers)	Turbocompressor: 9 kg max Controller: 6.5 kg max

controller were initiated in mid-2001. Baseline (standard configuration) and predicted (mixed flow, variable nozzle turbine) performance curves are shown in Figure 4.

Conclusions

The turbocompressor concept in which self-sustaining compliant foil air bearings are used has demonstrated low power consumption and moderate pressure ratio at low flow rates in a compact, lightweight package. Power consumption can be further lowered if the increased expander/turbine temperatures can be provided by the fuel cell system. A turbocompressor capable of increased expander/turbine temperatures has been demonstrated in the DOE/Honeywell fuel-cell-brassboard system. The latest turbocompressor/variable-speed motor controller incorporates a mixed-flow compressor and a variable inlet nozzle turbine to improve the pressure ratio at the low flows; the size, weight, and reliability of the variable-speed motor controller are being addressed with the new sensorless design. Testing of the latest design was initiated in mid-2001.

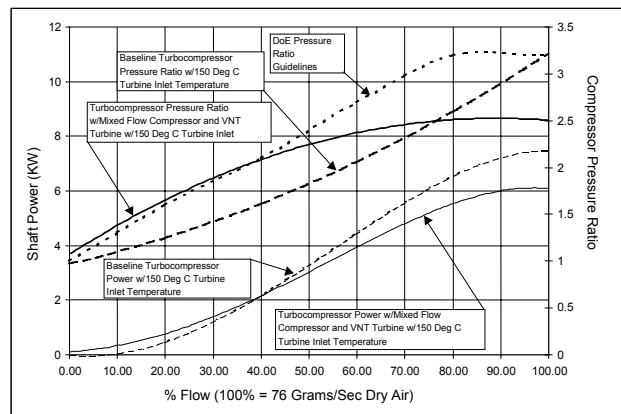


Figure 4. Turbocompressor shaft power/compressor outlet pressure ratio vs. percent flow. Baseline curves are based on actual data; mixed flow and VNT curves are predicted.

B. Innovative, High-Efficiency, Integrated Compressor/Expander based on TIVM Geometry

*Sterling Bailey, Ph.D., PE (primary contact), and Steve Chomyszak
Mechanology, LLC
453 South Main Street
Attleboro, MA 02703
(408) 356-5520, fax: (408) 358-4012, email: sterling@mechanology.com*

*DOE Program Manager: Patrick Davis
(202) 586-8061, fax: (202) 586-9811, e-mail: patrick.davis@ee.doe.gov*

*ANL Technical Advisor: George Fenske, Ph.D.
(630) 252-5190, fax: (630) 252-4798, e-mail: gfenske@anl.gov*

*Contractor: Mechanology, LLC, Attleboro, Massachusetts
ANL Contract No. 0F-00505, March 2000–September 2001*

Objectives

- Design a first-generation prototype compressor/expander based on the Toroidal Intersecting Vane Machine (TIVM) geometry.
- Fabricate and test the first-generation prototype TIVM compressor/expander.
- Identify the technology developments necessary for a commercially viable TIVM compressor/expander that satisfies all of the DOE requirements.

OAAT R&D Plan: Task 13; Barrier D

Approach

- Complete the detailed design for the prototype by using the conceptual design developed in FY2000.
- Fabricate the first-generation prototype compressor expander by using conventional materials.
- Design and construct a test stand to measure compressor/expander performance.
- Perform initial tests on a partial compressor/expander and use the results to refine the full prototype design.
- Conduct performance tests of the full prototype, covering the full operating range.
- Plan and initiate development for the key technology requirements.

Accomplishments

- Completed the detailed design of the TIVM compressor/expander prototype and produced fabrication drawings.
- Fabricated hardware for the initial partial assembly and for the full prototype.
- Designed and built a test stand for testing compressor/expander hardware.
- Used the results from testing the partial assembly to refine the full prototype hardware.
- Performed additional tests by using the generic prototype with temporary sealing to demonstrate the flow and pressure capabilities of the TIVM concept.
- Assembled the full prototype and initiated testing.
- Initiated key technology tasks in cooperation with national laboratories and commercial vendors.

Future Directions

- Test the first generation compressor/expander prototype over the full range of operating variables and compare measured performance with predictions.
- On the basis of analysis of the experimental data, refine design features to optimize performance.
- In parallel with the design evolution, conduct development tasks for seals, materials, and manufacturing, as well as for cost and noise minimization.
- Use the results of testing of subsequent prototypes, combined with the results from technology tasks, to evolve a mature TIVM compressor/expander component suitable for use in a commercially viable automotive fuel cell system.

Introduction

TIVM is an innovative mechanical concept, invented and patented by Mechanology, that can be configured as an integrated, positive displacement compressor/expander. In FY1999, the U.S. Department of Energy (DOE) investigated the TIVM concept for potential application in automotive fuel cell systems and determined that the inherent efficiency, compactness, and thermodynamic attributes of this concept might be of significant benefit. Mechanology was asked to develop a design specifically for the 50-kW_e automotive system and evaluate its potential performance. On the basis of the encouraging results obtained, the detailed design, fabrication, and testing of a first-generation prototype compressor/expander was authorized.

Approach

The approach followed during this period was to finalize the detailed prototype design, which is illustrated in Figure 1 (schematic diagram), fabricate the hardware, and then measure the performance across the operating range. This first-generation prototype is constructed of conventional materials and is not expected to satisfy all of the DOE requirements but rather to demonstrate the viability of the TIVM as a commercial air-management system. Future development of the concept will involve iterative prototypes, as well as concurrent technology and manufacturing tasks, to satisfy performance, cost, and noise requirements.

A test stand was designed and built to drive the compressor/expander and measure its operation. The test stand includes a drive motor instrumented for speed and torque; instrumentation for measuring the flow, pressure, and temperature of the inlet and outlet of the compression and expansion stages; and

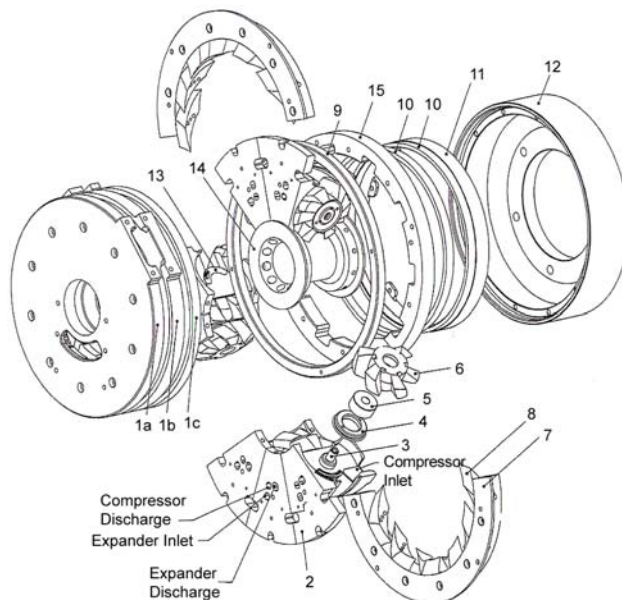


Figure 1. Design of the first-generation TIVM prototype compressor/expander.

a high-speed data acquisition system to record test data. Mechanology's test stand is shown in Figure 2.

A partial set of hardware was fabricated. The partial assembly was tested, and the results were used to refine the full prototype design and hardware. On the basis of the initial test results, several auxiliary tests were performed to better understand the design features necessary to satisfy the DOE flow and pressure requirements and to demonstrate the capability of the TIVM to meet these requirements.

Results

The first-generation TIVM compressor/expander prototype hardware was fabricated and is shown in Figures 3, 4, and 5. A partial set of this hardware



Figure 2. Mechanology's compressor/expander test stand.



Figure 4. TIVM prototype assembled housings and expander rotor.



Figure 3. TIVM prototype compressor and expander vanes.

was used for initial testing to finalize the design details for the full prototype.

To facilitate eventual integration with a drive motor, the structural support of the primary rotor and vanes was independent from the structural support of the secondary rotors and housings in the compressor/expander prototype. This approach was a deviation from that used in the generic prototype. Initial tests with the partial compressor/expander prototype assembly showed that this feature created a need for increased internal clearances in the TIVM

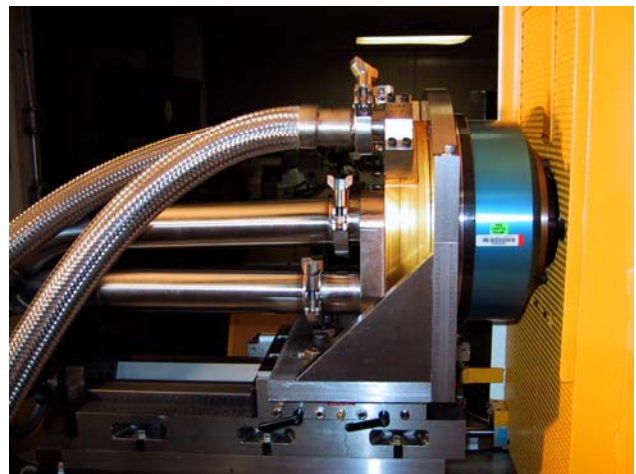


Figure 5. Compressor/expander prototype on performance test stand.

and required very precise alignment with the test stand. The structural design of the prototype was modified to provide a common structural support for the primary and secondary rotors. This modification was incorporated in the hardware for the full prototype and allowed reduced internal clearances and greatly reduced the alignment requirements for the test article with respect to the test stand. This integrated structural design approach will be maintained in future TIVM compressor/expander designs.

Initial testing of the partial assembly with large clearances showed that the compressor mass flow rate was only approximately 60% of the design values and that the pressure generated was well below the desired 3.2 atm. Analysis of these results

indicated that, in addition to the large internal clearances, the arrangement of inlet and outlet ports and the simplified seals contributed to significant leakage both within the TIVM chambers and from the chambers to the environment. On the basis of these observations, the porting design has been modified, and enhanced seal designs are being investigated.

To provide further empirical data related to the flow and pressure performance of the TIVM, auxiliary tests were run by using the generic prototype, which is shown in Figure 6. To temporarily simulate internal seals, the vanes of the generic prototype were greased. The first series of tests measured the flow, which was compared with the theoretical flow for the design. The measurements presented in Figure 7 are typical of several flow test runs. The data represent the design, or theoretical, flow rates for the compressor and the expander sections and the actual measured flow from the expander outlet. With perfect sealing, the actual flow rate would be limited to the compressor design rates because the compressors are intended to be the sole source of air for the expanders. The measured data indicate that, at low speeds, the flow rate is close to the expander design rate, indicating that the expander inlet is drawing additional air in from leakage paths. As speed increases, the time for in-leakage is less, and the flow approaches the compressor design rates. Overall, these sets of test

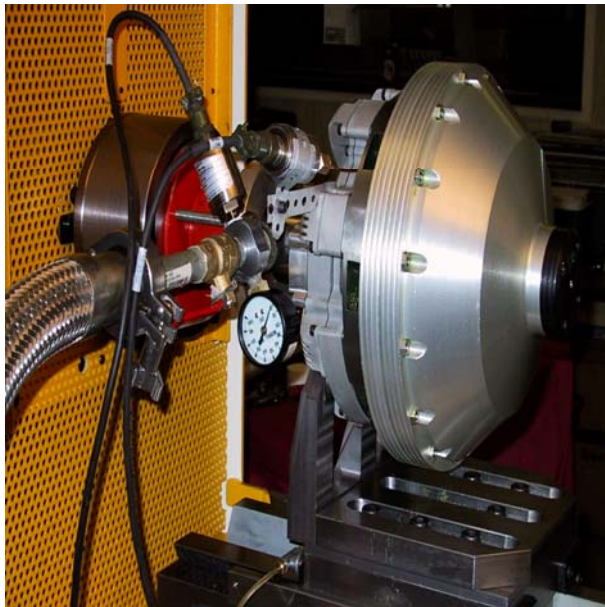


Figure 6. Generic prototype flow and pressure test assembly.

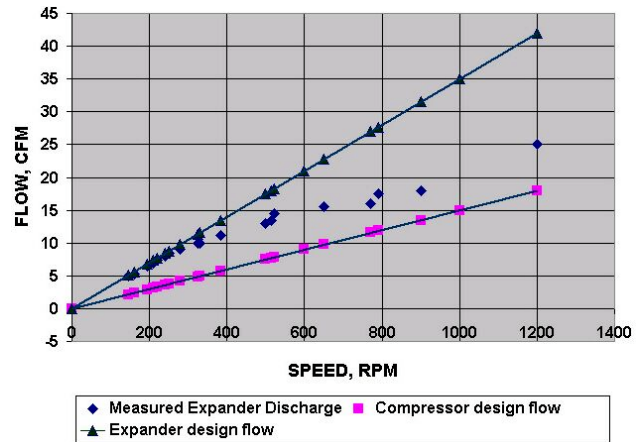


Figure 7. Generic TIVM prototype flow test results.

data indicate that the measured TIVM flow rates are consistent with the design values. The conclusion from this observation is that, with appropriate seals, the TIVM compressor/expander will provide the desired mass flow rate.

To measure the TIVM pressure capability, the prototype was brought to a speed of 1,200 rpm, which is 25% of full power speed, and a backpressure valve was closed to measure the maximum pressure the TIVM vanes could develop. Grease was used to simulate seals on the vanes. The TIVM vanes produced a pressure of 3.5 atm, which exceeds the DOE compressor outlet pressure requirement of 3.2 atm. The conclusion from this measurement is that a TIVM compressor with appropriate seals will meet the DOE outlet pressure requirement of 3.2 atm, even at 25% speed.

Conclusions/Future Work

Initial testing of the partial compressor/expander prototype has indicated the importance of an integrated structural support system and the importance of effective sealing in the TIVM. Testing the generic prototype with temporary sealing has demonstrated pressure and flow capabilities of the TIVM consistent with DOE requirements.

The future development work for the TIVM compressor/expander will include testing of the full first-generation prototype across the operating range and technology development tasks for seals, materials, manufacturing, and cost and noise minimization. Subsequent prototypes will incorporate design improvements and technology development results, leading to a compressor/expander that meets the DOE's technical targets.

C. Turbocompressor for Vehicular Fuel Cell Service

P. Fonda-Bonardi

Meruit, Inc.

1450 23rd Street

Santa Monica, CA 90404-2902

(310) 453-3259, fax: (310) 828-5830, e-mail: fbarch@concentric.net

DOE Program Manager: Patrick Davis

(202) 586-8061, fax: (202) 586-9811, e-mail: patrick.davis@ee.doe.gov

ANL Technical Advisor: Robert Sutton

(630) 252-4321, fax: (630) 252-4176, e-mail: sutton@cmt.anl.gov

Contractor: Meruit, Inc.

Prime Contract No. FE-FC02-97EE-50480, October 1997–December 2000

Subcontractor: FD Contours, Costa Mesa, CA

Objectives

- Test the design and performance of gas bearings for turbocompressor (under way).
- Test the performance of the expander and compressor for fuel cell service (under way).
- Test the endurance of DOE's/Argonne National Laboratory's (ANL's) near-frictionless carbon (NFC) coating in gas bearings (under way).

OAAT R&D Plan: Task 13; Barrier D

Approach

- Design, build, and test a specialized, instrumented test rig for measuring the performance of a new, high-performance gas bearing.
- Use the test rig for measuring the performance of the DOE/ANL NFC coating.
- Design, build, and test the prototype of a turbocompressor system supplying 76 g/s of air optimized for service over the full DOE-specified operating range.

Accomplishments

- Began the NFC endurance testing toward 100,000 start-stop cycles; completed one complete iteration with a strongly unbalanced bearing, and the balanced-bearing test currently under way has reached 5,500 start-stop cycles with minimal NFC wear.
- Completed 3,700 start-stop cycles with DuPont Vespel journals and 1,300 start-stop cycles with DuPont Delrin journals.
- Constructed the turbocompressor and the corresponding turbocompressor test bench, and the measurement system is being calibrated. We expect to meet the DOE-specified air delivery specification over the full operating range; performance testing will occur in July and August 2001.

Future Directions

- Performance test the turbocompressor prototype; continue NFC and bearing testing.
-

Introduction

Meruit has proposed a novel gas bearing for use in a small high-performance turbocompressor. A gas bearing suitable for automotive use must be inexpensive (i.e., mechanically simple with loose tolerances), durable (i.e., operate over many thousands of start-stop cycles), and able to survive mild collisions. The mechanical design of the Meruit bearing meets the first requirement; the second requirement has been demonstrated since the Meruit bearing only wears when not floating at speed, and its liftoff and landing speed with a ~1-kg rotor is about 900 rpm, which corresponds to a rubbing speed of about 1 m/s and a total rub of about 1 m per start-stop cycle. The third requirement is met by a demonstrated stiffness of 3.4 kn/mm (19.4 klb/in.) at 17,500 rpm, increasing to 6.80 knt/mm (38.8 klb/in.) at 21,000 rpm. The gas bearing performance must be stiff enough to support the rotor in the automotive environment (including minor collisions) and to float the rotor at speeds so low that the bearing does not wear out with many thousands of repeated start-stop cycles. The turbocompressor system must deliver the DOE-specified full mass flow (76 g/s) and pressure (3.2 pressure ratio) while maintaining pressure at lower mass flows. Finally, Meruit has undertaken to provide endurance testing for the ANL NFC coating. The gas-bearing and NFC programs are yielding experimental data that support Meruit's models.

Results

Air System and Turbocompressor Design

The design of the turbocompressor is constrained by several requirements; one of the most challenging is that the centrifugal compressor operates over a wide turn-down range, reflecting the fact that automobiles spend so much time idling and then shifting to nearly full power. Since Meruit has not been able to design one set of turbine and compressor wheels to cover the DOE-specified operating range, and since the expected polymer electrolyte membrane (PEM) cell exhaust may not have sufficient energy to achieve the desired 3.2 compressor pressure ratio, some source of make-up power will be necessary and is needed for starting the fuel cell. Meruit originally proposed the use of a coaxial high-speed electric motor to boost the

expander; however, Meruit has built its turbocompressor without the coaxial motor.

The most important reason for not using a coaxial motor in the prototype turbocompressor is that, while a coaxial booster motor may supply added shaft power to the compressor to cover an expander shortfall, this approach fails to cover the low-flow (i.e., idle) operating problem of centrifugal air compressors. Simply adding shaft power moves the entire performance curve to higher speed (rpm), but it does not help compressor performance in the low-flow area where automobiles spend so much of their time. A separate compressor in series with the turbocompressor can be used to cover the idle flow area, and the turbine can recover energy supplied by the positive-displacement compressor, as well as that supplied by the centrifugal compressor. Hence, to cover the entire specified operating range, Meruit will use a positive-displacement compressor driven by an electric motor in tandem with Meruit's turbocompressor.

Meruit designed a family of compressor wheels (designated by consecutive letters A to Z) with varying characteristics (specific speed, dimensional ratios, etc.) that represent different compromises in providing performance compatible with the DOE specifications. A similar series of expander wheels with variable inlet geometry was optimized for a variety of possible PEM exhaust flows. After an extensive evaluation, Meruit has chosen two wheels that provide an adequate compromise of pressure, turndown, efficiency, and energy recovery: compressor wheel 7016T and expander wheel 7016F (a detailed description of the modeled turbocompressor performance is presented in the DOE Office of Transportation Technologies 2000 Annual Progress Report for Transportation Fuel Cell Power Systems). To complement these wheels, Meruit selected an off-the-shelf Eaton M-45 Roots-type blower to be driven by an electric motor, the performance curves of which complement those of the proposed Meruit turbocompressor for the DOE fuel cell application.

Turbocompressor and Its Test Bench

The basic expander configuration consists of variable inlet vanes (nozzle segments) for the convenient control of back pressure and mass flow for matching the performance of the compressor. The gas is injected tangentially through a set of

openings adjustable from zero to maximum flow by rotating the nozzle segments about their pivots, which are driven by pins engaged in slots in a ring surrounding the structure. The gas enters the space at the OD of the turbine wheel at a velocity that depends on the inlet temperature and the pressure drop across the segments. Figure 1 shows the geometry of the inlet vanes and their relationship to the blades of the turbine wheel.

The turbocompressor uses Meruit's radial and thrust gas bearings with ANL's NFC coating. The rotor is illustrated in Figure 2, the turbocompressor body without the expander and compressor housings in Figure 3, and the housings in Figure 4 (the expander is on the left in each illustration).

The assembled turbocompressor (Figure 5) uses an inducer cage to condition the air flow into the compressor wheel and has two proximity probes to observe bearing performance (one radial and one axial), one speed probe, a bearing feed air pressure indicator, and a nozzle control position indicator.

The turbocompressor is mounted in a shippable test bench that includes the Eaton compressor and its motor, an instrumentation table carrying the



Figure 1. Meruit variable nozzle expander.



Figure 2. Meruit turbocompressor rotor.

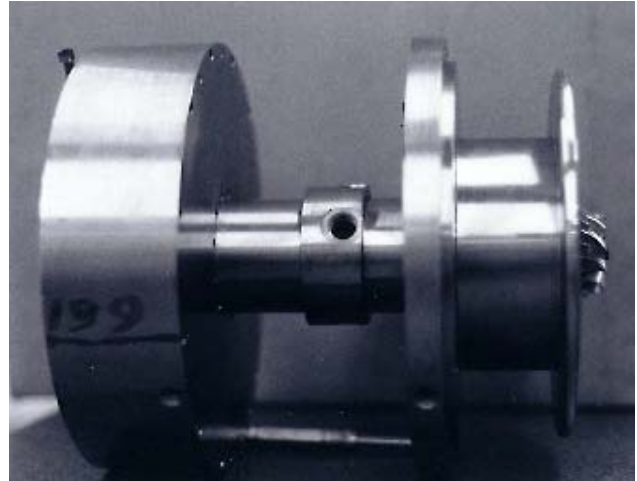


Figure 3. Meruit turbocompressor body.



Figure 4. Meruit turbocompressor housings.

electronics for probe power supply and signal conditioning, a logging computer with its associated monitor, printer and keyboard, an instrumentation and control panel, and the ducting necessary for the precise measurement of pressure and mass flow. The logging computer is a Pentium PC equipped with National Instruments "Labview" software; the Eaton

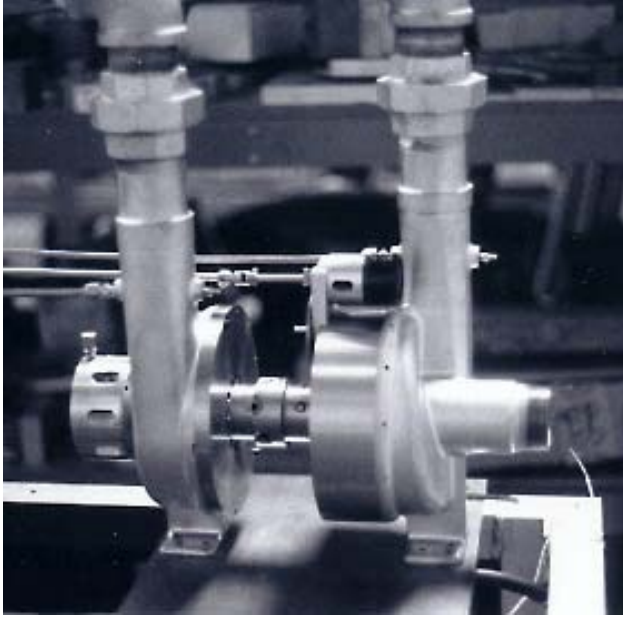


Figure 5. Assembled Meruit turbocompressor.

compressor is belt-driven by a Dayton 5N-134 10-hp electric motor. The air system instrumentation includes six pressure sensors (at the inlet, at the wheel OD, and at the exhaust of both compressor and expander), four corresponding temperature probes, and two orifice flow meters designed to ASME MFC-3M-1989 standards. Several electronic probes are paralleled by dial indicators. The ducting is valved to allow switching air flow between the two compressors and the expander in series or parallel or bleeding off mass flow and pressure at various points. Figure 6 shows the test bench instrumentation panel, and Figure 7 shows a side view of the turbocompressor test bench with its orifice flowmeters. Over the next few months, we plan to exercise the auxiliary compressor and turbocompressor in different configurations, speed ranges, and pressure settings to evaluate the performance of the Meruit gas bearing turbocompressor.

NFC Testing

Early in the gas bearing test program, it was experimentally found that, while a large-diameter (>75 mm) radial (journal) gas bearing would easily float a steel bearing in steel journals, the smaller-diameter (~20 mm) gas bearings intended for the DOE application would not lift off (“float”) satisfactorily. This condition, extant only when the shaft begins to turn from rest, could be remedied by

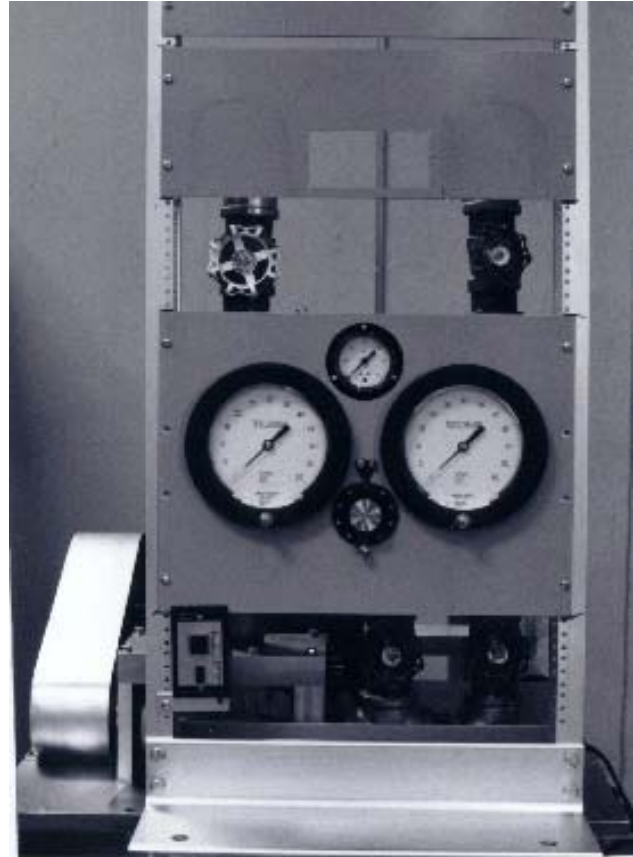


Figure 6. Test bench instrumentation panel.

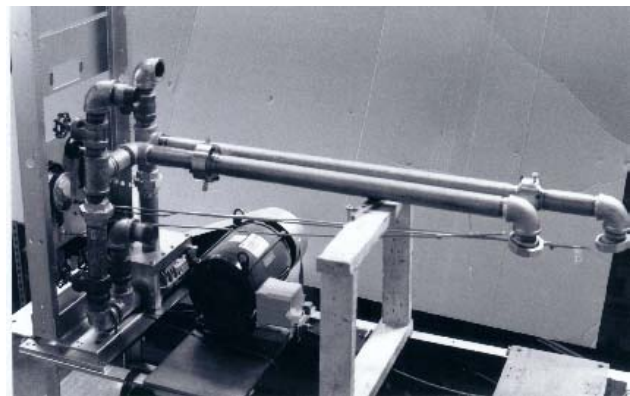


Figure 7. Test bench side view.

lowering the coefficient of friction between journal and bearing, and several remedies were found to work: DuPont *Vespel*, *Delrin*, and NFC. Delrin and Vespel are both commercially available low-friction plastics.

The Meruit gas bearing was tested with steel bearings in Vespel bushings in the journal up to 3,700 start-stop cycles; both bearing and bushing could have continued for more cycles. Another

tested remedy was the steel bearing with Delrin bushings in the journal; this configuration was tested to 1,300 start-stop cycles, and again both bearings and bushing could have withstood more cycles.

The ANL NFC was applied to the bearing. The NFC bearing runs in steel bushings and has been tested in two configurations: (1) with a strongly unbalanced rotor and (2) with a finely balanced rotor. In the unbalanced configuration, the gas bearing would float the rotor at ~8,700 rpm and land at about the same speed. When starting in the unbalanced configuration, the bearing rotor would turn about its geometric center. After a critical point was reached, the rotor would begin turning about its center of mass. When turning about the center of mass, the outside diameter of the bearing's rotation was very close to the available clearance in the journal, providing a great deal of physical contact between bearing and journal. After about 850 stop-start cycles, one point on the perimeter of the bearing had worn through the NFC; all other points showed either minimal wear or no wear at all. The worn point had accumulated an estimated 97,000 m of rubbing contact before the NFC was worn through and the bearing stopped working.

In the finely balanced configuration, it was found that the bearing floated the ~1-kg rotor somewhere between 900 and 1,000 rpm. This value is very close to Meruit's prediction that the bearing would float at about 1% of the 95,000 rpm turbocompressor design speed. To date, the bearing has accumulated 5,500 start-stop cycles. Because the liftoff and landing speeds are so low, the NFC coating should wear very little, and, when last measured, very little wear was evident (see Table 1). We expect to continue testing for 100,000 cycles or NFC wear-through, whichever comes first.

Gas Bearing Testing

Another aspect of the bearing test program is the experimental measurement of the thrust bearing's stiffness, force, and damping properties. The thrust bearing's stiffness is computed to increase with bearing feed air pressure, air temperature, and rpm. Any increase in these values should lead to a stiffer bearing with a more strongly damped response to shocks. While temperature testing is outside the scope of this contract, the thrust bearing stiffness has so far been tested at 17,500 and 21,000 rpm and at

Table 1. ANL NFC wear rate.

NFC2 Run May through June 2001			Balanced Rotor						
Rotor Mass (kg)		1.20	Weight per bearing (N)			5.89			
Start-Stop Cycles		250	1000	2000	4000	7000	10000	15000	20000
	Dimple Number	Summd Wear (micron)	Summd Wear (micron)	Summd Wear (micron)	Summd Wear (micron)				
Side 1	1	0.0347	0.0347	0.3782	1.2078				
	2	0.0487	0.0649	0.869	1.4693				
	3	0.0000	0.0000	0.0707	0.0707				
	4	0.0176	0.1927	0.5379	0.7924				
	5	0.0611	0.3144	0.8097	1.2899				
	6	0.0930	0.3534	0.3534	0.7275				
	7	0.0938	0.4023	0.4023	0.4023				
	8	0.0148	0.6915	1.0364	1.0364				
	9	0.0483	0.5779	1.4383	1.5073				
	10	0.0153	0.9997	0.9997	0.9997				
	11	0.1095	0.418	0.5697	0.5697				
Side 2	1	0.0141	0.0282	0.0984	0.5784				
	2	0.0882	0.5228	0.5228	0.6937				
	3	0.0669	0.0669	0.0669	0.3303				
	4	0.0295	0.1782	0.1782	0.1782				
	5	0.0834	0.5428	0.5751	0.6235				
	6	0.0290	0.1732	0.2447	0.2447				
	7	0.0567	0.099	0.1412	0.1692				
	8	0.0485	0.0807	0.2408	1.3882				
	9	0.0147	0.0735	0.1467	1.5222				
	10	0.0782	0.3102	0.3867	0.3867				

bearing feed pressures of 69 and 83 kPa (10 and 12 psig). Bearing air consumption was measured at about 0.08 g/s, which is negligible in comparison with the 76 g/s design air flow of the DOE turbocompressor.

The measured stiffness is shown in Figure 8, where the abscissa $Z/B2$ is the fractional displacement of the bearing from the center of the clearance (i.e., at $Z/B2=0$, the bearing is centered in its clearance, and at $Z/B2=1$, the bearing is in contact with the thrust washer), and the ellipses represent the measured points. The measured stiffness values vary with displacement between 6.80 and 3.63 kn/mm (38.8 to 20.7 klb/in.) at 21,000 rpm and 3.4 and 2.5 kn/mm (19.4 to 14.3 klb/in.) at 17,500 rpm.

Since the above values of required feed air mass flow and pressure are so modest in comparison with what the air system is designed to deliver, Meruit believes that this bearing will work very well for the intended automotive applications.

Reference

- Fonda-Bonardi, G. 2000. "Turbocompressor for Fuel Cell Service," in *Transportation Fuel Cell Power Systems 2000 Annual Progress Report (FY2000 Progress Report for Fuel Cell Power Systems)*, U.S. Department of Energy Office of Transportation Technology, October 2000, pg. 137.

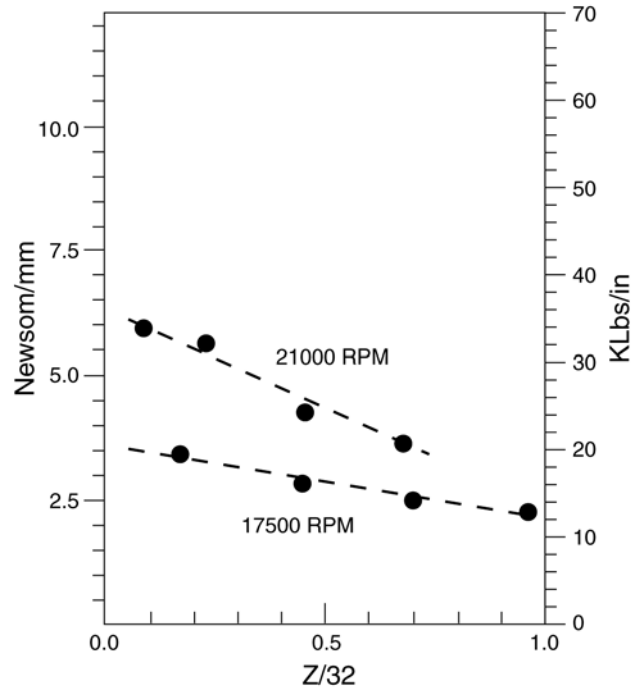


Figure 8. Meruit gas bearing stiffness.

APPENDIX A: ACRONYMS, INITIALISMS, AND ABBREVIATIONS

AB	air bleed
ACO	adsorption/catalytic oxidation
ADVISOR	Advanced Vehicle SimulatOR
AFM	atomic force microscopy
ANL	Argonne National Laboratory
AOP	anode over-potential
Ar	argon
ASTM	American Society for Testing and Materials
atm	pressure in atmospheres
ATR	autothermal reformer (reforming, Chapters 3B, 3E, 3I)
BPS	biphenyl sulfone
C ₂ H ₂	acetylene
C ₂ H ₄	ethylene
CaFCP	California Fuel Cell Partnership
CARAT	Cooperative Automotive Research for Advanced Technologies
CCM	catalyst-coated membrane
CEM	continuous emissions monitoring
CFD	computational fluid dynamics
CGO	gadolinium-doped cerium oxide
CMEU	compressor/motor/expander unit
CNG	compressed natural gas
CO	carbon monoxide
spi	cells per inch
pspi	cells per square inch
CS	constant stoichiometry
CVI	chemical vapor infiltration
CZO	zirconium-doped cerium oxide
DC	direct current
DFMA	design for manufacturing and assembly
DFT	density functional theory
DGO	direct gradient optimization
DMFC	direct methanol fuel cell
DOE	U.S. Department of Energy
DSC	differential scanning calorimetry
e ⁻	electron
EB	electrode backing
ECO	electrochemical oxidation
Fe	iron
FTIR	Fourier transform infrared
FTP	Federal Test Procedure
GC	gas chromatography
GC/MS	gas chromatograph/mass spectrometer
GDL	gas diffusion layer
GDM	gas diffusion media
GHSV	gas hourly space velocity
GM	General Motors

H ⁺	proton (hydrogen ion)
H ₂	hydrogen gas
H ₂ O	water
H ₂ SO ₄	sulfuric acid
HAD	hydrogen adsorption/desorption
HCN	hydrogen cyanide
HTS	high-temperature shift
ICE	internal combustion engine
IEC	ion-exchange capacity
IFC	International Fuel Cells
kg	kilograms
kN	kilonewtons
kW	kilowatts
kW _e	electrical power in kilowatts
L	liters
LANL	Los Alamos National Laboratory
LHV	lower heating value
LTS	low-temperature shift
MEA	matrix electrode assembly (Chapter 5I)
MEA	membrane electrode assembly
MEEM	Modal Energy and Emissions Model
Mequiv	milli-equivalent
mpgge	miles per gallon, gasoline equivalent
msec	milliseconds
MTI/CES	McDermott Technology, Inc./Catalytica Energy Systems, Inc.
MTS	medium-temperature shift
NFC	near-frictionless carbon
NH ₃	ammonia
NHE	normal hydrogen electrode
NMOG	non-methane organic gases
NREL	National Renewable Energy Laboratory
NRL	Naval Research Laboratory
NSLS	National Synchrotron Light Source
O/C	atomic oxygen to atomic carbon ratio (oxygen from air only)
O ₂	oxygen gas
OAAT	Office of Advanced Automotive Technologies
ORNL	Oak Ridge National Laboratory
ORR	oxidation reduction reaction
PC	personal computer
Pd	palladium
PDF-XRD	pair-density function analysis of X-ray diffraction
PEM	polymer electrolyte membrane
PEMFC	polymer electrolyte membrane fuel cell
PM	platinum metals
PNGV	Partnership for a New Generation of Vehicles
POx	partial oxidation
ppbv	parts per billion by volume
ppm	parts per million
PRDA	Program Research and Development Agreement
PrOx	preferential oxidation
PSAT	PNGV Systems Analysis Toolkit

Pt	platinum
PTFE	poly-tetra fluoro-ethylene
RCA	reconfigured anode
rpm	revolutions per minute
RPS	rapid prototype system
RSA	response surface approximation
RuO_xH_y	hydrous ruthenium oxide
S/C	steam to carbon ratio
SAE	Society of Automotive Engineers
SCE	saturated calomel electrode
SO	selective oxidation
SO_3^{2-}	sulfonate group
SOA	state of the art
SOC	state of charge
SOFC	solid oxide fuel cell
SR	stoichiometric ratio
SULEV	super ultra-low emissions vehicle
SUV	sport utility vehicle
SwRI	Southwest Research Institute
TGC	tail gas combustor
THC	total hydrocarbons
TIM	traction inverter module
TIVM	toroidal intersecting vane machine
TMO	transition metal oxide
VC	vulcan carbon, XC-72
VNT [®]	Variable Nozzle Turbine
VPT	Virginia Power Technologies
WGS	water-gas shift
XPS	X-ray photoelectron spectroscopy

APPENDIX B: DRAFT DOE TECHNICAL TARGETS FOR FUEL CELL SYSTEMS, SUBSYSTEMS, AND COMPONENTS

Table 1. Draft technical targets: integrated fuel cell power systems operating on Tier 2 gasoline containing average 30 ppm sulfur (50-kW peak power [continuous], including fuel processor, stack, auxiliaries, and start-up devices, if required; excluding gasoline tank and vehicle traction electronics). All targets require simultaneous achievement.

Characteristic	Units	Calendar Year		
		2001 (status)	2005	2010
Energy efficiency ^a @ 25% of peak power	%	34	40	45
Energy efficiency @ peak power	%	31	33	35
Power density	W/L	140	250	325
Specific power	W/kg	140	250	325
Cost ^b	\$/kW	300	125	45
Transient response (time from 10% to 90% power)	s	15	5	1
Cold start-up @ -20°C to maximum power	min	TBD	2	1
Cold start-up @ 20°C to maximum power	min	<10	1	<0.5
Survivability ^c	°C	TBD	-30	-40
Emissions ^d	-	<Tier 2 Bin 5 ^e	<Tier 2 Bin 5 ^e	<Tier 2 Bin 5 ^e
Durability ^f	h	1,000 ^g	2,000 ^h	5,000 ⁱ

- ^a Ratio of dc output energy to the lower heating value of the input fuel (gasoline).
- ^b Includes projected cost advantage of high-volume production (500,000 units per year) and includes cost for assembling/integrating the fuel cell system and fuel processor.
- ^c Achieve performance targets at 8-h cold-soak at temperature.
- ^d Emissions levels will comply with emissions regulations projected to be in place when the technology is available for market introduction.
- ^e 0.07 g/mi NO_x and 0.01 g/mi PM.
- ^f Performance targets must be achieved at the end of the durability period.
- ^g Continuous operation.
- ^h Includes thermal cycling.
- ⁱ Includes thermal and realistic drive cycles.

Table 2a. Draft technical targets: fuel-flexible fuel processors operating on Tier 2 gasoline containing average 30 ppm sulfur^a (50 kW peak power [continuous], excludes fuel storage; includes controls, shift reactors, CO cleanup, heat exchangers). All targets require simultaneous achievement.

Characteristic	Units	Calendar Year		
		2001 (status)	2005	2010
Energy efficiency ^b	%	78	78	80
Power density	W/L	500	700	800
Specific power	W/kg	450	700	800
Cost ^c	\$/kW	85	25	10
Cold start-up @ -20°C to maximum power	min	TBD	2.0	1.0
Cold start-up @ 20°C to maximum power	min	<10	<1	<0.5
Transient response (time from 10% to 90% power)	s	15	5	1
Emissions ^d	-	<Tier 2 Bin 5	<Tier 2 Bin 5	<Tier 2 Bin 5
Durability ^e	h	1,000 ^f	2,000 ^g	5,000 ^h
Survivability ⁱ	°C	TBD	-30	-40
CO content steady-state ^j	ppm	10	10	10
CO content transient ^j	ppm	100	100	100
H ₂ S content in product stream	ppb	<200	<50	<10
NH ₃ content in product stream	ppm	<10	<0.5	<0.1

^a With catalyst system suitable for use in vehicles.

^b Fuel processor efficiency = total fuel cell system efficiency/fuel cell stack system efficiency, where total fuel cell system efficiency accounts for thermal integration. For purposes of testing fuel-processor-only systems, the efficiency can be estimated by measuring the derated heating value efficiency (lower heating value H₂ × 0.95/ lower heating value of the fuel in), where the derating factor represents parasitic system power losses attributable to the fuel processor.

^c High-volume production: 500,000 units per year.

^d 0.07 g/mi NO_x and 0.01 g/mi PM.

^e Time between catalyst and major component replacement; performance targets must be achieved at end of durability period.

^f Continuous operation.

^g Includes thermal cycling.

^h Includes thermal and realistic drive cycles.

ⁱ Performance targets must be achieved at the end of 8-h cold-soak at temperature.

^j Dependent on stack development (CO tolerance) progress.

Table 2b. Draft technical targets for fuel processor catalysts (gasoline w/30 ppm sulfur) (autothermal reformer = ATR, sulfur = S, water-gas shift = WGS, preferential oxidizer = PrOx).

Characteristic	Units	ATR	S Removal	WGS	PrOx
GHSV ^{a, b}	h ⁻¹	200,000	50,000	30,000	150,000
Conversion ^c	%	>99.9	>99.95	>90	>99.8
H ₂ Selectivity ^d	% (or consumption)	>80	<0.1	>99	<0.2
Volume ^e	L/kW _e	<0.013	<0.06	<0.1	<0.02
Weight ^e	kg/kW _e	<0.015	<0.06	<0.1	<0.03
Durability ^f	h	5,000	5,000	5,000	5,000
Cost	\$/kW _e	<5	<1	<1	<1

^a GHSV = gas hourly space velocity: The volumetric flow rate of the product gases at 25°C and 1 atm, divided by the bulk volume of the catalyst.

^b STP equivalents for wet inlet gas; target values are guidelines for single reactor R&D; system/subsystem targets take precedence.

^c Conversion: (moles of reactant in–moles of reactant out) × 100/(moles of reactant in).

^d Selectivity: At the ATR: (moles of H₂ in product) × 100/(moles of H₂ “extractable” from ATR feed); at the shift reactor: (moles CO converted to H₂) × 100/(total moles of CO converted).

^e The volume and weight targets include only the catalysts, not the hardware needed to house the catalysts or the heat exchangers.

^f Over standard drive cycle.

Table 3. Draft technical targets: fuel cell stack systems running on hydrogen-rich fuel from fuel-flexible fuel processor 50-kW peak power (continuous)^a (excludes fuel processing/delivery system; includes fuel cell ancillaries: heat, water, air management systems). All targets must be achieved simultaneously.

Characteristic	Units	Calendar Year		
		2001 (status)	2005	2010
Stack system power density ^{a, b}	W/L	200	400	550
Stack system specific power	W/kg	200	400	550
Stack system efficiency ^c @ 25% of peak power	%	45	50	55
Stack system efficiency ^c @ peak power	%	40	42	44
Precious metal loading	g/peak kW	2.0	0.6	0.2
Cost ^d	\$/kW	200	100	35
Durability ^e	h	1,000 ^f	>2,000 ^g	>5,000 ^h
Transient response (time from 10% to 90% power)	s	3	2	1
Cold start-up @ -20°C to maximum power	min	2	1	0.5
Cold start-up @ 20°C to maximum power	min	1	0.5	0.25
Survivability ⁱ	°C	-20	-30	-40
CO tolerance (steady-state — 2% maximum air bleed)	ppm	50	500	500
CO tolerance (transient)	ppm	100	500	1,000

^a Power refers to net power (i.e., stack power minus auxiliary power requirements).

^b Volume is “box” volume (including dead space) and is defined as the water-displaced volume \times 1.5 (packaging factor).

^c Ratio of output dc energy to lower heating value of hydrogen-rich fuel stream (includes converter for 300-V bus).

^d High-volume production: 500,000 units per year.

^e Performance targets must be achieved at the conclusion of the durability period; durability includes tolerance to H₂S and NH₃ impurities.

^f Continuous operation.

^g Includes thermal cycling.

^h Includes thermal and realistic drive cycles.

ⁱ Performance targets must be achieved at the end of 8-h cold-soak at temperature.

Table 4a. Draft technical targets for fuel cell stack components^a.

Component	Requirement
Membranes ^b	Cost: \$5/kW Stability: w/RH 20–100%, <10% swelling, <2-mV degradation H ₂ crossover: <1mA/cm ² Area-specific resistance: 0.1 ohm-cm ²
Electrodes	Cost: \$5/kW CO tolerance: 500 ppm steady-state, 1,000 ppm transient @ 0.2 g Pt/peak kW Durability: 5,000 h Utilization: 85% H ₂ , 60% O ₂
Membrane-electrode assembly	Cost: \$10/kW Voltage/current density: 0.8 V @ 0.4 A/cm ² Power Density: 0.32 W/cm ² @ 0.8 V
Bipolar plates	Cost: \$10/kW; <1 kg/kW H ₂ permeation rate: < 2 × 10 ⁻⁶ cm ³ /s-cm ² @ 80°C, 3 atm (<0.1mA/cm ²) Corrosion limit: 16 μA/cm ² Resistivity: 0.02 ohm-cm ²

^a For operation on gasoline reformat: 40% H₂.

^b Targets listed are for conventional membrane technologies (operating temperatures of 60–90°C); high-temperature membranes for operation above 100°C might have different characteristics.

Table 4b. Draft technical targets for fuel cell sensors ^a.

Sensor	Requirements
Carbon monoxide	<p>a) <u>1–100-ppm reformat pre-stack sensor</u></p> <ul style="list-style-type: none"> – Operating temperature: <150°C – Response time: 0.1–1 s – Gas environment: high-humidity reformer/partial oxidation gas: H₂ 30–75%, CO₂, CO, N₂, H₂O @ 1–3 atm total pressure – Accuracy: 1–10% full scale <p>b) <u>100–1,000-ppm CO sensors</u></p> <ul style="list-style-type: none"> – Operational temperature: 250°C – Response time: 0.1–1 s – Gas environment: high-humidity reformer/partial oxidation gas: H₂ 30–75%, CO₂, CO, N₂, H₂O @ 1–3 atm total pressure – Accuracy: 1–10% full scale <p>c) <u>0.1–2% CO sensor</u></p> <ul style="list-style-type: none"> – Operational temperature: 250–800°C – Response time: 0.1–1 s – Gas environment: high-humidity reformer/partial oxidation gas: H₂ 30–75%, CO₂, CO, N₂, H₂O @ 1–3 atm total pressure – Accuracy: 1–10% full scale
Hydrogen in fuel processor product gas	<ul style="list-style-type: none"> – Measurement range: 1–100% – Operating temperature: 70–150°C – Response time: 0.1–1 s for 90% response of step function – Gas environment: 1–3 atm total pressure, 10–30 mol % water, total H₂ 30–75%, CO₂, N₂ – Accuracy: 1–10% full scale
Hydrogen in ambient air (safety sensor)	<ul style="list-style-type: none"> – Measurement range: 0.1–10% – Operating temperature: –30–80°C – Response time: <1 s – Accuracy: 5% – Gas environment: ambient air, 10–98% RH range – Lifetime: 5 yr – Selectivity from interference gases, such as hydrocarbons, is needed.
Sulfur compounds (H ₂ S, SO ₂ , organic sulfur)	<ul style="list-style-type: none"> – Measurement range: 0.05–0.5 ppm – Operating temperature: <400°C – Response time: <1 min @ 0.05 ppm – Gas environment: Hydrogen, CO, CO₂, hydrocarbons, water vapor
Flow rate of product gas from fuel processor	<ul style="list-style-type: none"> – Flow rates: 30–300 standard L/min – Temperature: 80°C – Gas environment: high-humidity reformer/partial oxidation gas: H₂ 30–75%, CO₂, N₂, H₂O, CO @ 1–3 atm total pressure
Ammonia	<ul style="list-style-type: none"> – Measurement range: 1–10 ppm – Operating temperature: 70–150°C – Selectivity: <1 ppm from matrix gases – Lifetime: 5–10 yr – Response time: s – Gas environment: high-humidity reformer/partial oxidation gas: H₂ 30–75%, CO₂, N₂, H₂O, CO @ 1–3 atm total pressure

Table 4b. Cont.

Sensor	Requirements
Temperature	<ul style="list-style-type: none"> - Operating range: -40–150°C - Response time: in the -40–100°C range <0.5 s with 1.5% accuracy; in the 100–150°C range, a response time <1 s with 2 % accuracy is sufficient - Gas environment: high-humidity reformer/partial oxidation gas: H₂ 30–75%, CO₂, N₂, H₂O, CO @ 1–3 atm total pressure - Needs to be insensitive to flow velocity.
Relative humidity for cathode and anode gas streams	<ul style="list-style-type: none"> - Operating temperature: 30–110°C - Relative humidity: 20–100% - Accuracy: 1% - Gas environment: high-humidity reformer/partial oxidation gas: H₂ 30–75%, CO₂, N₂, H₂O, CO @ 1–3 atm
Oxygen concentration in fuel processor and at cathode exit	<p><u>(a) Oxygen sensors for fuel processor reactor control</u></p> <ul style="list-style-type: none"> - Measurement range: 0–20% O₂ - Operating temperature: 200–800°C - Response time: <0.5 s - Accuracy: 2% of full scale - Gas environment: high-humidity reformer/partial oxidation gas: H₂ 30–75%, CO₂, N₂, H₂O, CO @ 1–3 atm <p><u>b) Oxygen sensors at the cathode exit</u></p> <ul style="list-style-type: none"> - Measurement range: 0–50% O₂ - Operating temperature: 30–110°C - Response time: <0.5 s - Accuracy: 1% of full scale - Gas environment: H₂, CO₂, N₂, H₂O @ 1–3 atm total pressure
Differential pressure in fuel cell stack	<ul style="list-style-type: none"> - Measurement range: 0–1 psig or (0–10 or 1–3 psig, depending on design of fuel cell system) - Temperature range: 30–100°C; -40°C survivability - Response time: <1 s - Accuracy: 1% - Size: Needs to be small — 1 in.² — and orientation cannot be a problem. - Other: Has to be able to withstand and measure liquid and gas phases.

^a Sensors must conform to size, weight, and cost constraints required for automotive applications.

Table 5. Draft technical targets for compressor(c)/expander(e) systems.

Characteristic	Units	Requirement
Input power ^a @ maximum flow	kW	4.3
Efficiency @ 100% flow	%	c-75% @ 3.2 PR e-90%
Efficiency @ 20% flow	%	c-65% @ 1.6 PR e-80%
Volume ^b	L	4
Weight ^b	kg	3
Cost ^b @ 100K/yr	\$	200
Turndown ratio	-	10
Noise	db	<80

^a Input power to the controller to power a compressor/expander system producing 76 g/s (dry) maximum flow. This flow rate roughly corresponds to maximum power for a 50-kW fuel cell system. A 20% flow is approximately equivalent to 25% system power point. Input power and expander efficiency numbers calculated assuming tail gas composition specified by DOE (@100% flow, 82 g/s, 150°C, and 2.8 atm inlet, unless otherwise specified).

^b DOE guidelines for weight, volume, and cost do not include the motor/controller or heat rejection (if required).

Table 6. Technical targets for on-board hydrogen storage^{a, b, c}.

Characteristic	Units	Target	2001 Status	
			Physical Storage ^d	Chemical Storage ^e
Storage weight percent ^f	%	6	5.2	3.4
Recoverable usable H ₂ ^g	%	90	99.7	90
Energy density (gas)	W-h/L ^{h, i}	1,100	813	1,300
Specific energy ^j	W-h/kg ^{h, i}	2,000	1,745	TBD
Cost ^k	\$/kW-h	5	50 ^l	18 ^m
Cycle life	cycles	500	500	>500
Operating temperature ⁿ	°C	-40 to 90	-40 to 80	TBD
Start-up delivery time to full flow	from 20°C	15	near zero	<15
	from -20°C	30	TBD	TBD
Refueling time	min	5	TBD	TBD
Hydrogen loss	scf/h•L	1.0	TBD	<1.0

^a Based on lower heating value of hydrogen — includes both physical and chemical methods of hydrogen storage; enables greater than 300-mi range based on an aerodynamic 2,500-lb vehicle.

^b R&D carried out in collaboration with DOE Hydrogen Program.

^c Retail H₂ refueling infrastructure targets: 70% well-to-pump energy efficiency, \$1.50 (untaxed) per gasoline gallon equivalent, and delivery of 150 kg of H₂ per day.

^d Based on 5,000-psi tanks; 10,000-psi tanks have been built and tested, but not yet certified.

^e Based on a 5-kg alanate hydride storage system.

^f Weight percent H₂ is assumed to be the weight of H₂ divided by the weight of (H₂ + tank).

^g Recoverable stored hydrogen; for example, in a 100-kg H₂ containing 6 kg of stored hydrogen, at least 5.4 kg of useful hydrogen must be recoverable.

^h Based on 5 kg of hydrogen for >300-mi range at 10,000 psia (volume of stored hydrogen is 135 L). Allowing for 10% containment volume, system volume is 150 L.

ⁱ Watts thermal.

^j Specific energy is assumed to be the lower heating value energy of H₂ contained divided by the weight of (H₂ + tank).

^k Based on high-volume production of 500,000 units.

^l Based on individual tanks.

^m Cost of hydride material only.

ⁿ Hydrogen storage system must provide hydrogen to the fuel cell at these ambient temperatures.

Table 7. Draft DOE technical targets for integrated fuel cell power systems operating on direct hydrogen^a (50-kW peak power [continuous]). All targets require simultaneous achievement.

Characteristic	Units	Calendar Year		
		2001 (status)	2005	2010
Energy efficiency ^b @ 25% of peak power	%	59	60	60
Energy efficiency @ peak power	%	50	50	50
Power density (excluding H ₂ storage)	W/L	400	500	650
Power density (including H ₂ storage)	W/L	TBD	150	220
Specific power (excluding H ₂ storage)	W/kg	400	500	650
Specific power (including H ₂ storage)	W/kg	TBD	250	325
Cost ^c (including H ₂ storage)	\$/kW	200	125	45
Transient response (time from 10 to 90% power)	s	3	2	1
Cold start-up @ -20°C to maximum power	s	120	60	30
Cold start-up @ 20°C to maximum power	s	60	30	15
Emissions	-	0	0	0
Durability ^d	h	1,000	2,000 ^e	5,000 ^f
Survivability ^g	°C	-20	-30	-40

^a Targets are based on hydrogen storage targets in an aerodynamic 2,500-lb vehicle.

^b Ratio of dc output energy to the lower heating value of the input fuel (hydrogen).

^c Includes projected cost advantage of high-volume production (500,000 units per year).

^d Performance targets must be achieved at the end of the durability period.

^e Includes thermal cycling.

^f Includes thermal and realistic drive cycles.

^g Achieve performance targets at 8-h cold-soak at temperature.

This document highlights work sponsored by agencies of the U.S. Government. Neither the U.S. Government nor any agency thereof, nor any of their employees, makes any warranty, express or implied, or assumes any legal liability or responsibility for the accuracy, completeness, or usefulness of any information, apparatus, product, or process disclosed, or represents that its use would not infringe privately owned rights. Reference herein to any specific commercial product, process, or service by trade name, trademark, manufacturer, or otherwise does not necessarily constitute or imply its endorsement, recommendation, or favoring by the U.S. Government or any agency thereof. The views and opinions of authors expressed herein do not necessarily state or reflect those of the U.S. Government or any agency thereof.

Office of Transportation Technologies Series of 2001 Annual Progress Reports

- Office of Advanced Automotive Technologies FY 2001 Program Highlights
- Vehicle Propulsion and Ancillary Subsystems
- Automotive Lightweighting Materials
- Automotive Propulsion Materials
- Fuels for Advanced CIDI Engines and Fuel Cells
- Spark Ignition, Direct Injection Engine R&D
- Combustion and Emission Control for Advanced CIDI Engines
- Fuel Cells for Transportation
- Advanced Technology Development (High-Power Battery)
- Batteries for Advanced Transportation Technologies (High-Energy Battery)
- Vehicle Power Electronics and Electric Machines
- Vehicle High-Power Energy Storage
- Electric Vehicle Batteries R&D



www.carttech.doe.gov

DOE/EERE/OTT/OAAT - 2001/008